Department of AERONAUTICS and ASTRONAUTICS
STANFORD UNIVERSITY

URY PASSY

SIMULATION AND OPTIMIZATION STUDIES OF DRAG FREE SATELLITE

NOVEMBER 1966

This work was performed in association with research sponsored by the National Aeronautics and Space Administration Under Research Grant NsG 582 And NASA Grant NGR-05-020-073

SUDAAR NO. 295

Department of Aeronautics and Astronautics
Stanford University
Stanford, California

SIMULATION AND OPTIMIZATION STUDIES OF DRAG FREE SATELLITE

By

Ury Passy

SUDAAR No. 295
November 1966

This work was performed in association with research sponsored by the
National Aeronautics and Space Administration
under Research Grant NsG 582
and NASA Grant NGR-05-020-073

TABLE OF CONTENTS

LIST OF ILLUSTRATIONS

CHAPTER I

INTRODUCTION

Research on the behavior of a "zero-g satellite" [Reference 1] is being done at Stanford University. The drag-free satellite can be used to perform several different experiments.

a) Geodesy: the departure of the figure of the earth from perfect sphere;

b) Aeronomy: the density measurements of the upper atmosphere.

Several other possible applications are described by Lange [Reference 1].

For the purpose of studying the behavior of the "zero-g satellite" a large dynamic simulator ACV (Air Cushion Vehicle the name given to the simulator) was designed. The main features of this simulator are described later. Four air jets which are actuated by a pulse-width,. pulse frequency (P.W.P.F.) [Reference 2] control law keep the ACV at the desired position. It is intended to use the same control law and the same position sensor on the satellite itself.

The lifetime of that satellite depends on the limit cycle fuel consumption of the control jets. Therefore the parameters of P.W.P.F. must be chosen so that the limit cycle fuel consumption is minimized. The present research is concerned with this optimization problem. The research consists of three different phases:

Phase 1: The ACV should be brought into operating conditions, and all the necessary modifications should be done so that thebehavior of the ACV could be studied;

Phase 2: Based on the data and experimental results obtained in Phase 1, a model of the ACV system is to be constructed on the analog computer.

Phase 3: At this phase the optimization is done. There are two stages to the optimization process:

1) Slaving the analog computer to the digital computer (hybrid system) and

2) Constructing an efficient search method for the optimum gain setting.

The present report consists mainly of these three parts.

CHAPTER II

THE EXPERIMENTAL SET-UP AND RESULTS

2.1 Introduction

It is not the purpose of this report to describe the ACV (Air Cushion Vehicle), but in order to understand the experiments and the analog simulation, and since there is no report which describes the ACV, a short and simplified description is included.

The ACV is actually an air bearing which floats horizontally over a granite table with negligible friction. Thus it can be used as a simulator for a "zero-g satellite". The simulator is an important tool in the development of circuitry and sensors of the control loop, and it will give accurate information on propellant consumption of the "zero-g satellite".

2.2 General Description of the ACV Operation

The air-cushion vehicle is floated on an air film over a granite table. The table (Fig. 2.2.1) can be tipped so that the air cushion vehicle tends to move across the table. This simulates a disturbing force acting on the "zero-g satellite". Table angles corresponding to drag at different altitudes for a typical satellite are shown in Figure 2.2.2. A proof mass is supported above the table to simulate the proof mass in the "zero-g satellite". The ball is located within a hemispherical capacitor (Figure 2.2.3) which is connected rigidly to the vehicle. As the vehicle moves across the table, its position with respect to the ball is sensed, and the control system causes a gas valve

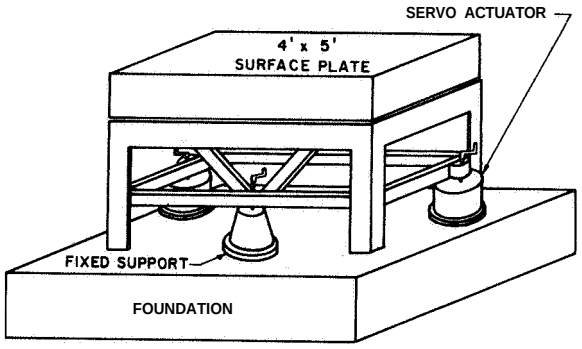

Figure 2.2.1. Table support system

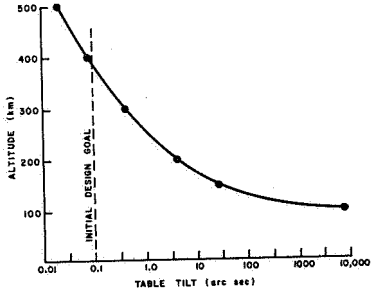

Figure 2.2.2. Table tilt required to simulate aerodynamics drag on a typical satellite vs. altitude

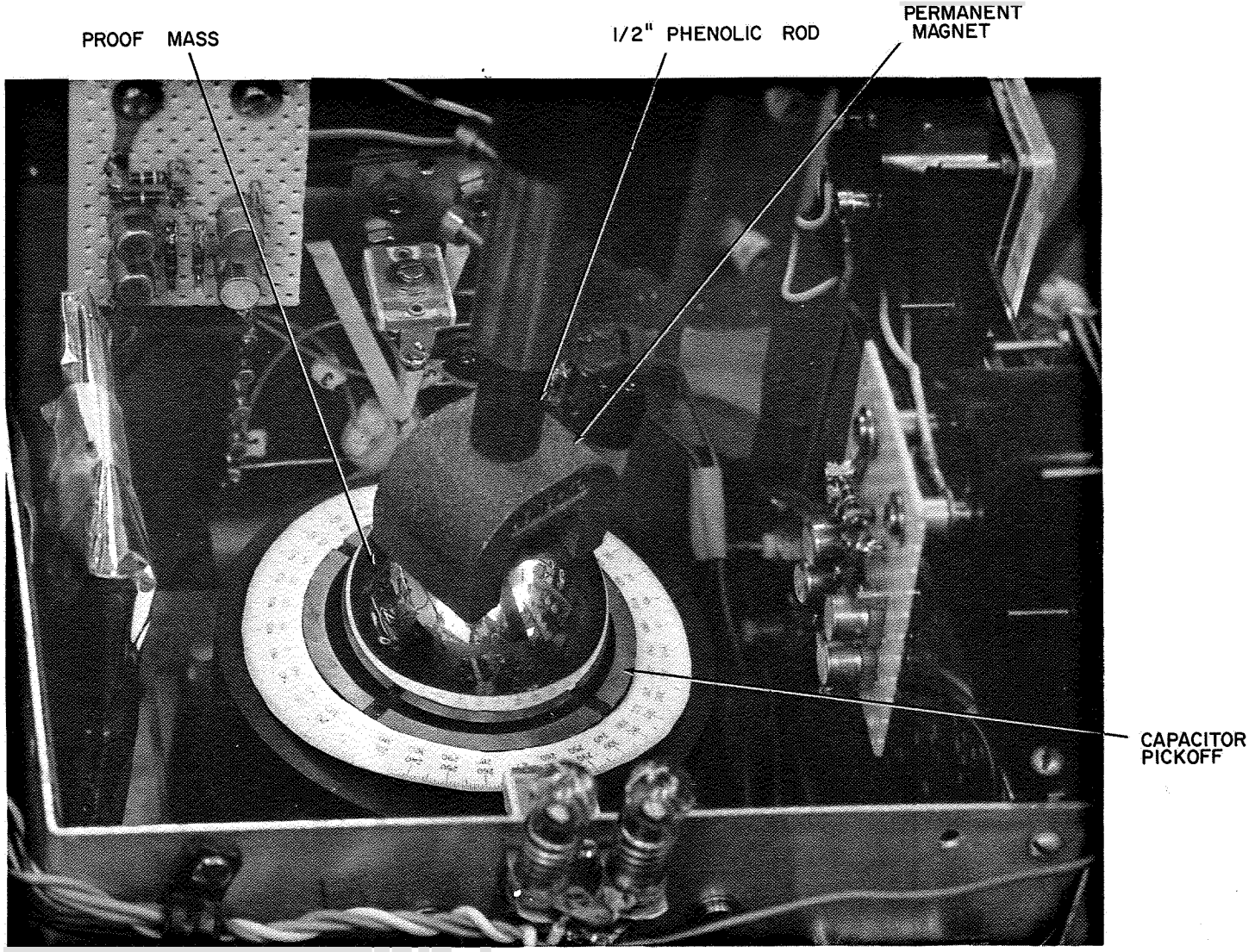

Figure 2.2.3. The simulated proof mass and the capacitor pickoff

(Fig. 2.2.4) to fire in order to bring the vehicle back to its proper location centered underneath the ball. The granite table is kept at a proper leveling by an automatic table leveling system described in details elsewhere [Reference 3].

2.3 Structural Description

The present simulator vehicle was developed mainly by a "try and learn" method. Most of its components have been built by Dr. R. Bourke and Mr. R. Tuffias. It consists of a 3/4" thick and 28" diameter circular aluminum base (Fig. 2.3.1) with central gas supply and 2" diameter recess at the center. This recess is necessary to lift the vehicle off the ground when it is not yet afloat. (Fig. 2.3.3a) Then the total lift is provided by the pressure of the gas flowing in, times the area of the recess, until a gap is formed between the vehicle and the ground which allows the gas to spread out and to form the normal supporting gas film. A second 1/4" aluminum plate of hexagonal planform and of 26" width between opposite edges is located on the base plate. The two plates are separated by an O-ring. This is done in order to have a completely axisymmetric load distribution on the lower base plate. All the instrumentation and the gas supply systems are connected to the hexagonal base.

The support gas is stored in four vertical high-pressure steel bottles, size number 4, each holding approximately 1 pound of nitrogen (Fig. 2.2.4). The gas is let out through a pressure regulator and a flowmeter into the base plate.

The control gas is stored in two horizontal steel bottles similar to the support gas.

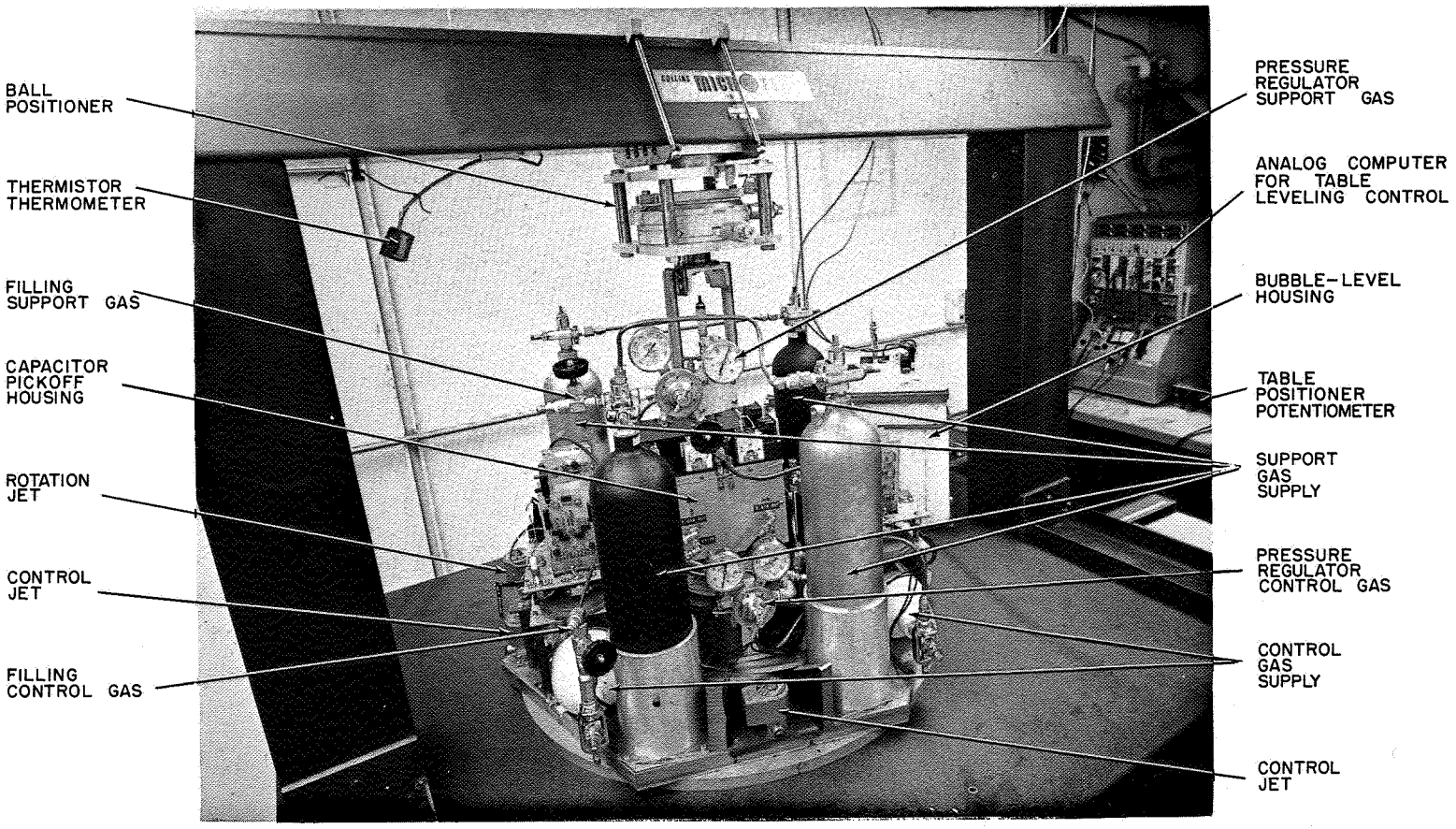

Figure 2.2.4. A.C.V. Front View

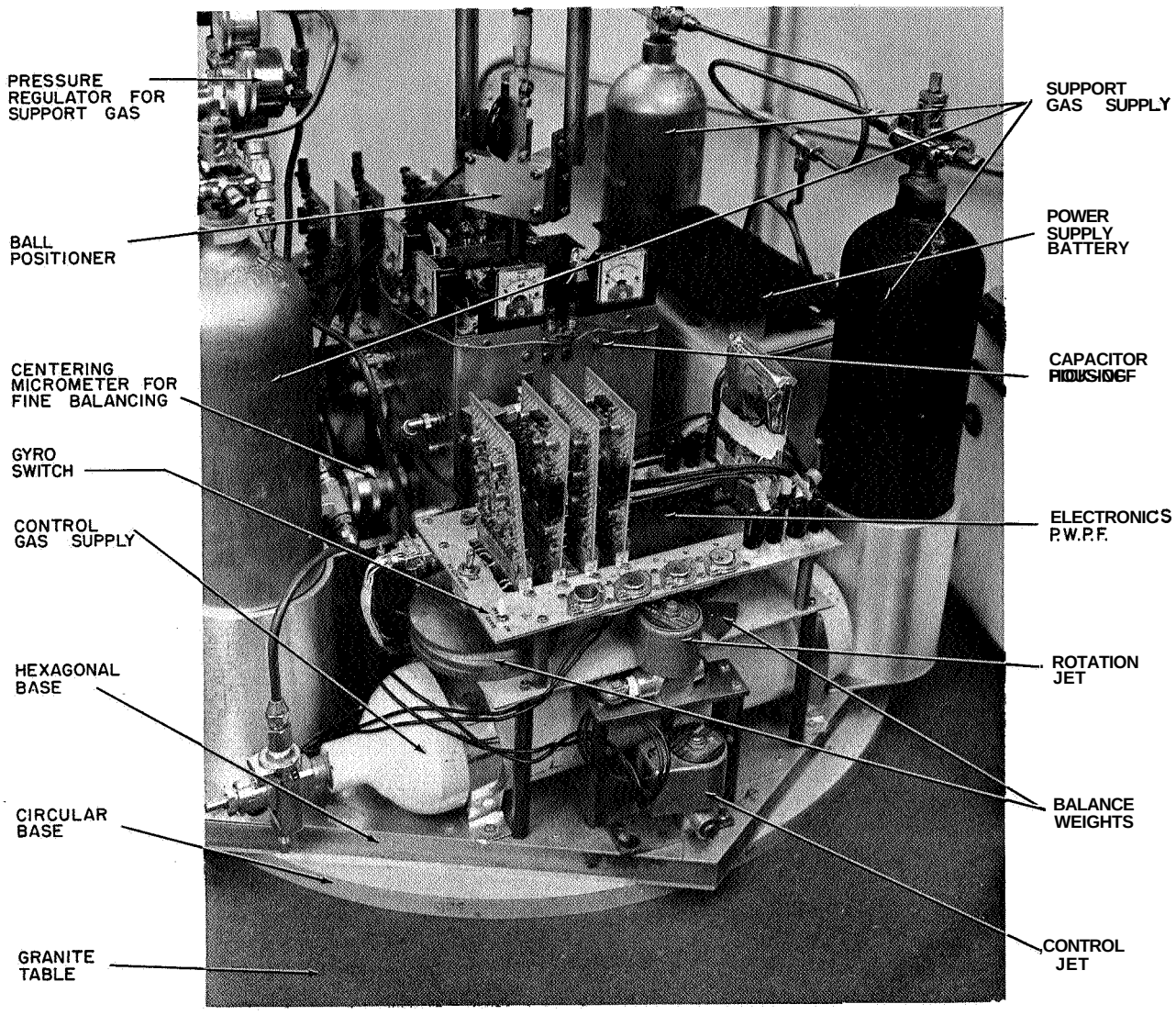

Figure 2.3.1. A.C.V. Side View

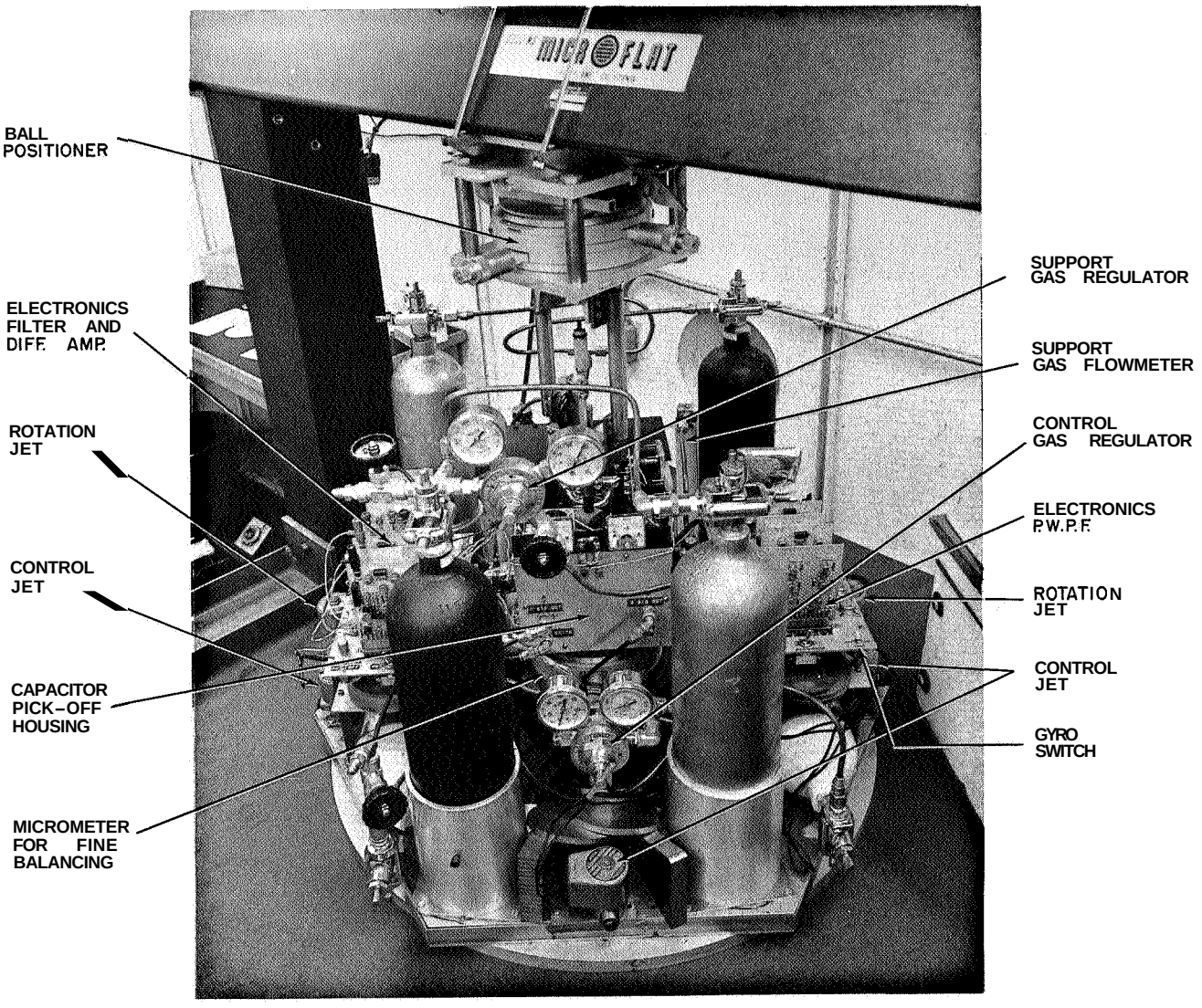

Figure 2.3.2. A.C.V. Front View

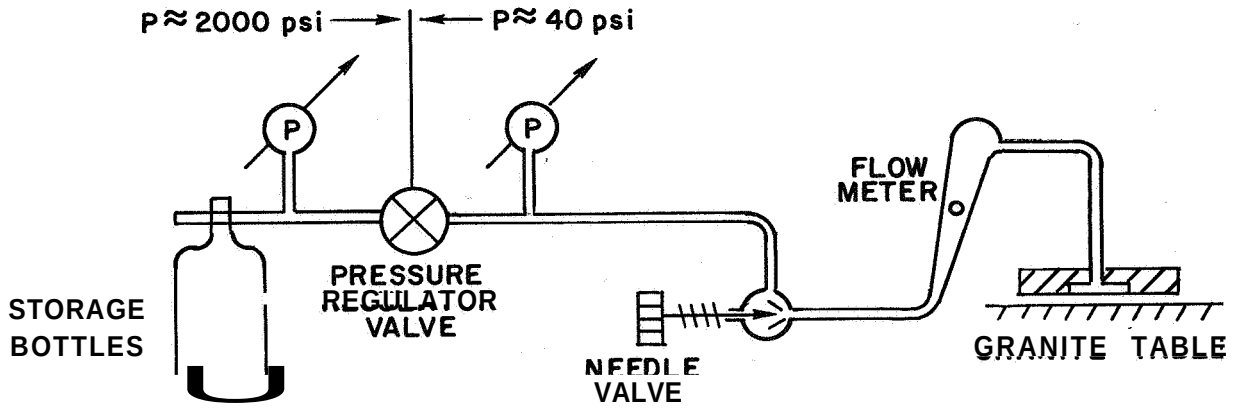

(a)

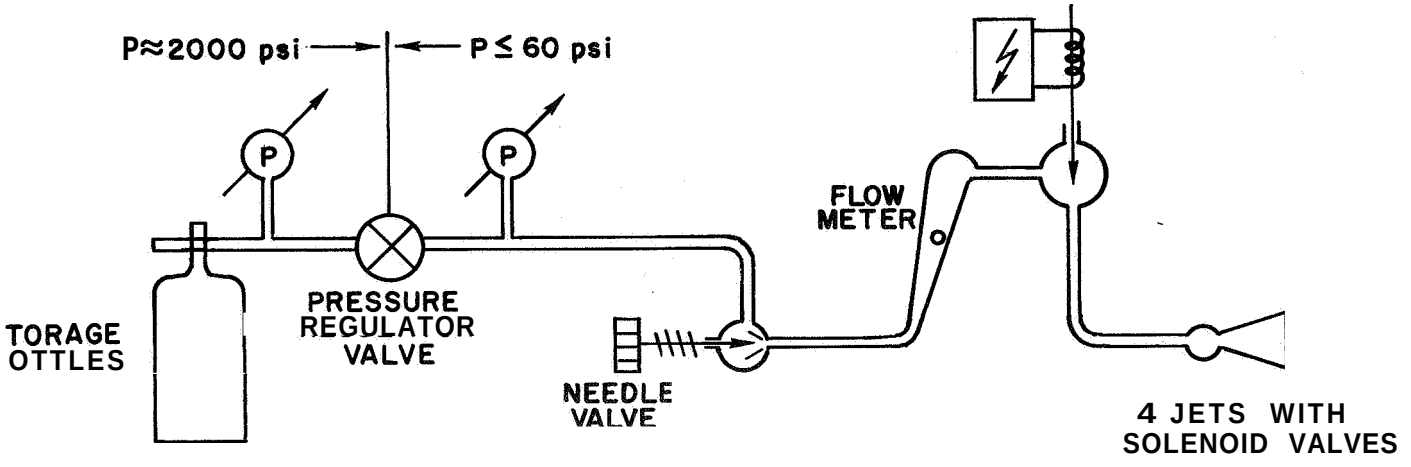

(b)

Figure 2.3.3. Flow diagram of the two gas systems:
(a) support gas flow diagram
(b) control gas flow diagram

Four radial jets for two-dimensional lateral control had been mounted on the vehicle at 90^{o} apart (Fig. 2.3.2). The nozzles are 3/64" diameter holes drilled into pipe plugs, the edges of the holes being well rounded to yield a convergent-divergent shape. The plugs were then screwed into the outlets of a commercial solenoid valve, "ASCO" No. 826222.

The two gas systems, the support and control, are described schematically in Figure 2.3.3.

The electrical equipment consists of the position sensor, a large 12-volt battery as general power supply, and the control circuitry. Finally, two "Nikon" cross travelling micrometer carriages are located one under the battery, (Fig. 2.3.4) and one under the position sensor (Fig. 2.3.2). By manipulating the micrometer-carriage it was possible to get fine symmetrical mass distribution.

The metallic ball which represents the proof mass in the actual satellite was positioned by a special device (Fig. 2.4.1) which allows accurate (0.0001 inch) positioning in three dimensions.

2.4 Position Sensor

The position sensor consists of two main parts:

1) Precision Ball Positioner (Fig. 2.4.1).

2) Capacitive Pickoff Sensor (Fig. 2.4.2).

Precision Ball Positioner:

For various purposes, a device has been built which allows accurate (0.0001 in.) positioning in three dimensions of the steel ball which represents the proof mass in the actual satellite.

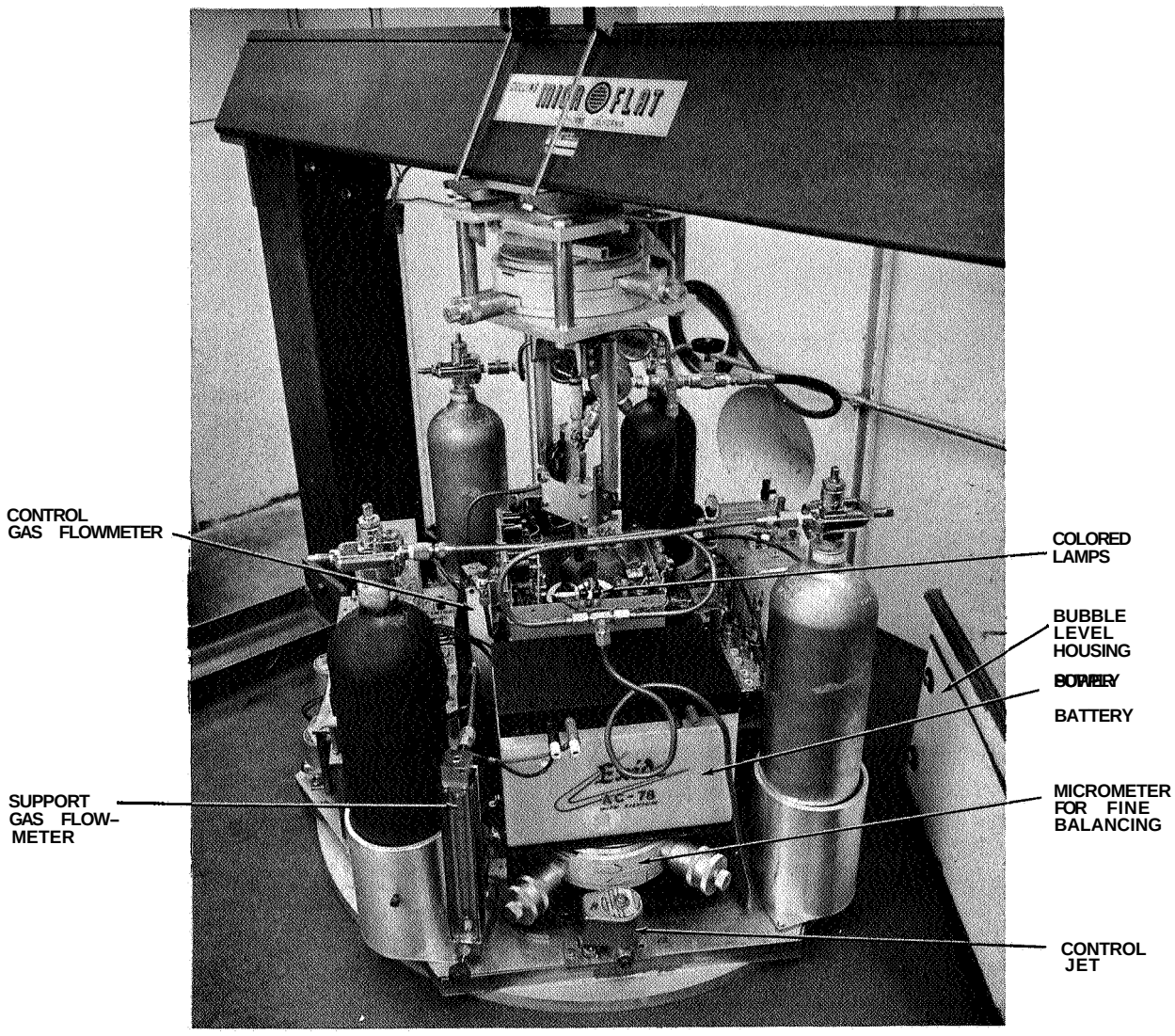

Figure 2.3.4. A.C.V. Back View

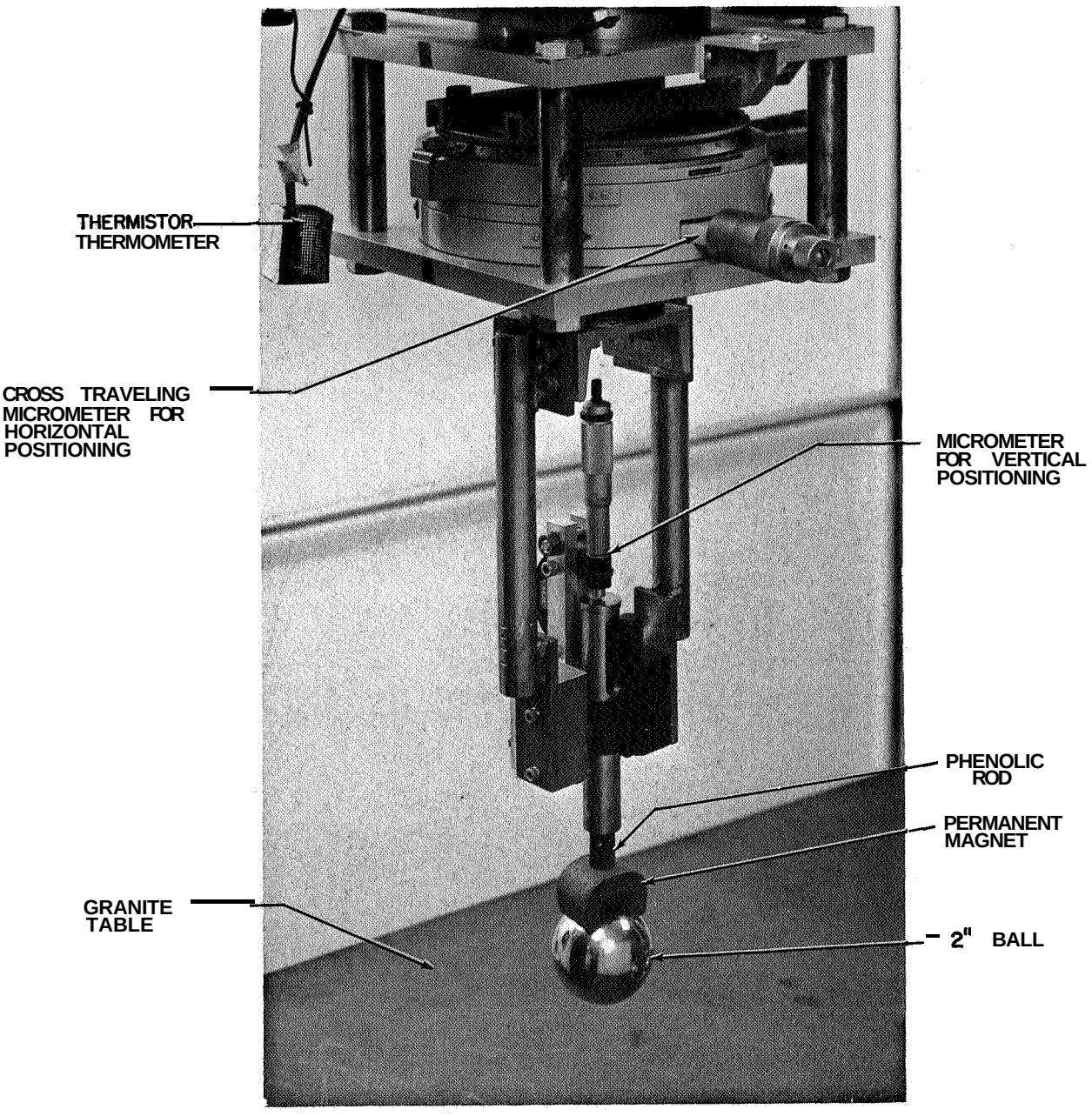

Figure 2.4.1. Precision ball position with 2" ball

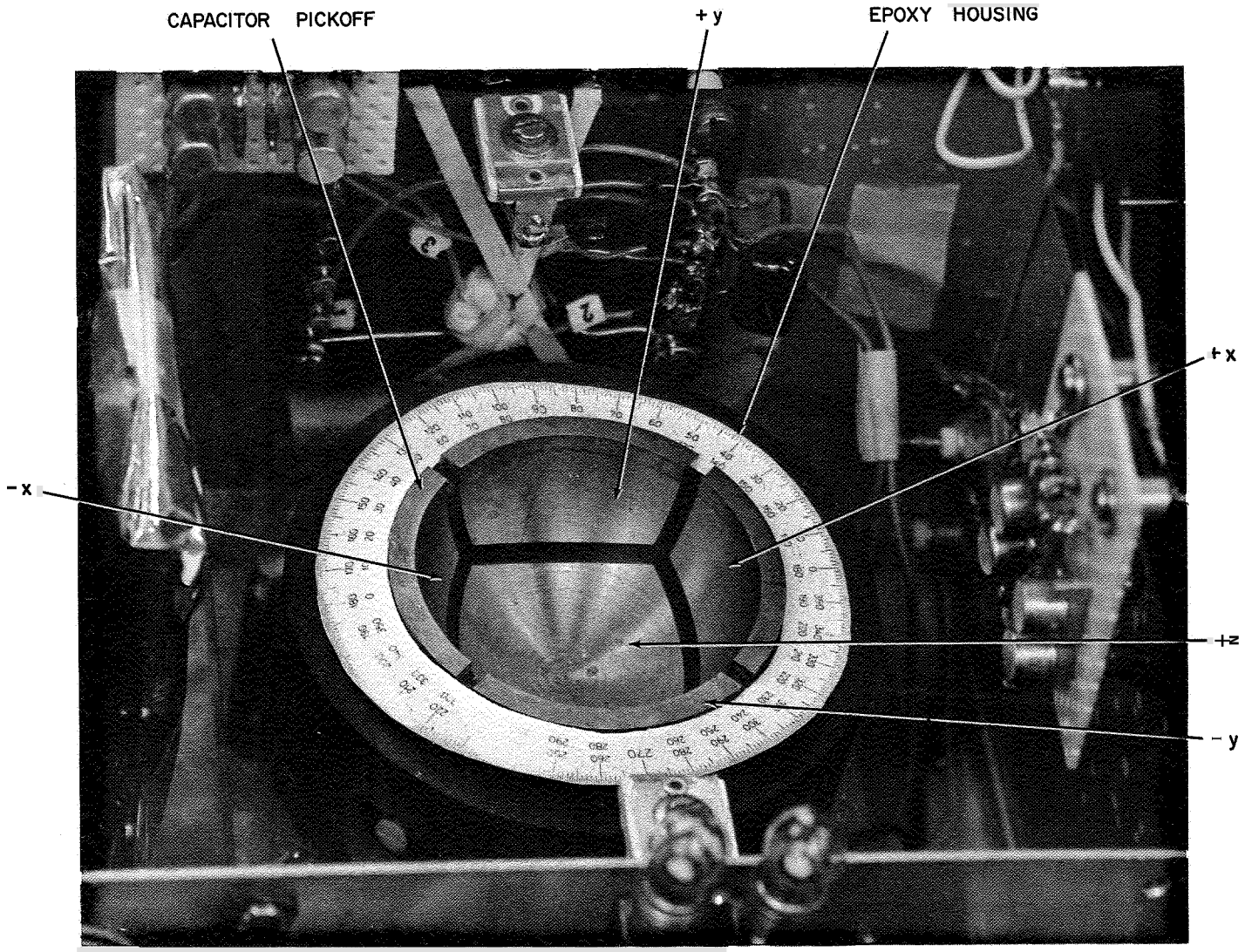

Figure 2.4.2. Capacitor pickoff sensor

A "Nikon" cross-travelling micrometer carriage (accessory to Nikon Model 6C Comparator) provides 1-inch travel in the two horizontal directions. It sits in a cage which is clamped via a rotation head to the granite rail. A 1-3/4 in. diameter steel tube whose upper end is fixed to the moving head of the micrometer carriage goes through its central 3-inch diameter hole. It carries the vertical positioner whose essential parts are a micrometer measuring the vertical position of the actual ball holder, and a microscope sled (taken from an "Edmund Scientific" microscope) which carries the ball. By this construction, the micrometer is completely unloaded and should allow accurate position readings even after long use. The ball itself sticks to a permanent horseshoe magnet which in turn sits at the end of a 1/2 inch phenolic rod. Thus, it is insulated against the large metal mass of the positioner head, and while its suspension is plenty stable for "no touch" conditions, it is still flexible enough to prevent damage of either the vehicle or the positioner in case the vehicle bumps into it.

Capacitive Pickoff Sensor:

The capacitive pickoff sensor consists of four or six sphere sections arranged for two-axis or three-axis operation as well as two- or three-impedance matching transformers and associated circuitry as shown in Figure 2.4.3. The sphere to be position-sensed is nominally located concentrically with'respect to the sphere sections.

The capacitive pickoff used with the existing ACV employs one full plate (nearly 1/6 of total sphere area) located at the bottom and grounded, and four half plates located in the +X, -X, +Y, and -Y positions. The inside diameter of the sections is 55.3 mm, and the ball

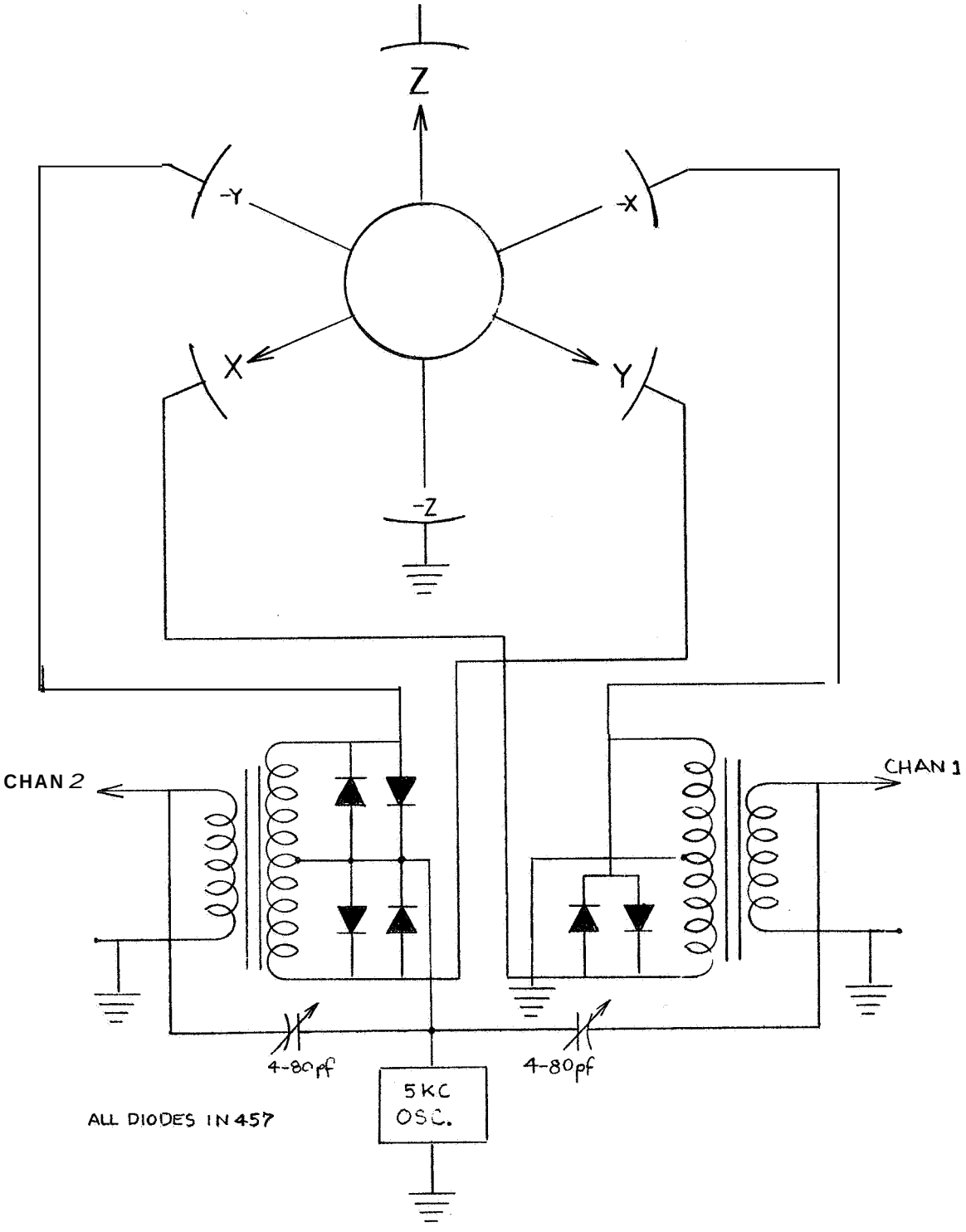

Figure 2.4.3. Capacitive pickoff schematics

used is 50.8 mm diameter. Thus the ,nominal gap is 2.25 mm.

The transformers used with the capacitive pickoff are special units having an exciting impedance of about 1.8 megohms at 5 kc and a step down ratio of about 88 to 1 with an output impedance of about 300 ohms at 5 kc. Capacitive balance is extremely critical, as is the exciting impedance phase angle. The dielectric and loss factors associated with the sphere section insulating support are also very important in determining the pickoff design. The impedance of the legs making up the capacitive bridges are approximately -j 15 megohms at 5 kc.

The capacitive pickoff produces a hard nonlinearity resulting from the nonlinear capacitance vs. displacement function. The extent of this nonlinearity is shown in Figure 2.4.4. It should be noted that the nominal threshold of the control system is set at 30 mils, which is within the reasonably linear range of the pickoff.

2.5 Control System Description

The control system block diagram is shown in Figure 2.5.1. The electrostatic capacitive pickoff sensor provides a two-dimensional position indication in the form of a phase-polarized D.C. signal of the order of ± 0.5 mv R.M.S. Two high-gain amplifiers amplify the signal from millivolt range to volt range. The amplified D.C. signals are converted to differential DC signals by means of a transformerless differential demodulator circuit. The electrostatic pickoff and demodulators both employ an excitation signal derived from a 5 kc oscillator. The differential DC signals drive the differential operational amplifiers and excite 'the rate gyro potentiometers. The differential operational

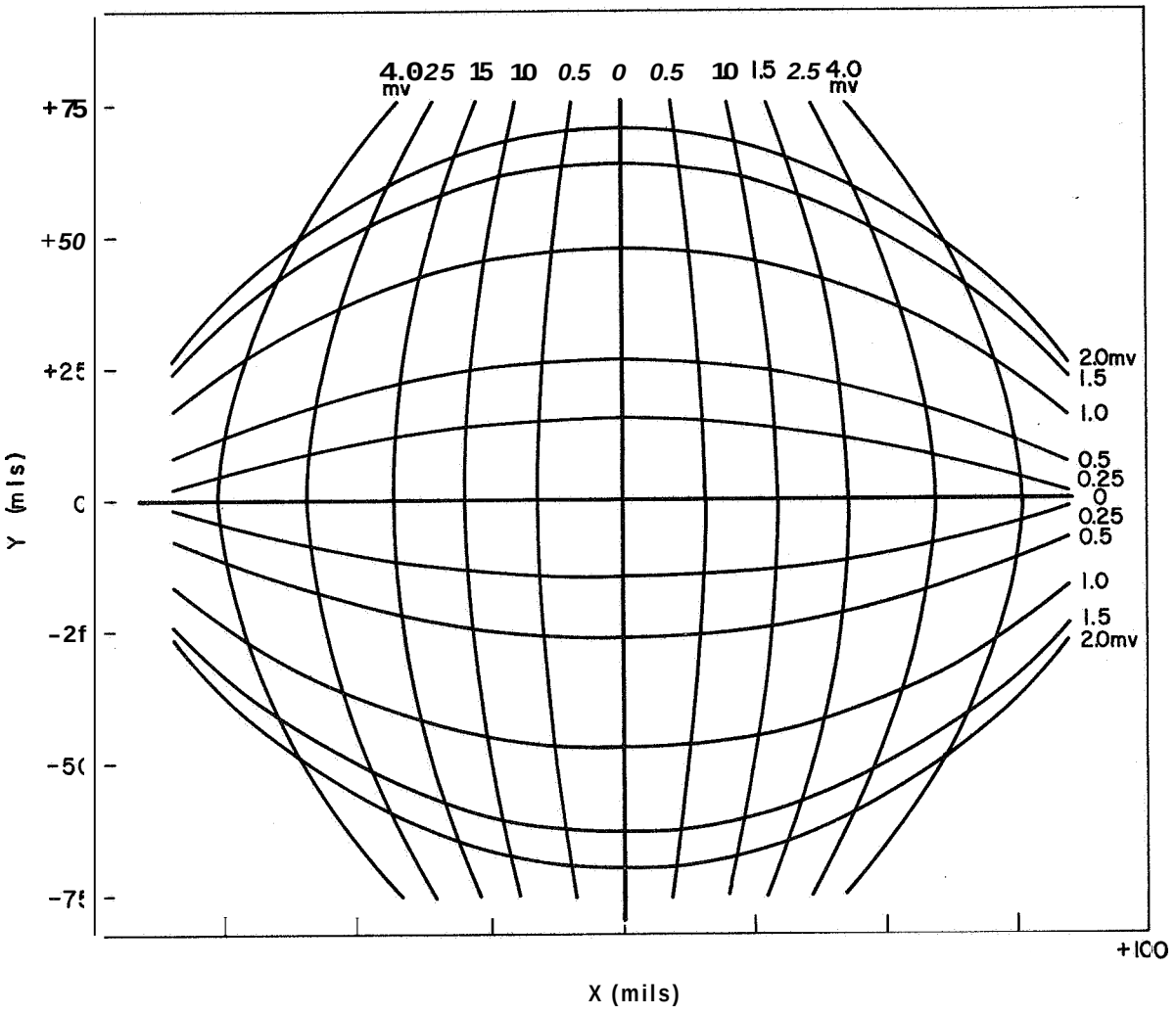

Figure 2.4.4. Output of position sensor (Accuracy ± 10%)

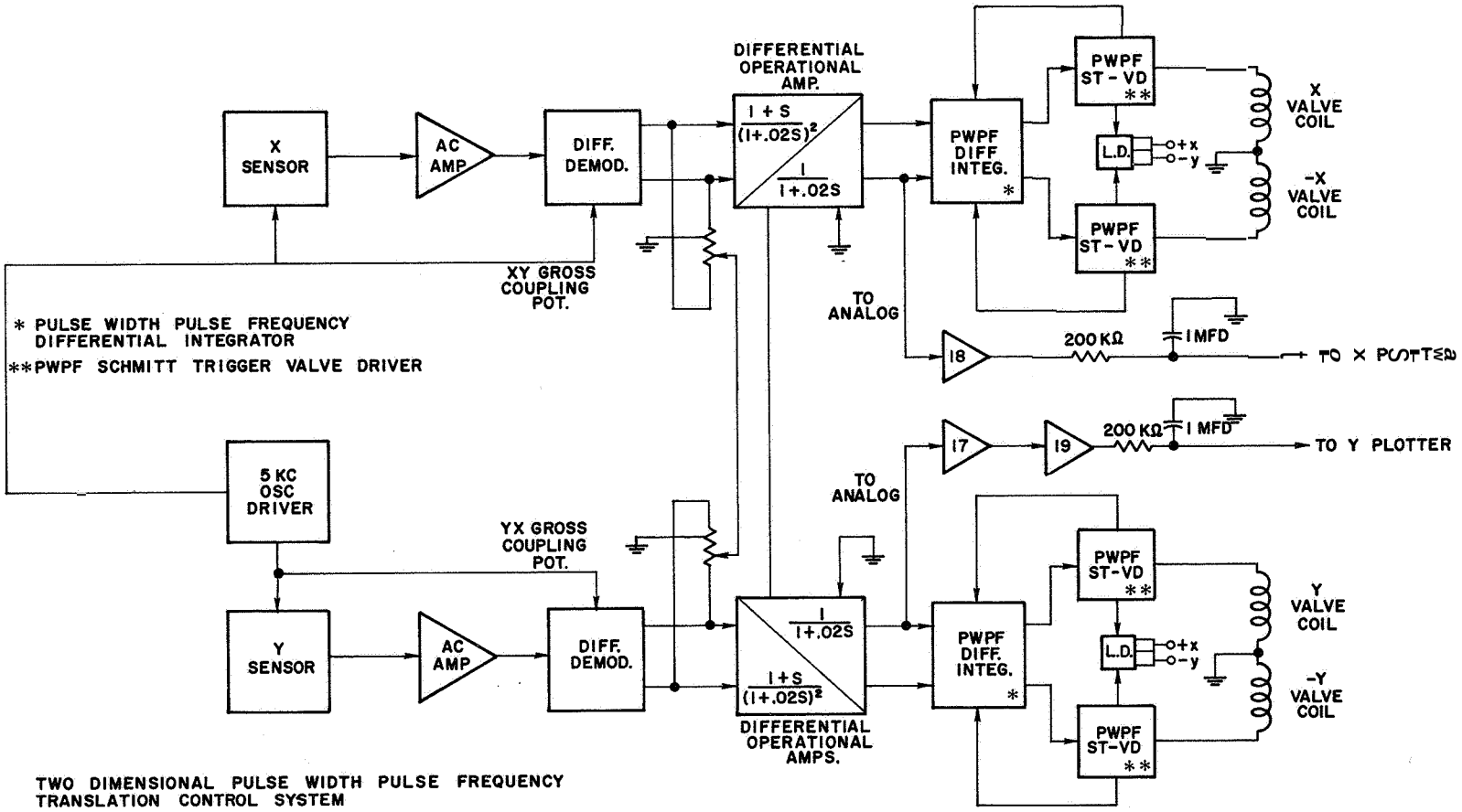

Figure 2.5.1. Flow diagram of the position sensor and control circuit.

amplifiers provide a lead lag lag transfer function for rate sensing and noise filtering. The modified DC signal which now includes rate information as well as position, drive pulse width pulse frequency valve control circuits. The pulse width pulse frequency valve control circuits consist of integrators with Schmitt trigger reset feedback. The system is arranged in a bipolar manner such that positive inputs cause the positive Schmitt trigger to fire and negative inputs cause the negative Schmitt trigger to fire. A dead band is provided to prevent the use of excessive fuel. The error signals seen by the P.W.P.F. circuits are effectively the following:

$$E_X = X + \dot{X} - (\omega_Z Y)$$
$$EY = Y + \dot{Y} + (\omega_Z X) \qquad (2.5.1)$$

where

X = X-axis position error

Y = Y-axis position error

$\dot{X}$ = X-axis rate

$\dot{Y}$ = Y-axis rate

ω_Z = Z-axis angular rate (by using the rate gyro switch, Fig. 2.3.2, it can be included in the error signal).

The P.W.P.F. characteristics are given in Figure 2.5.2. Observe that the dead band is $\pm$ 12 mils and saturation occurs at around 30 mils.

Lamp drivers are provided for visual display of valve operation. Lamps are color coded to permit visual determination of valve axis and polarity, Figure 2.3.4.

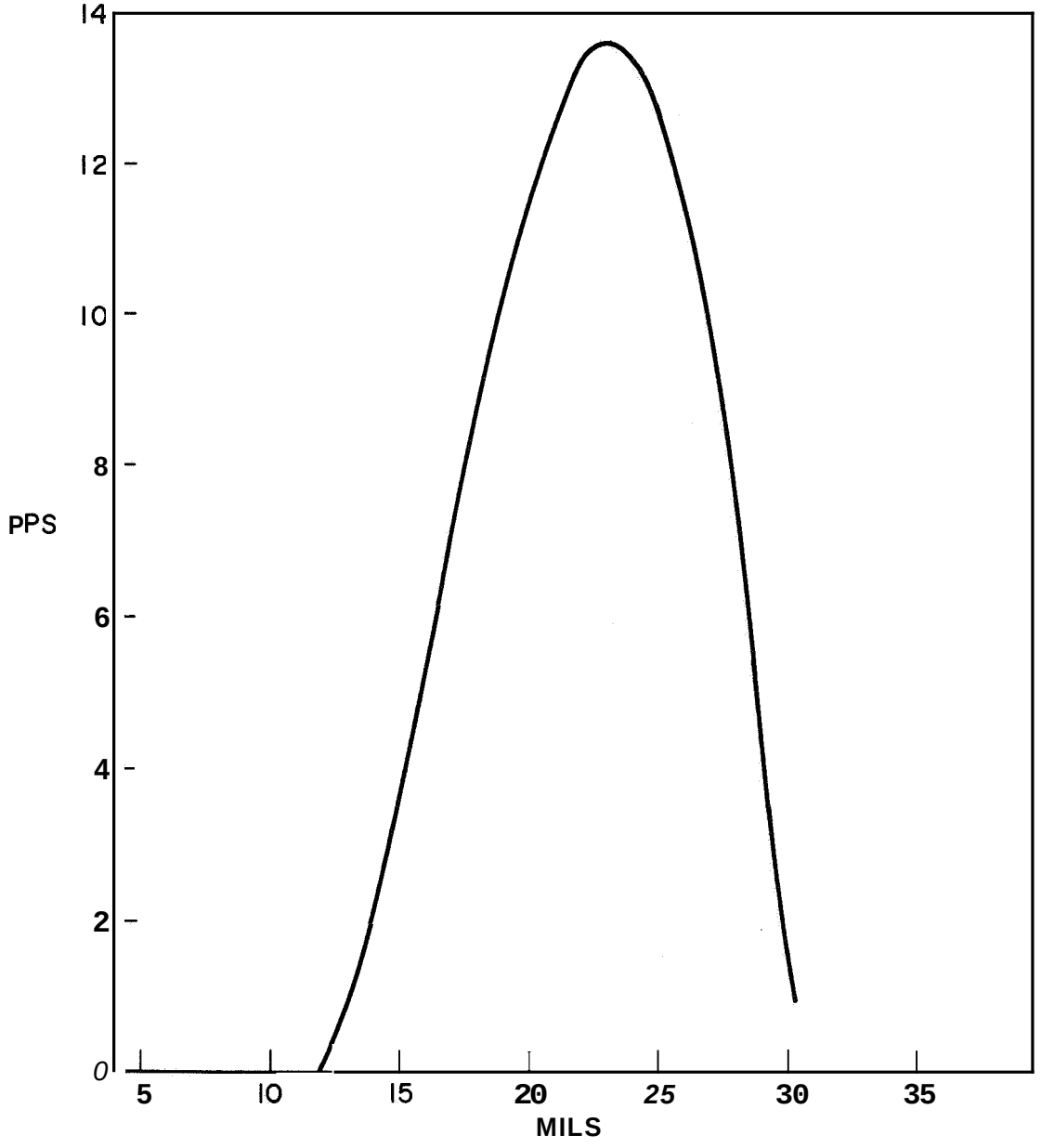

Figure 2.5.2. P.W.P.F. characteristics (Accuracy ± 10%).

The error signals are fed into an analog computer TR-20 and filtered, and the filtered error signals are available for plotting or measuring.

2.6 Balancing Procedure

The experiments were performed during a period of one month; during all this time the table was kept at a zero tilt position by the automatic table levelling system.

After bringing the vehicle into operating conditions it was necessary to balance it and to level the table; these two operations must be done simultaneously, since the vehicle behavior determines both the table tilt and the mass distribution on the vehicle. The table position can be adjusted by changing the table angle biases, Figure 2.6.1, while changing the mass distribution on the vehicle is achieved by putting brass weights, Figure 2.3.1, on the ACV and adjusting the micrometer carriage, under the battery, Figure 2.3.4, and under the capacitor pickoff housing, Figure 2.3.2.

An initial rough levelling was obtained by levelling the bubble level which is located on the granite table.

The values of the table angle bias are then recorded and the vehicle trajectory is observed. If the system is unbalanced, the mass distribution on the ACV is adjusted. A typical trajectory of an unbalanced system is shown in Figure 2.6.2b. By changing the mass distribution it is possible to improve the system balance.. A trajectory of such a system is shown in Figure 2.6.2a. At this stage the vehicle is turned 180° and again its trajectory is obtained. If the trajectory is the same as the

Figure 2.6.1. Table angle bias potentiometers.

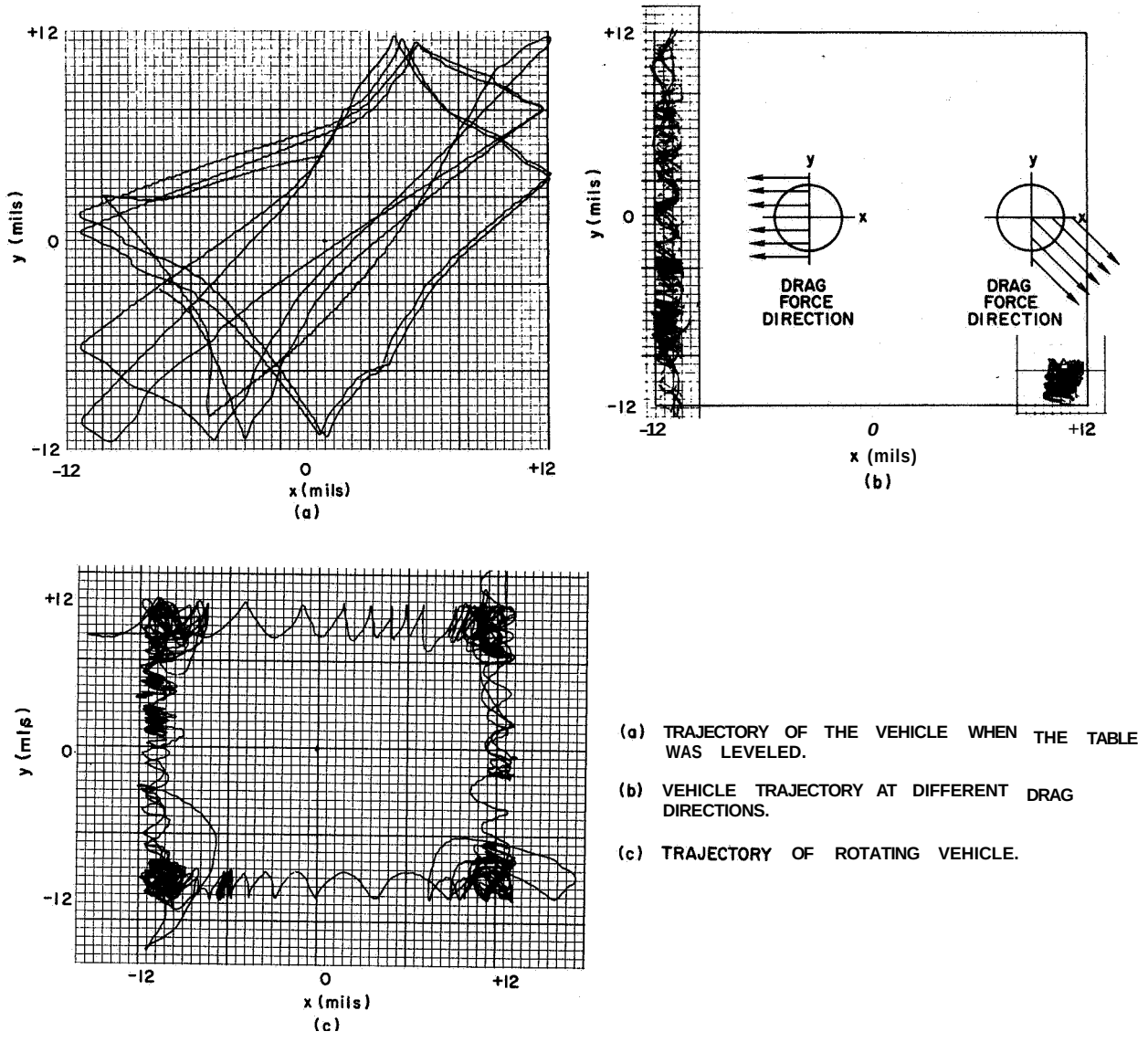

Figure 2.6.2. Vehicle trajectory at different conditions:

(a) Vehicle trajectory of balanced vehicle and leveled table, vehicle travel over all its allowable range ± 12 mils. (control jet pressure 60 p.s.i.).

(b) Left Side: vehicle trajectory when table is tilted 3 arcsec, and the direction of the gravitational force coincides with the X direction.

Right Side: vehicle trajectory when table **tilt** is 3 arcsec, and the direction of the gravitational force is 45° with the control jet axis.

(c) Trajectory of rotating vehicle when table **tilt** is 3" arcsec.

previous one, the system is balanced; if it is similar to that shown in Figure 2.6.2b, the table level is changed until the system is balanced. At this stage the initial values of the table angle bias potentiometer are compared with the present values, and a new set of values are obtained by setting the potentiometers at a mid-value. The vehicle is then turned back to its initial position and the above steps are repeated. This procedure continues until a turn of 180^{o} does not cause a change in the vehicle trajectory.

This procedure was carried only once, since the system was kept almost balanced by the automatic table levelling control and only slight daily adjustments of the table bias potentiometers were needed for bringing the system back to its proper position.

2.7 The Experiments

In order to identify the ACV system equations it was necessary to get as much information as possible from each experiment. Three different sets of experiments were conducted.

In the first set of experiments the effect of the granite table surface on the vehicle was checked. These experiments were performed in order to estimate the magnitude of the error introduced by performing different experiments at different locations on the table. Since all the experiments were done during a period of one month, it was possible to keep the location of the vehicle approximately constant. Therefore, the effect of the table surface was checked only over an area which is slightly bigger than the diameter of the vehicle (precisely 1.5" bigger).

In the remaining experiments both fuel consumption and vehicle trajectory were recorded as a function of the granite table tilt and the control jet pressure.

The amount of gas consumed by the support jet and control jets was measured by an accurate pressure gauge (± 5 p.s.i.). In order to reproduce the same initial conditions the initial pressures of both support and control tanks were 1000 ± 5 p.s.i.

The vehicle jets were aligned with the table corners so whenever the table was tilted only one channel fired, while the second channel trajectory was uneffected (see Fig. 2.8.4).

The temperature in the experimental area remains constant; therefore, the pressure difference ($P_{initial} - P_{final}$) of both control and support tanks was directly proportional to the gas consumption.

The table angle tilt was adjusted by the table angle bias potentiometers (Fig. 2.6.1). Table tilt angles range from 0" ± 0.1" to 4" ± 0.3", which corresponds to height range of 400 to 200 km.

The control jet pressure was adjusted by changing the low pressure side of the pressure regulator. Three different values were used ± 20, 40, and 60 p.s.i.

The support low pressure side was kept at 30 p.s.i., while the support flowmeter was kept at 3 (Stainless Steel ball).

Information on the vehicle trajectory was obtained from signals leaving the lead lag lag filter (Fig. 2.5.1).

2.8 Results

The results are represented in two different ways:

a) Fuel Consumption (lb/hr - nitrogen consumed)

b) Vehicle trajectory.

Pressure difference was the measured parameter, and the fuel rate consumption is calculated by

$$G = \frac{273}{293.5} \frac{28 \times 3}{1.54 \times 10^{-4} \times 22.4} \Delta P N = 5.4 \times 10^{-4} \Delta P N$$

where

$293.5\,^{o}K$ is the room temperature

28 - molecular weight of nitrogen

3 - volume of storage tank (liters)

AP - pressure difference (p.s.i./hr)

N - number of storage tanks

(N = 2 for control system)

(N = 4 for support system)

22.4 - molar volume at standard conditions

1.54×10^{-4} - conversion factor $\frac{inch^2}{gr}$

From the first set of experiments it is clear that the granite table surface does not influence the gas consumption, at least in the vicinity where all experiments were performed.

Position on the Table		Gas Consumption
X(inches)	Y(inches)	lb/hr
-0.5	-0.5	0.118
0	0	0.129
0.5	0.5	0.124

Table 1 - Gas consumption (lb/hr) vs. different locations on the table.

The gas consumption rate does not depend on the control jet pressure over a wide range. At very high altitudes there is an increase in fuel consumption because all four jets fire and some of the fuel is wasted to counteract the acceleration given to the vehicle by the opposite jet. This phenomenon can be observed clearly from the analog computation results, See 3.10.3, and also from Figure 2.8.1.

Since each day the level position was slightly changed the correlation found between different experiments done on the same day is higher compared to that found between experiments that were done on different days. Therefore, the dependence of the fuel consumption on table tilt cannot be deduced accurately from Figure 2.8.1. However, in another set of four experiments, all done on the Same day, the fuel consumption variation with table tilt was determined. These results are shownin Figure 2.8.2.

The vehicle trajectory in the usual sense is a spatial description of the vehicle position as shown in Figure 2.6.2, but in order to extract more information from the analysis of the results it is more convenient to have the vehicle "trajectory" in each channel as a function of time.

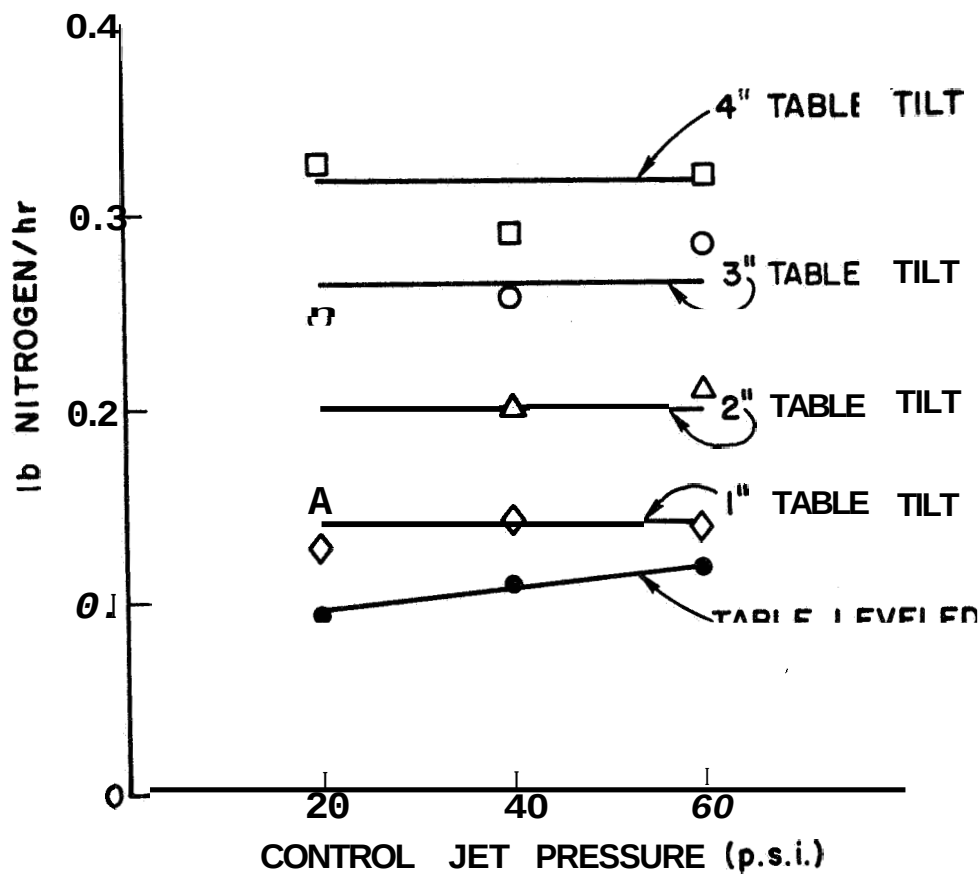

Figure 2.8.1. Gas consumption as a function of control jet pressure (Each contour was obtained on a different day).

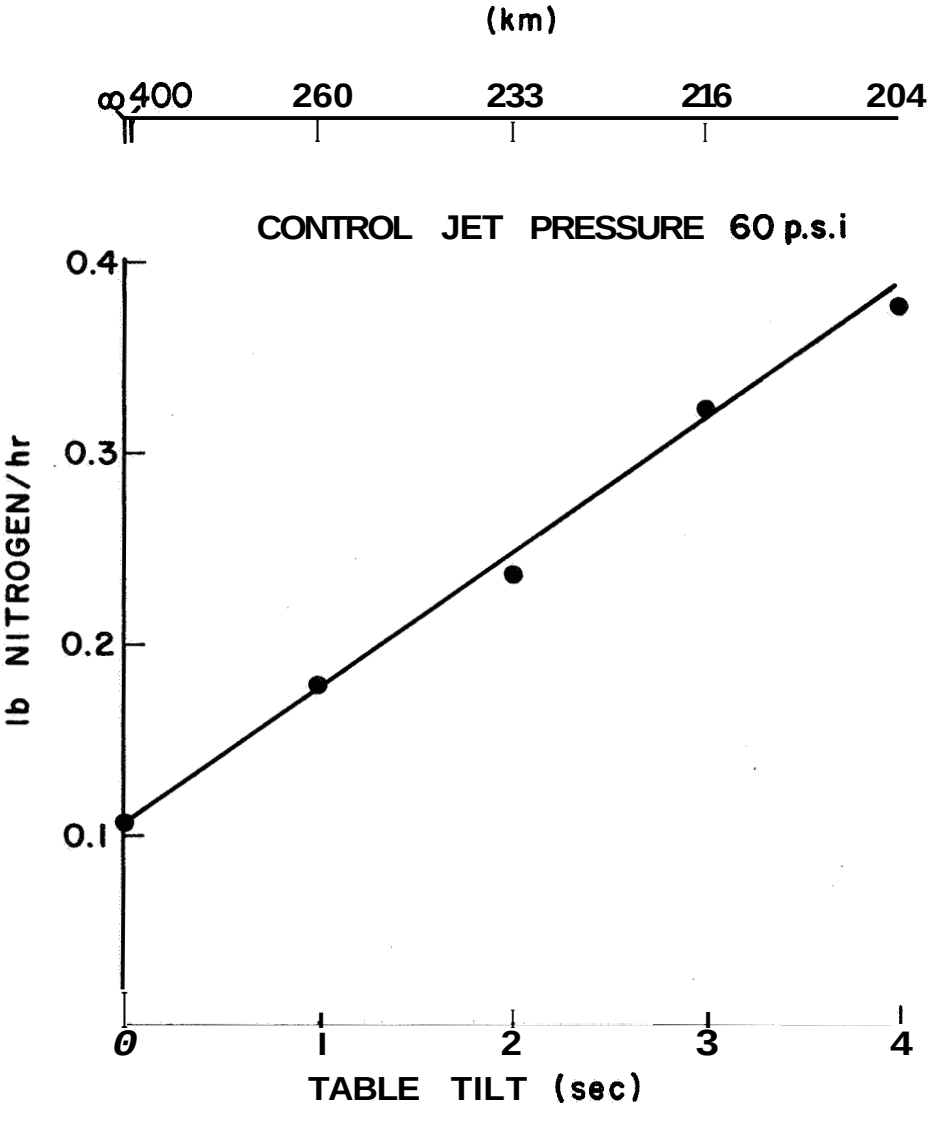

Figure 2.8.2. Gas consumption as a function of table tilt

In all the following figures the trajectory of the vehicle in both directions is given as a function of time and various other parameters. Each figure consists of several pairs of curves. The upper curve is always the trajectory of the vehicle in x-direction (channel 1), while the lower curve is the trajectory of the vehicle in y-direction (channel 2).

The maximum travelling distance in any direction is around ±12 mils, which is the point where the control jets opened.

In Figure 2.8.3 the vehicle trajectory is given as a function of time when the control jet pressure is varied from 20 to 60 p.s.i. The table is leveled; therefore the vehicle is travelling over all its range |12| mils in each direction. As the control jet pressure increased, the velocity of the vehicle increased; therefore, the frequency of firing is also increased. Moreover, in the low range pressures any external disturbance due to nonideal behavior of the jets or minor rotation of the vehicle can be observed, and in these cases the shape of the curve is not regular.

The effect of different table tilts on the shape of the trajectory, for control jet pressure of 60 p.s.i., is shown in Figure 2.8.4. When the table is leveled, both trajectories are alike since the vehicle is travelling over all its allowable range. Note that the gravitational force is aligned with the vehicle axis. Therefore the force is felt only in one channel. (See also Fig. 2.6.2b.) Since it was not possible to avoid minor angular velocity, the pulses are not always uniform. However, the effects of increasing table tilt are clearly observed. The

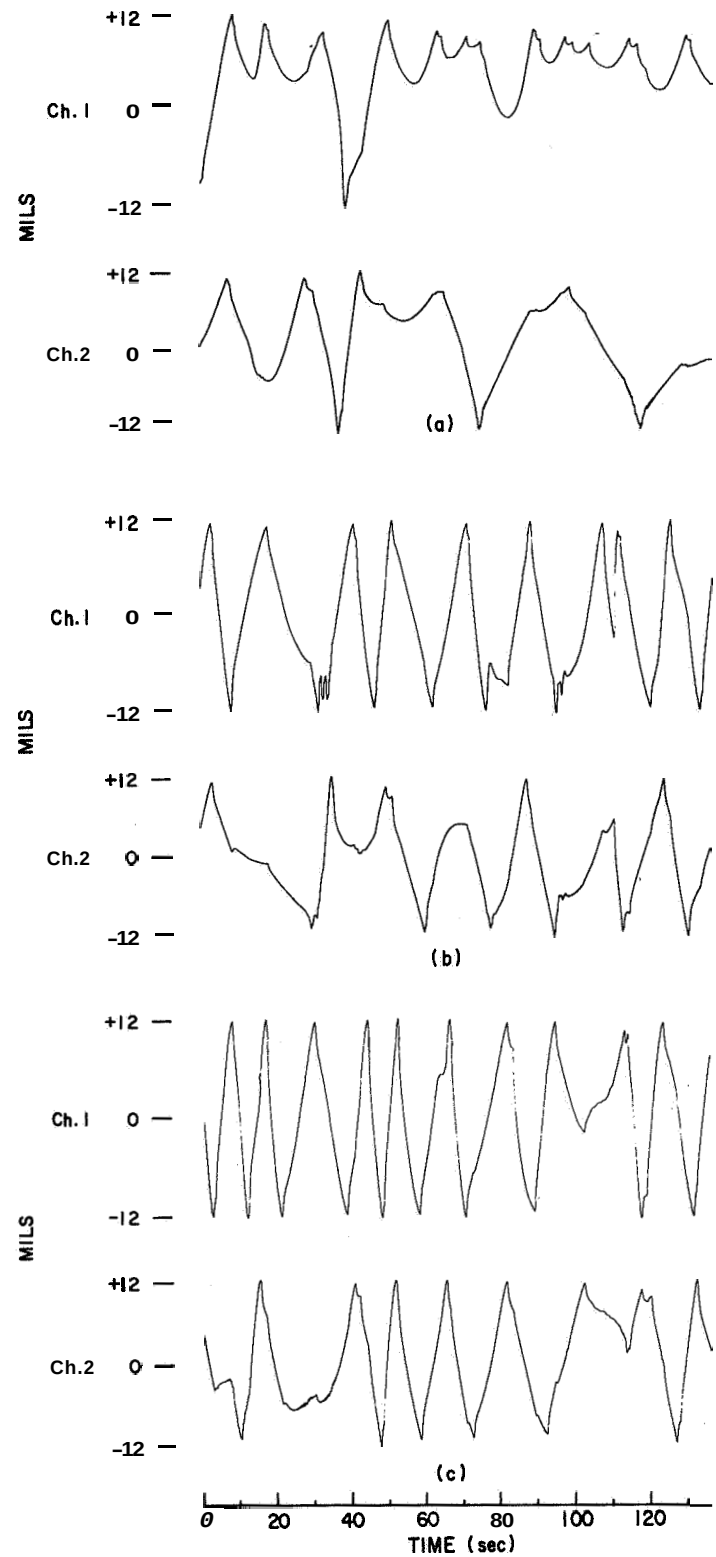

Figure 2.8.3. Vehicle trajectories of leveled and balanced system as a function of control jet pressure:
(a) Control jet pressure 20 p.s.i.
(b) Control jet pressure 40 p.s.i.
(c) Control jet pressure 60 p.s.i.

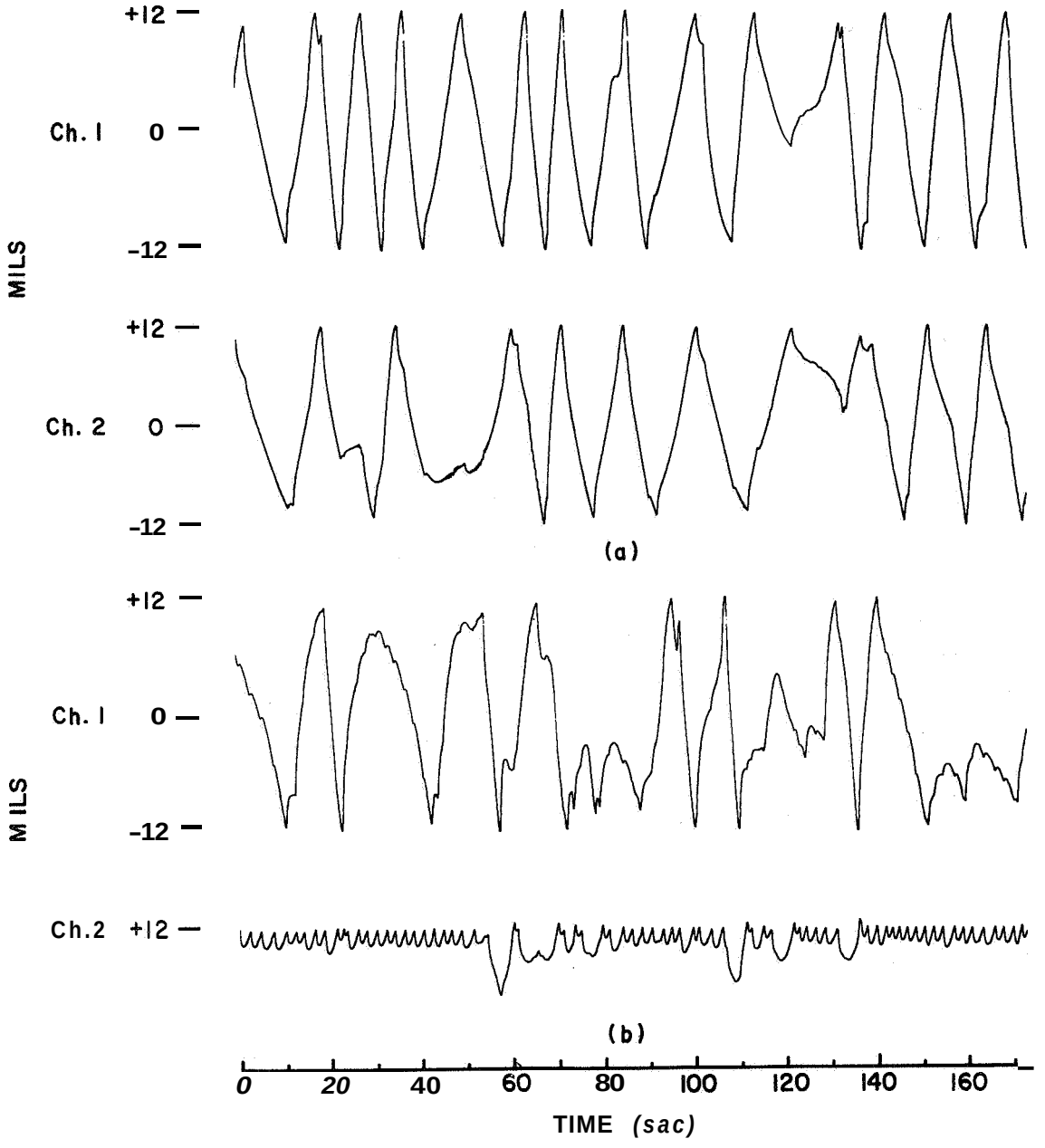

Figure 2.8.4. Vehicle trajectory as a function of different table tilts; note that the gravitational force is aligned with the axis of the control jet in channel 2.

(a) Table leveled
(b) Table tilt 1 arcsec

(continued)

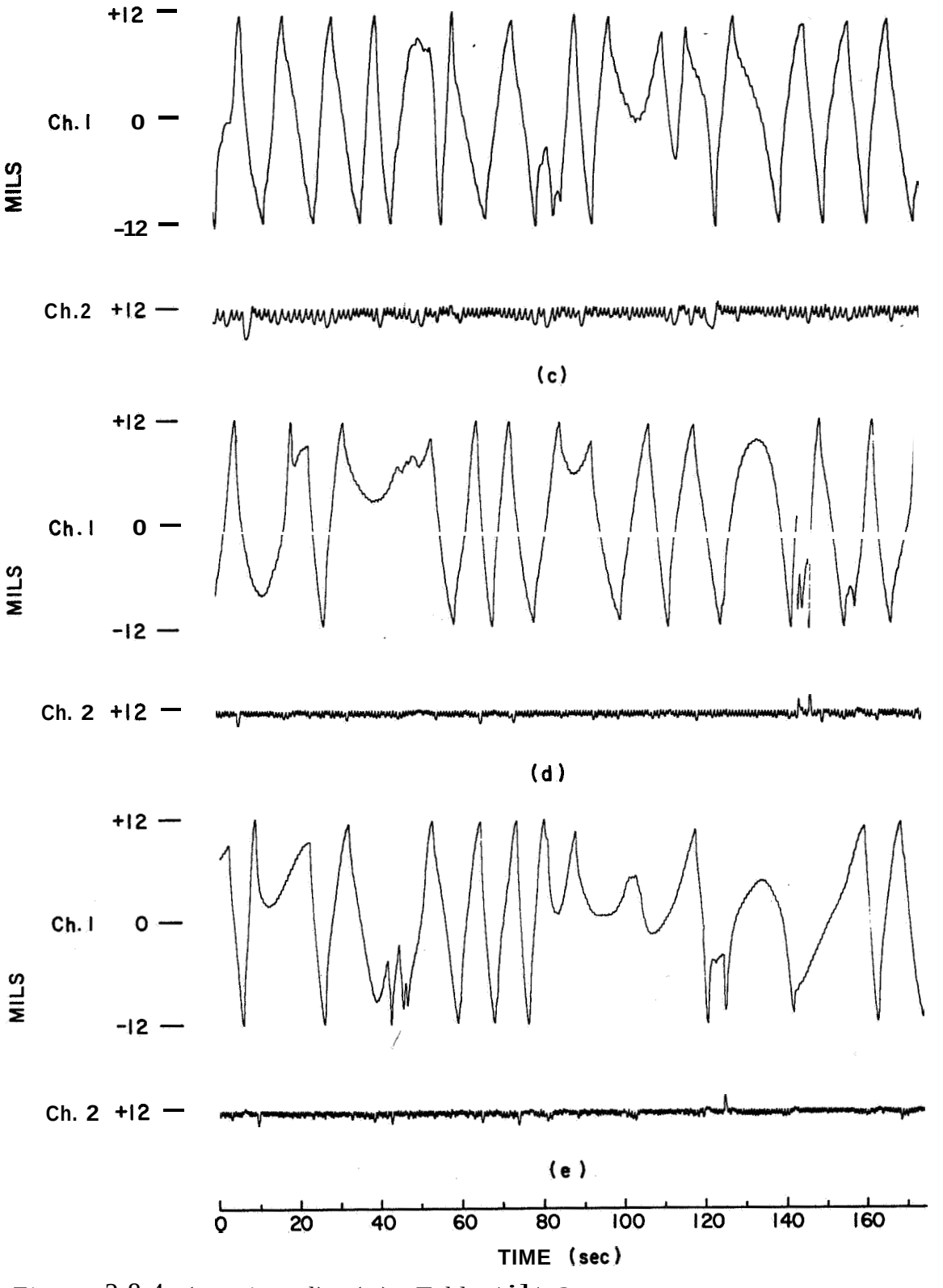

Figure 2.8.4 (continued) (c) Table tilt 2 arcsec
(d) Table tilt 3 arcsec
(e) Table tilt 4 arcsec

frequency of firing is increased, while the height of the parabolas is decreased.

The same curves but with different time scale are shown in Figure 2.8.5. This figure was included in order to show the electronic cross coupling effect. It was felt that this effect does not influence the fuel consumption; therefore, this effect was not included in the simulation (see sec. 3.5).

The effect of different control jet pressures on vehicle trajectory, when table tilt is 4 arc sec, is shown in Figure 2.8.6. When control jet pressure is 20 p.s.i., the frequency of firing is very high and it is almost impossible to distinguish between the individual pulses. The pulse height is increased with the pressure, while the pulse frequency is decreased.

The trajectory of the rotating vehicle when table tilt was 3 arc sec and control jet pressure was 60 p.s.i. is shown in Figure 2.8.7. This is the only data of rotating vehicle available in the present report.

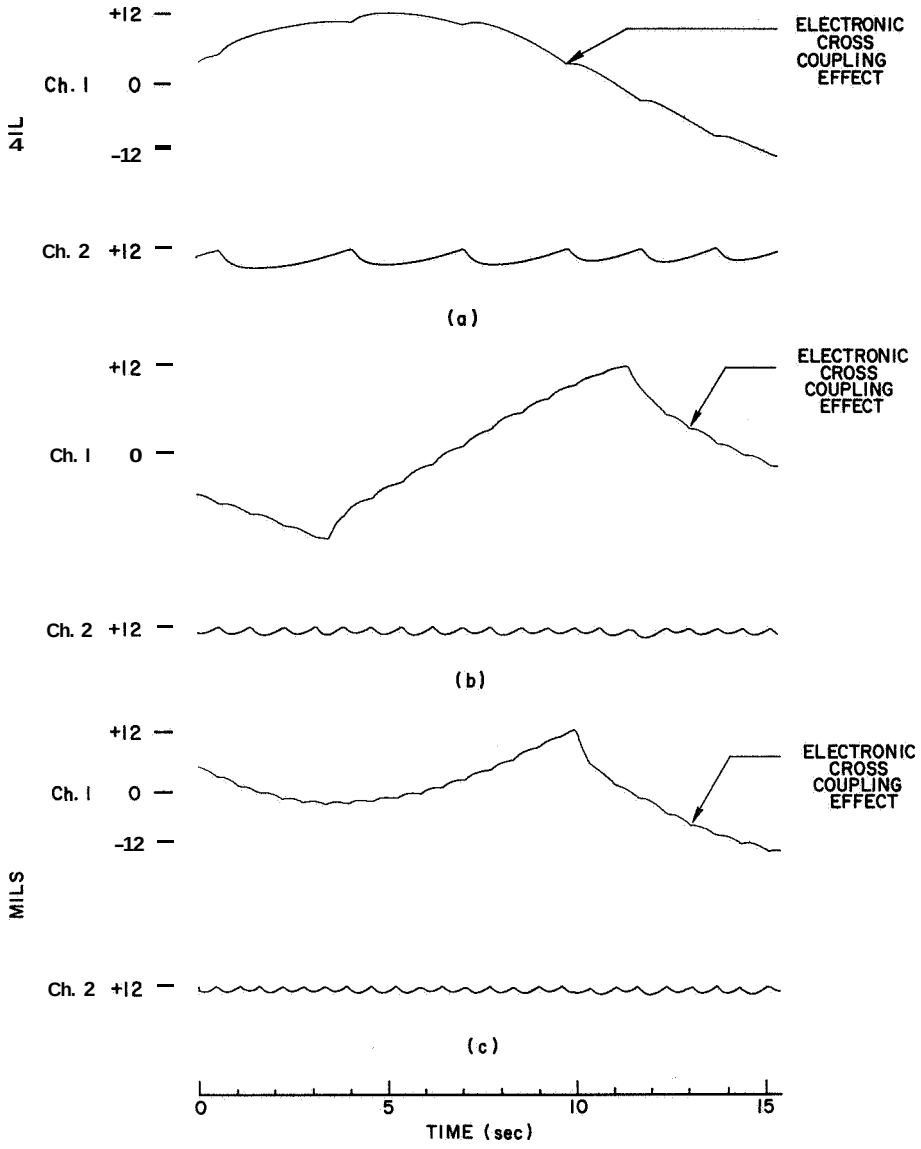

Figure 2.8.5. Vehicle trajectory as a function of different table tilt:

(a) Table tilt 1 arc see

(b) Table tilt 2 arc sec

(c) Table tilt 4 arc sec

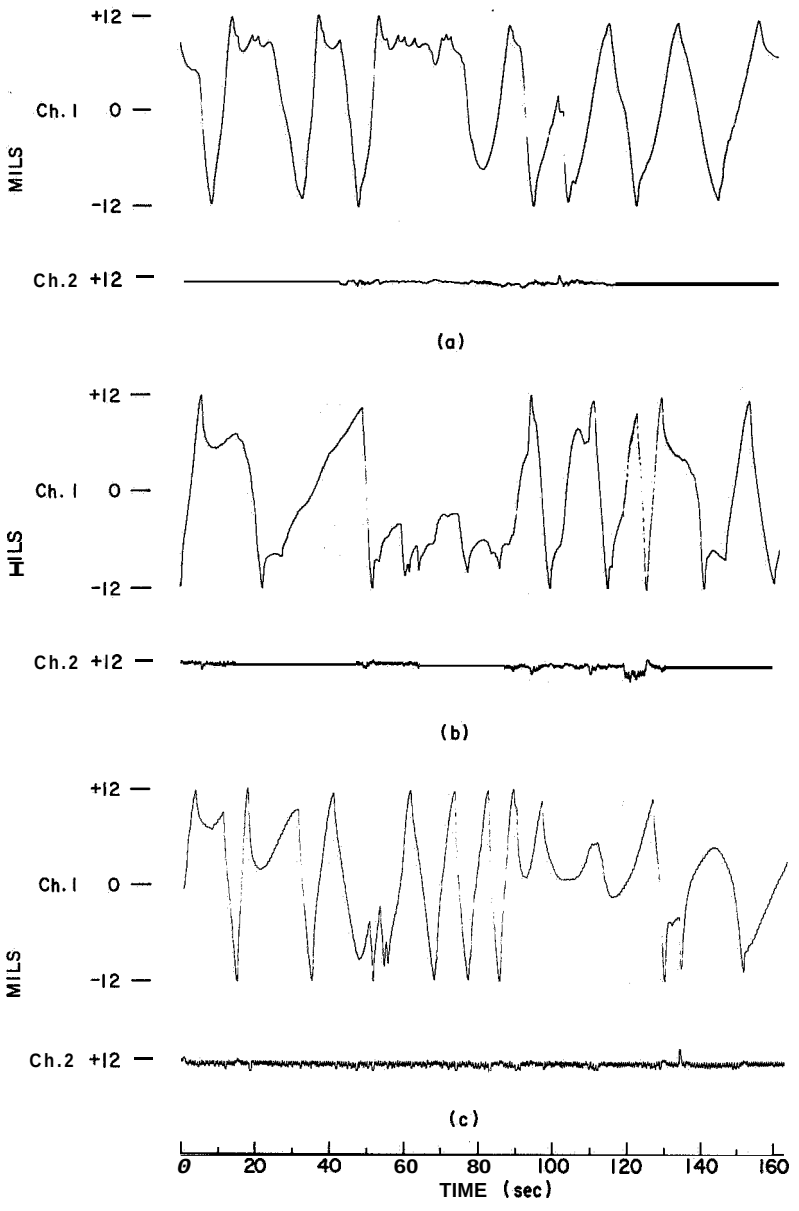

Figure 2.8.6. Vehicle trajectory, when table tilt is 4 arc sec, as a function of different control jet pressures:

(a) Control jet pressure 20 p.s.i.

(b) Control jet pressure 40 p.s.i.

(c) Control jet pressure 60 p.s.i.

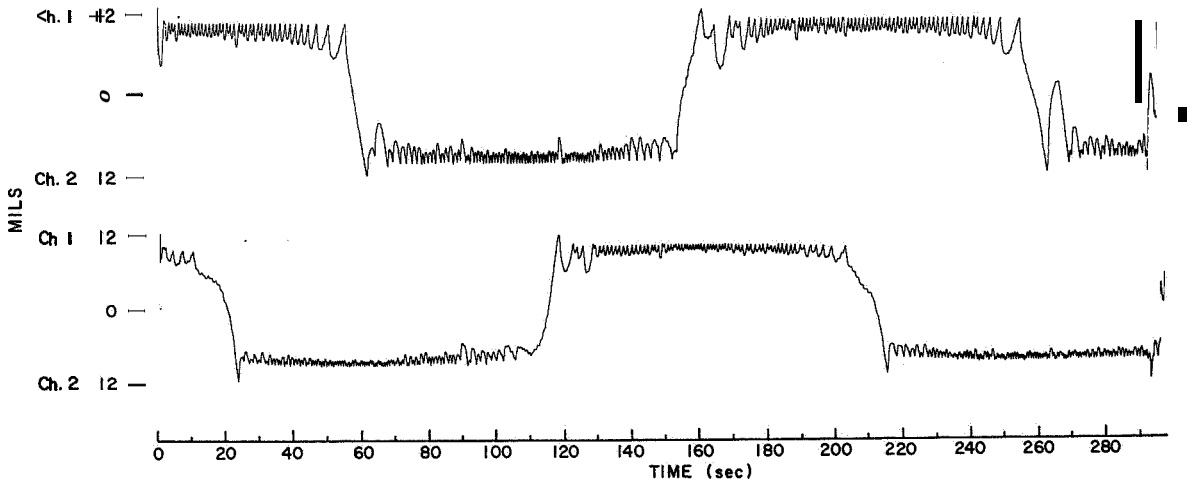

Figure 2.8.7. Trajectory of rotating vehicle
(Body-fixed coordinates)

CHAPTER III

ANALOG SIMULATION

3.1 Introduction

Two PACE TR-48 analog computers were used to simulate the ACV. The TR-48 computer is a fully transistorized analog; a detail description of the unit can be found in [Reference 4]. The program on the analog was divided into two main parts:

a) ACV Simulation, and

b) Measuring devices and relays for slaving the analog to the digital computer for the optimization purposes (described later).

ACV Simulation:

The program consists of nine parts:

1) Dynamics of the ACV. As described later two different programs were used,

2) Coordinate Transofrmation,

3) Position sensor,

4) Velocity and position filter,

5) Schmitt trigger (as part of the control mechanism),

6) P.W.P.F. with Dead-Zone,

7) Fuel consumption measurements

8) Maximum range measurements

9) Noise generator and filter for analyzing the noise.

Two different simulations were used. In the first case the equations of motion were given in body-fixed coordinates, while in the second case

the equations of motion were given in inertial coordinates. Both programs are shown in Figures 3.10.1 and 3.10.2.

3.2 ACV Dynamics

Derivation of the equations of motion for the three-dimensional "zero-g satellite" have been given by Lange [Reference 1]. The equations of motion of the two-dimensional ACV are obtained similarly

$$\begin{aligned} \ddot{x} - \omega^2 x - 2\omega\dot{y} &= F_g \cos \omega t + F_{cx} \\ \ddot{y} - \omega^2 y + 2\omega\dot{x} &= - F_g \sin \omega t + F_{cy} \end{aligned} \tag{3.2.1}$$

where

ω - is the angular velocity of the ACV rad/sec.

F_g - is the magnitude of the gravitational acceleration (which can be adjusted by changing the table **tilt** on which the ACV is floating).

F_{cx}, F_{cy} - are the control acceleration along the x and y coordinates.

x, y - are the coordinates of the ACV; the most convenient coordinate system is a body-fixed frame.

In order to observe the motion in inertial frame, a coordinate transformation was programmed on the analog (Sec 3.3).

The analog computer program, together with sin and cos generators, is given in Figure (3.2.1). For reasons of clarity some of the outputs were not included in this figure. The parameter β appearing in the diagram is a scale factor, and the numbers refer to attenuators and

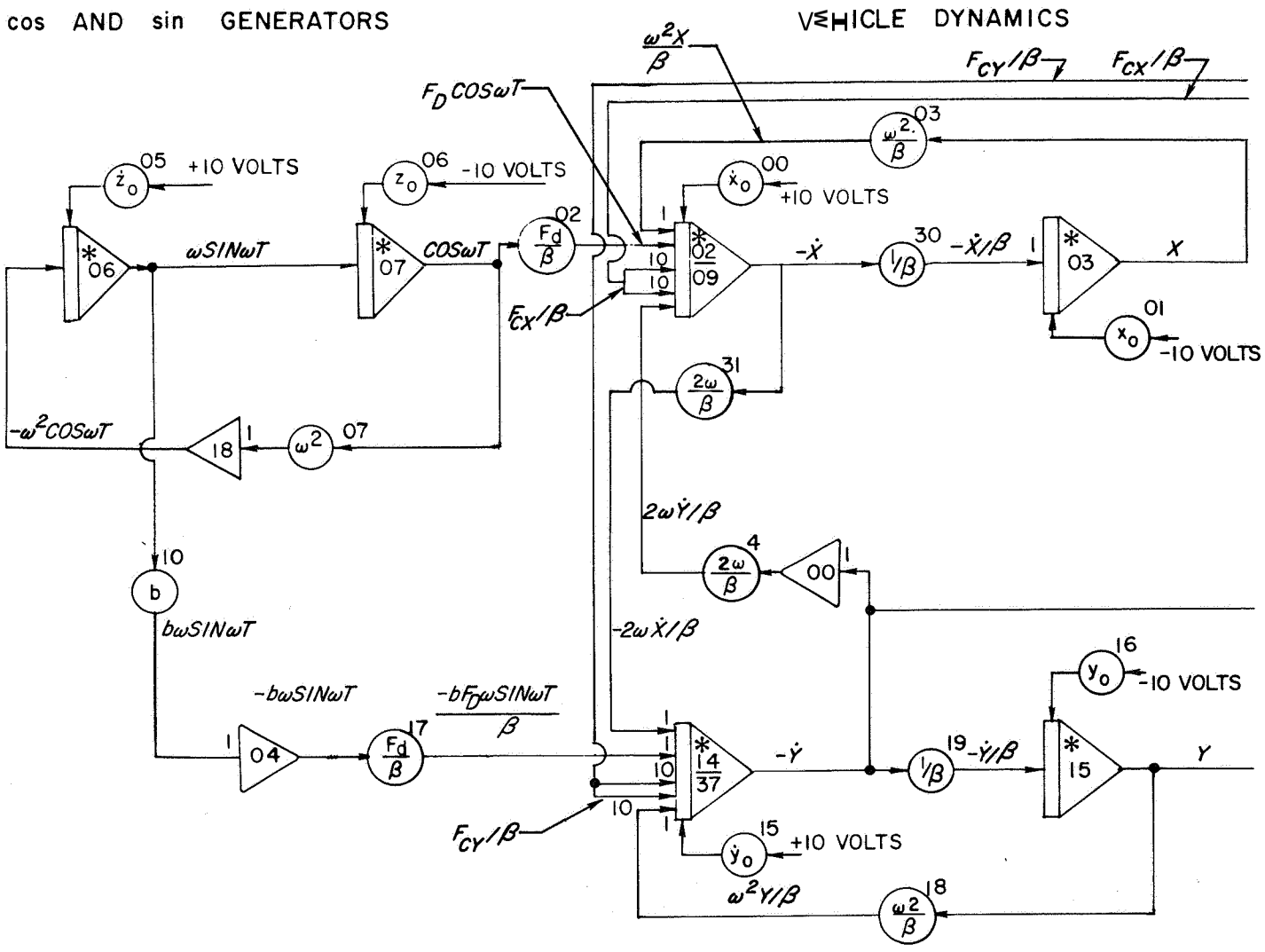

Figure 3.2.1. Dynamics simulation - body-fixed coordinates.

amplifiers of the TR-48 No. 2 analog computer. The voltage as read on the amplifiers is related to the position of the ACV by the following equations:

$$X_{ACV} = \text{'analog} \cdot 10[\text{mils/volt}]$$
$$Y_{ACV} = \text{'analog} \cdot 10[\text{mils/volt}] \qquad (3.2.2)$$

By defining

$$\xi = x + iy$$

it is possible to reduce Equation (3.2.1) to

$$\ddot{\xi} + 2i\omega\dot{\xi} - \omega^2\xi = F_C + F_D \qquad (3.2.4)$$

where

$$i = \sqrt{-1}$$

$$F_C = F_{Cx} + i\,F_{Cy} \qquad (3.2.5)$$

$$F_D = F_{Dx} + i\,F_{Dy} \ .$$

Equation (3.2.4) can be written as

$$(D^2 + 2i\omega D - \omega^2)\xi = F_C + F_D \ . \qquad (3.2.6)$$

The roots of Equation (3.2.6) are given by

$$D_{1,2} = -i\omega \pm \sqrt{\omega^2 - \omega^2} \qquad (3.2.7)$$

It was found that when $\omega \neq 0$ it was rather difficult to simulate the double root, for this reason, a simulation in which the vehicle

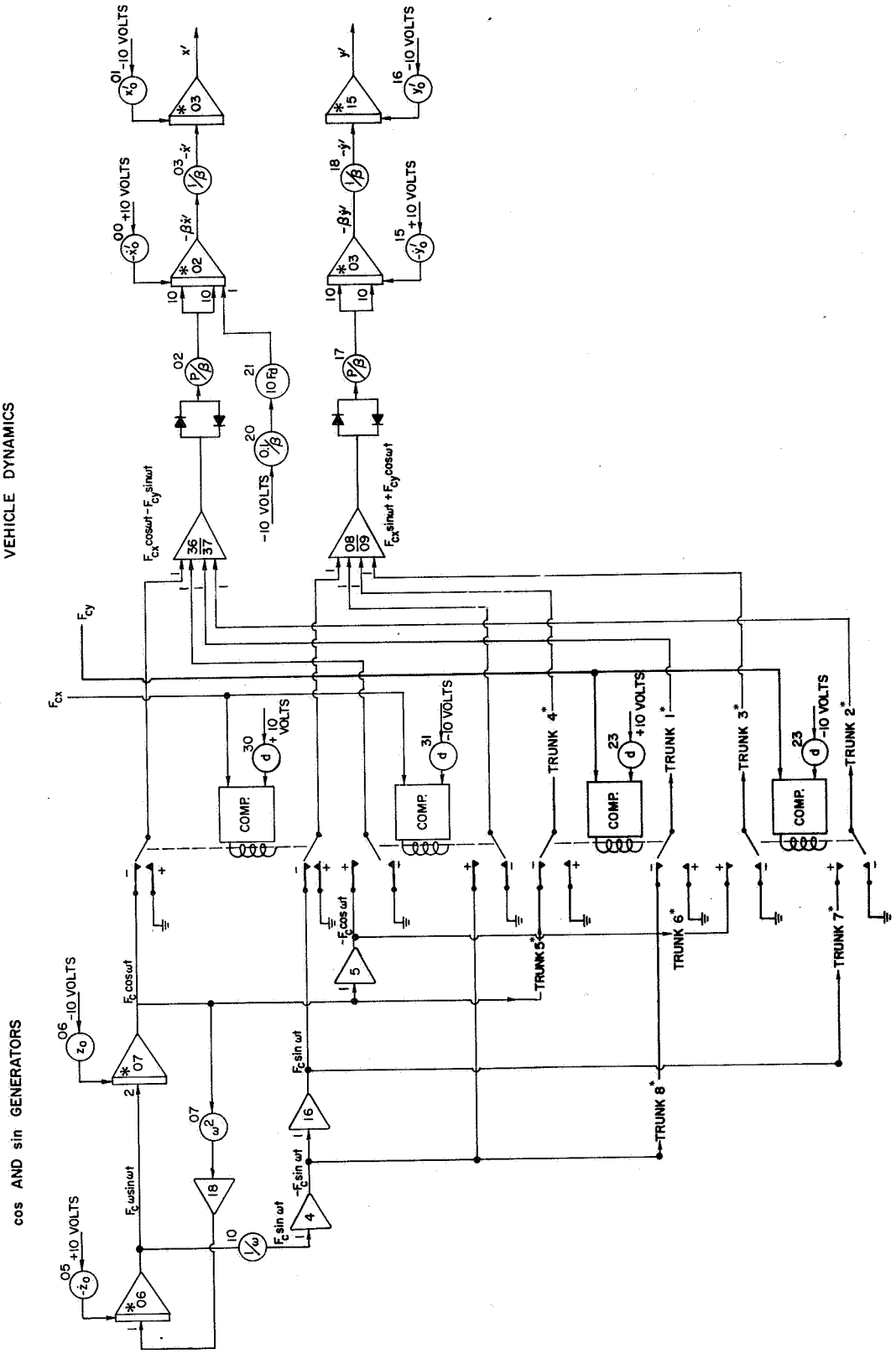

Figure 3.2.2. Dynamics simulation (inertial frame of reference)

dynamics is given in inertial coordinates was constructed. In this form the equations of motion are given by

$$\ddot{x}' = F_D + F_{C_{x'}}$$
$$\ddot{y}' = F_{C_{y'}} \tag{3.2.8}$$

where

$$F_{Cx'} = F_{Cx} \cos \omega t - F_{Cy} \sin \omega t$$
$$F_{Cy'} = F_{Cx} \sin \omega t + F_{Cy} \cos \omega t \tag{3.2.9}$$

The simulation of this equation of motion is shown by Figure 3.2.2, together with sine and cosine generators, and control acceleration transformation (Eq. 3.2.9).

3.3 Coordinate Transformation

The position and velocity of the ACV in inertial reference frame (x', y') are related to the position and velocity coordinates (x,y) in the body-fixed frame by:

a) Position in inertial frame

$$x' = x \cos \omega t - y \sin \omega t$$
$$y' = y \cos \omega t + x \sin \omega t \tag{3.3.1}$$

b) Velocity in inertial frame

$$\dot{x}' = (\dot{x} - \omega y) \cos \omega t - (\dot{y} + \omega x) \sin \omega t$$
$$\dot{y}' = (\dot{y} + \omega x) \cos \omega t + (\dot{x} - \omega y) \sin \omega t \tag{3.3.2}$$

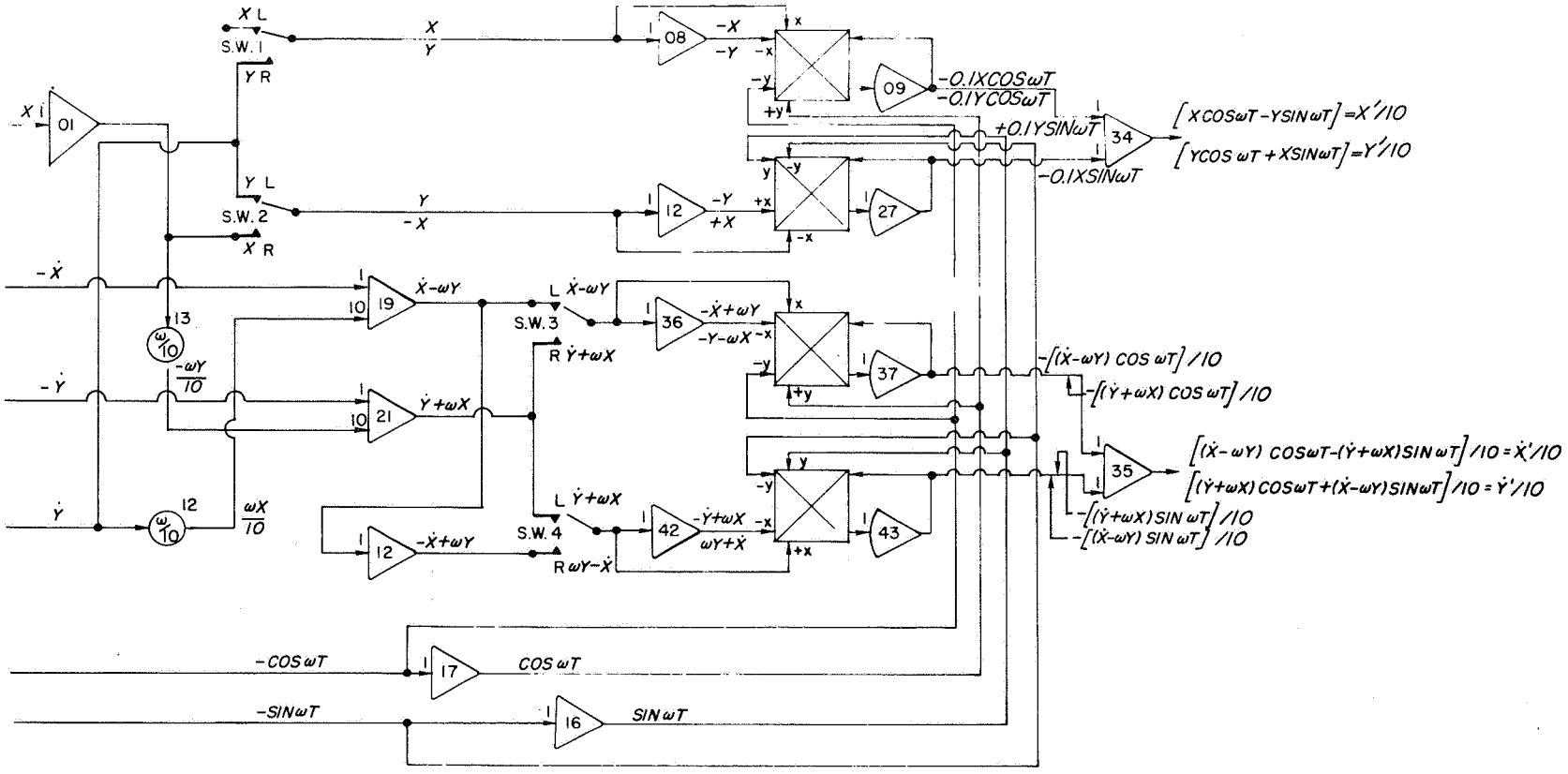

Figure 3.3.1. Coordinate transformation simulation (body-fixed to inertial coordinates)

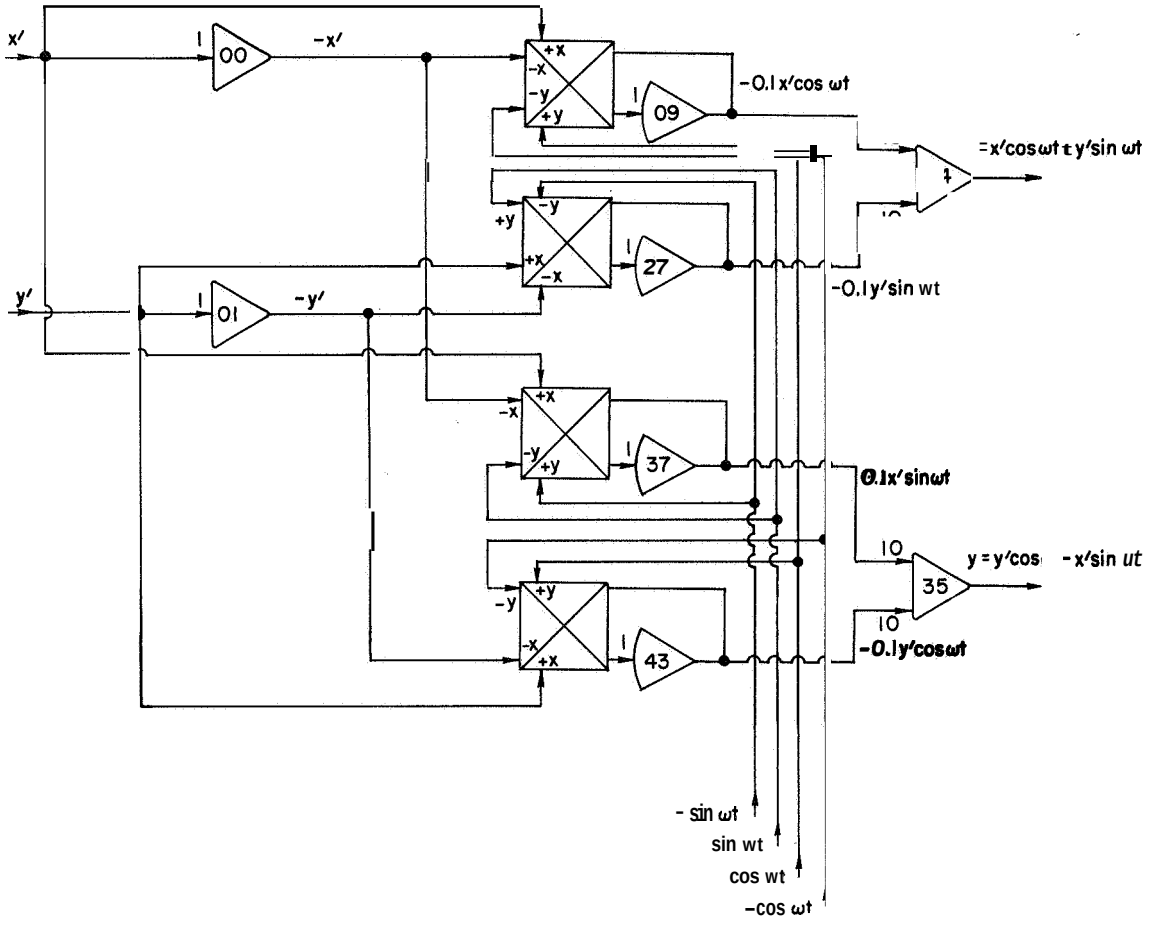

Figure 3.3.2. Coordinate transformation simulation (Inertial coordinates to body-fixed coordinates). This transformation is the inverse of the transformation shown in Figure 3.3.1

where $\dot{x}$, $\dot{y}$ - are the velocities components in body-fixed coordinates

$\dot{x}'$, $\dot{y}'$ - are the velocities components in inertial frame.

The analog program which simulates this transformation is given in Figure 3.3.1. Some parts of the program which are not relevant to the transformation are not shown here. This program allows the observation of x' and $\dot{x}'$ or y' and $\dot{y}'$.

The control and sensing devices are on the vehicle and are rotating with it. Therefore, the complete simulation can be done in body-fixed coordinates without using the above coordinate transformation; the only reason for including this part was for checking purposes. Since intuition can be used if the trajectory is given in inertial coordinates. But if the equations of motion are given in inertial coordinates (Eq. 3.2.8) a transformation of coordinates is necessary because the control mechanism is actuated by error signals proportional to the position and velocity in the body-fixed coordinates. The coordinate transformation, which is the inverse to the one shown in Figure 3.3.1, is given in Figure 3.3.2.

3.4 Position Sensor

The position sensor simulation is shown in Figure 3.4.1. The outputs of the position sensor in both directions $F_1(x,y)$ and F2(x,y) depend on both x and y as can be seen from Figure 2.4.5. The simulation consists of two parts: 1) generation of contours, and 2) generating $F_1(x,y)$ and $F_2(x,y)$.

1) Generation of contours.

$$\left.\begin{aligned} F_1(x,y) &= \text{Const} \\ F_2(x,y) &= \text{Const} \end{aligned}\right\} \quad (3.4.1)$$

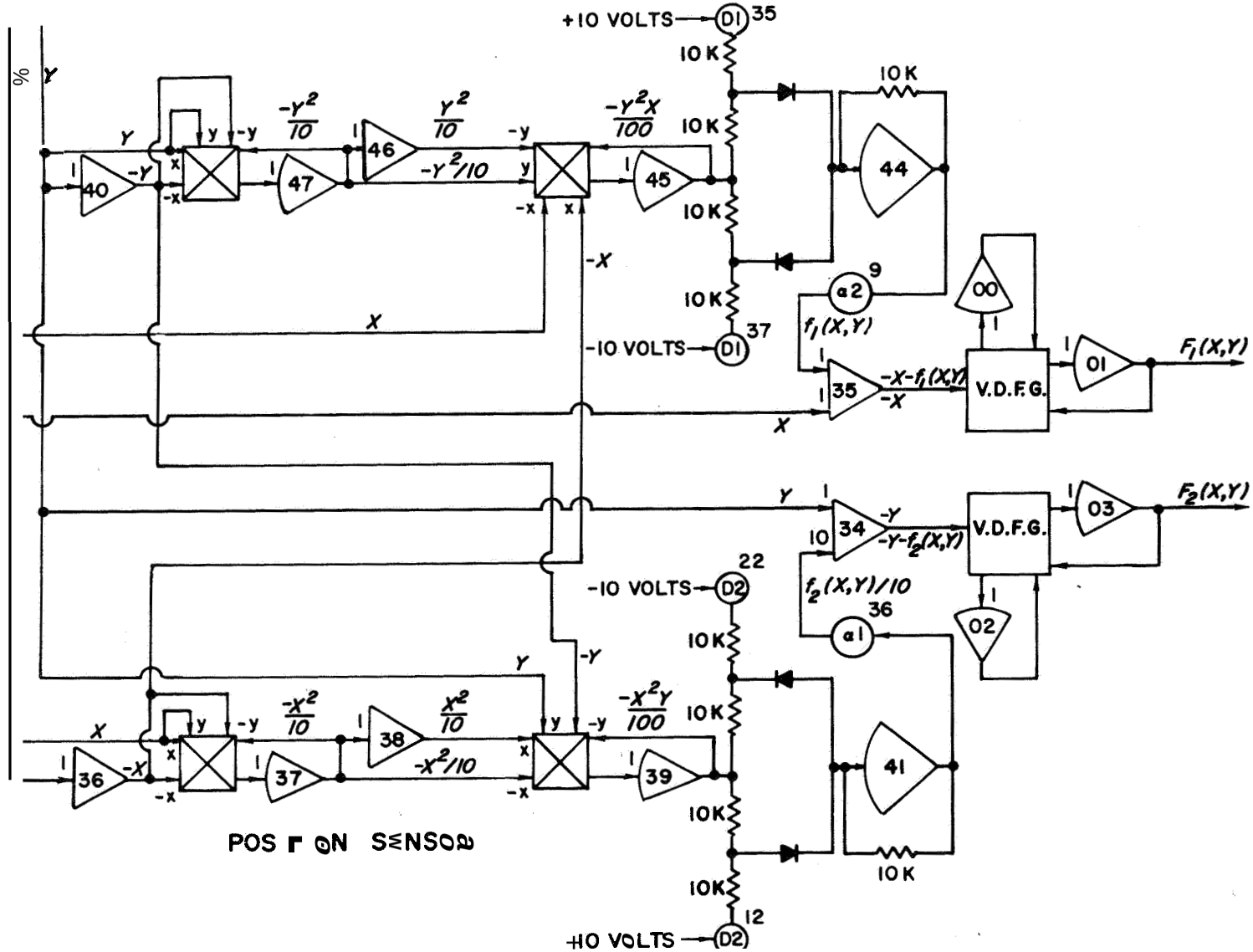

Figure 3.4.1. Position sensor simulation

It is assumed that near the origin F_1 depends only on x and F_2 depends only on y. Therefore, at this region the contours are given by the lines

$$\begin{aligned} x &= \text{Const} \\ y &= \text{Const} \end{aligned} \qquad (3.4.2)$$

As x and y increase, the dependence of both F_1 and F_2 on y and x respectively is increased. It is assumed that in that region the equation of the contours is given by

$$\begin{aligned} x(1 + A \times y^2) &\equiv x + f_1(x,y) \\ y(1 + B \times x2) &\equiv y + f_2(x,y) \end{aligned} \qquad (3.4.3)$$

The coefficients A and B and the breaking points are determined by attenuators numbers 35, 37, and 09 for the x-direction and by attenuators numbers 12, 22, and 36 for the y-direction. The values of the coefficients were not calculated explicitly; the attenuators were adjusted so that the contours obtained from the simulation will fit the experimental contours which were obtained from Figure 2.4.4.

F_1 / y mils	x mils 0.5mv	1.0mv	1.5mv	2.5mv	4.0mv
0	15	30.0	42.5	60.0	77.0
10	15	29.5	41.2	60.0	77.0
20	15	29.5	41.2	58.5	73.0
30	15	28.8	41.2	57.5	71.0
40	15	27.5	40.0	56.2	71.0
50	13.8	26.2	39.2	54.0	68.5
60	13.8	25.0	37.2	50.0	62.5
70	12.5	22.5	31.2	40.0	50.0

Table 3.4.1 Contours of constant output of the position sensor in X-direction ($F_1(x,y)$).

The corresponding controus, Table 3.4.1, were obtained by setting the values of attenuators 35, 36, and 09 to

$$D1 = 0.08 \quad \text{(Pot. 35, 36)}$$
$$\alpha 2 = 1.00 \quad \text{(Pot. 09)} \qquad (3.4.4)$$

(Since $\alpha 2 = 1.00$ it was not used in the complete program).

y volts	x volts				
0	1.5	3.00	4.25	6.00	7.7
1	1.5	2.99	4.23	5.99	7.68
2	1.48	2.98	4.19	5.92	7.56
3	1.46	2.91	4.06	5.72	7.25
4	1.42	2.74	3.86	5.38	6.87
5	1.35	2.58	3.60	5.04	6.40
6	1.26	2.39	3.35	4.63	5.93
7	1.16	2.21	3.05	4.25	5.39
8	1.07	2.00	2.78	3.87	4.90

Table 3.4.2 The corresponding analog computer contours for the position sensor in X direction.

Similarly for the y direction the experimental values of the contours are given in Table 3.4.3.

F_2 / X mils	y mils 0.25mv	0.5mv	1.0mv	1.5mv	2.0mv
0	15	23.8	47.5	68.5	77.5
10	15	23.8	47.5	68.5	77.5
20	15.8	23.8	46.4	67.5	76.3
30	13.8	23.0	45.0	65.0	73.7
40	13.8	22.4	43.0	61.3	70.0
50	12.5	21.3	40.0	57.5	65.0
60	12.5	19.2	36.7	52.5	57.5
70	11.8	17.5	32.5	45.0	51.3
80	11.2	15.0	27.5	37.5	43.7

Table 3.4.3 Contours of constant output of the position sensor in Y-direction $(F_2(x,y))$

The corresponding contours on the analog were obtained by setting attenuators numbers 12, 22, and 36 to

$$D2 = 0.08 \quad \text{(Pot. 12 and 22)}$$
$$\alpha 1 = 0.110 \quad \text{(Pot. 36)} \qquad (3.4.5)$$

X volts					
0	1.5	2.38	4.75	6.85	7.75
1	1.49	2.37	4.72	6.83	7.72
2	1.49	2.32	4.66	6.71	7.58
3	1.40	2.20	4.49	6.45	7.25
4	1.40	2.19	4.24	6.04	6.83
5	1.42	2.03	3.93	5.59	6.30
6	1.22	1.87	3.61	5.13	5.81
7	1.10	1.73	3.28	4.68	5.26
8	1.03	1.56	2.99	4.22	4.76

Table 3.5.3 Contours of constant output of the position sensor Y-direction as obtained from the analog simulation.

2) Generating $F_1(x,y)$ and $F_2(x,y)$

Once the signal is obtained on amplifiers numbers 35 and 36 for x and y directions respectively, it is fed into variable diode function generators. The potentiometer settings of the variable diode function generators are given in the following tables:

Output of V.D.F.G. $F_1(x,y)$ volts	±0.5	±0.75	±1.0	±1.5	±2.0	±2.5	±4.0	±4.3	±5.5	±6.33
Input to V.D.F.G. Amp. 35 volts	∓1.5	∓2.25	∓3.0	∓4.25	∓5.12	∓6.0	∓7.7	78.0	∓9.0	∓10.0

Table 3.6.4 V.D.F.G. Settings for position sensor in x direction.

Output of V.D.F.G. $F_2(x,y)$ (volt)	±0.5	±1.4	±2.4	±3.2	±4.4	±5.4	±6.8	±8.4	±10.4	±12.0
Input to V.D.F.G. Amp. 34(volt)	∓1.0	∓2.0	∓3.0	∓4.0	∓5.0	∓6.0	∓7.0	∓8.0	∓ 9.0	∓10.0

Table 3.7.5 V.D.F.G. Settings for position sensor in y direction.

Note that the signal in the y direction (Table 3.4.5) is twice the actual signal (see Figure 2.4.5). This is done to increase the accuracy of the V.D.F.G. In order to compensate for this deviation, the AC amplifiers (see Figure 2.5.1) simulation (see Figure 3.5.1) are set on the same gain, while on the ACV the gain in the y direction is twice that of the gain in the x direction.

3.5 Position and Velocity Filter

The error signals generated by the position sensor are passed through high gain amplifiers simulated by attenuators number 20 and 21, which are set at

$$AT2 = 0.4 \tag{3.5.1}$$

to avoid overload of the sensitive lead lag lag filter. The "amplified" signal is passed through a lead lag lag filter with the transfer function

$$G(s) = \frac{1 + s}{(0.02s+1)^2} \tag{3.5.2}$$

At this point noise is being introduced to the system (for details, see Section 3.9).

A cross coupling is added to the error signal by the rate gyro potentiometers (Figure 2.3.1), making the error signal proportional to

$$\begin{aligned} E_X &\approx x + \dot{x} - (\omega_z y) + N_x \\ E_Y &\approx y + \dot{y} + (\omega_z y) + N_y \end{aligned} \tag{3.5.3}$$

where

$x + \dot{x}$ - output of the lead lag lag filter

$\omega_z y$ - rate gyro cross coupling

N_X - noise in x channel

$y + \dot{y}$ - output of the lead lag lag filter

$\omega_z x$ - rate gyro cross coupling

N_Y - noise in y direction.

The rate gyro cross coupling can be disconnected by function switches numbers 1 and 2. The program is shown in Figure 3.5.1.

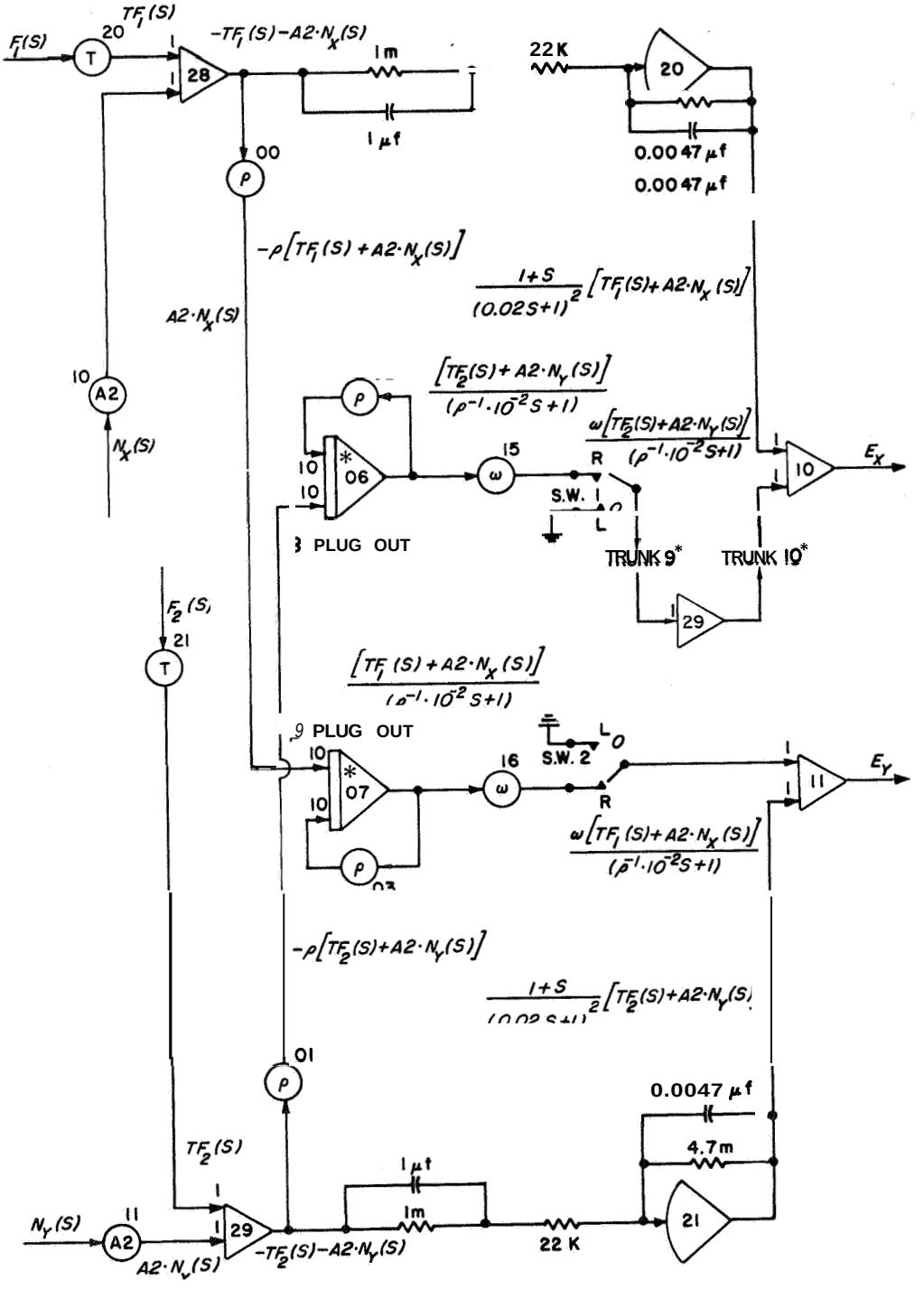

POSITION AND VELOCITY FILTER

Figure 3.5.1. Position and velocity filter simulation

As can be seen from Figure 2.8.5, there is an electronic cross coupling of both channels. Since it was felt that the fuel consumption is not affected by this cross coupling, it was not simulated, but it can be included very easily in the program if the following steps are followed:

1. Connect the output of Amp. 20 (TR-48 #1) through an attenuator to the input of amplifier 29 (TR-48 # 1).
2. Connect the output of Amp. 21 through an attenuator to the input of Amp. 28 (TR-48 # 1).
3. Set the attenuators that have been used in steps 1 and 2 to 0.01.

The effect of this electronic cross coupling is shown in Figure 3.5.2.

3.6 Control Circuit

The control simulation is given in Figure 3.6.1. It consists of dead band and P.W.P.F. valves which include two integrators with Schmitt trigger reset feedback.

The dead band is determined by attenuators 24 and 39 for the x channel and 29 and 14 for the y channel. The dead band on the vehicle is equivalent to 12.5 mils. In order to achieve the equivalent dead band (1.25 volt), the attenuator's setting should be

Pot. 24 = 0.0360
Pot. 39 = 0.0407 (3.6.1)
Pot. 29 = 0.03
Pot. 14 = 0.03

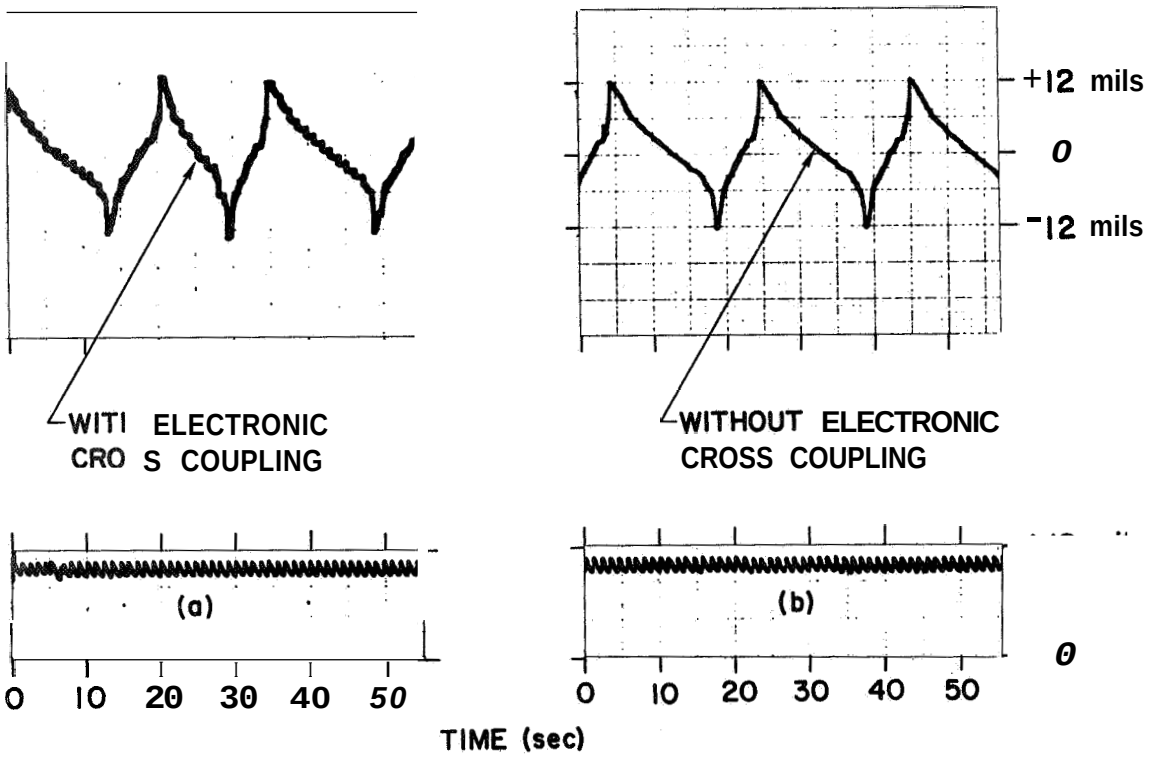

Figure 3.5.2. Electronic cross coupling effect.

(a) With cross coupling

(b) No cross coupling

Note: Gravitational Force coincides with X direction.

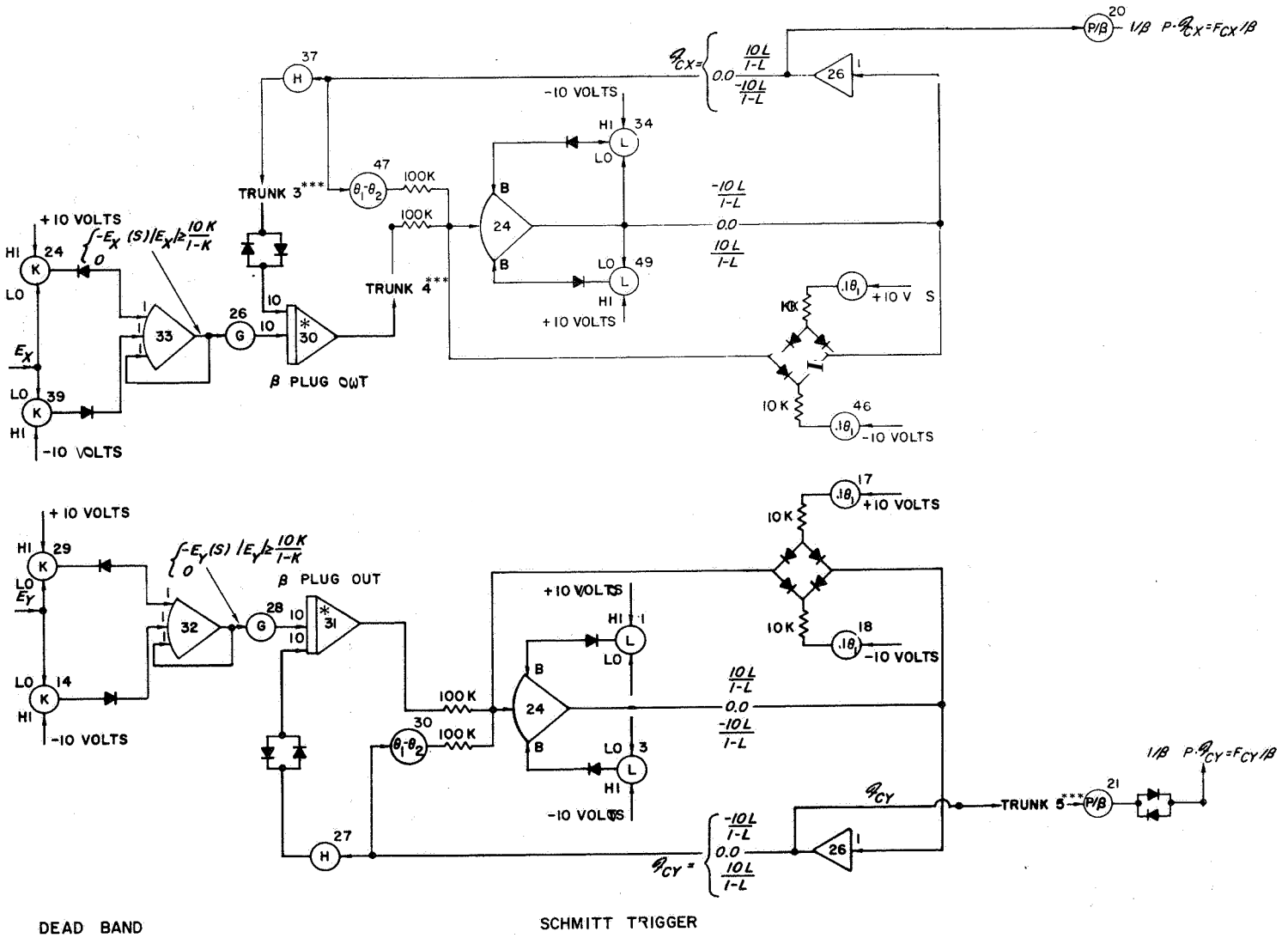

Figure 3.6.1. P.W.P.F. Simulation

The P.W.P.F. characteristics are determined by four parameters:

1) Integrator time constant determined by G, H, the input resistance into the integrators (100 kΩ or 10 kΩ) and by the value of the feedback capacitor determined by the "β plug".

2) Threshold of Schmitt trigger determined by $0.1\theta_1$.

3) The width of the Schmitt trigger, which is determined by $(\theta_1 - \theta_2)$.

4) The height of the pulse determined by L.

$$[\text{Pulse Height}] = \left|\frac{10L}{1-L}\right|$$

The value of L = 0.472 was kept constant, while all other parameters were adjusted *so* that the characteristic of the simulated system will be equal to that of the P.W.P.F. on the ACV (Fig. 2.5.2).

. The control jet pressure is simulated by attenuators 21 and 20. When inertial coordinates are used the control jet pressure is simulated by attenuators 02 and 17 (See Fig. 3.10.2). As it can be seen (Fig. 3.6.1) an arrangement of two diodes in parallel appears at several places. This is done in order to eliminate small signals due to nonideal behavior of the Schmitt trigger bang-bang circuit, especially when fed into integrators.

As mentioned later (see Sec. 3.11), the width of the Schmitt trigger hysteresis loop, the threshold of the Schmitt trigger and the width of the Dead-band were adjusted by the digital computer, using the digital attenuators called x_1, x_2, x_3 respectively. In the following Figures 3.6.3 and 3.6.4, a calibration curves are given for recalculating the control parameters from the values set by the digital computer. Observe

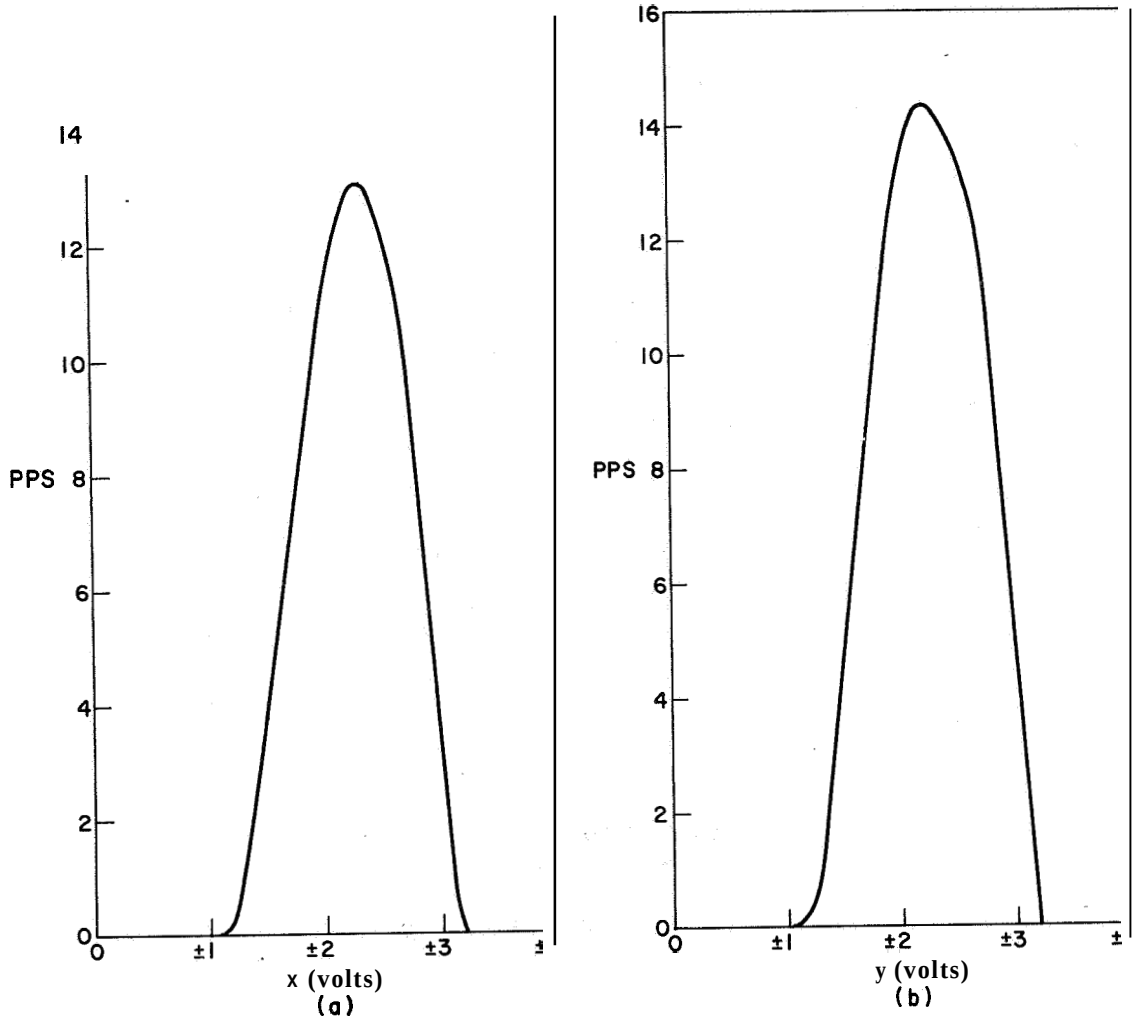

Figure 3.6.2. P.W.P.F. Characteristics

(a) Channel X

(b) Channel y

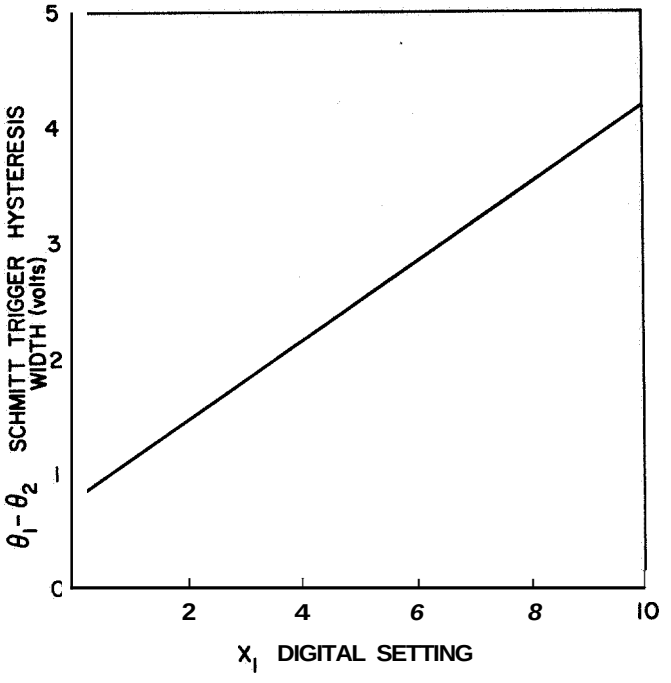

Figure 3.6.3. Calibration curve for Schmitt-Trigger hysterises loop

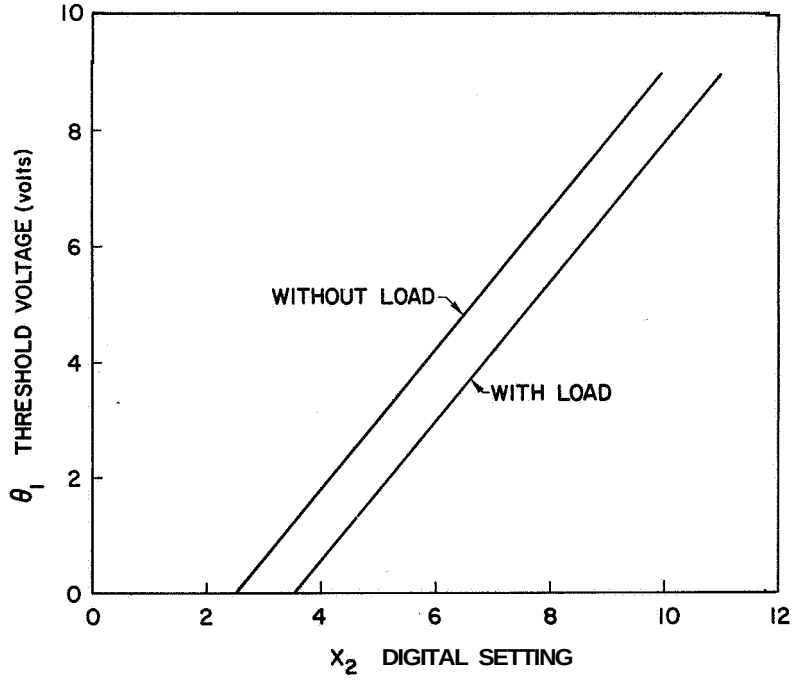

Figure 3.6.4. Calibration curve for Schmitt-Trigger treshold voltage

that all attenuators which are associated with the control simulation should be set equal to the setting shown in Table 3.10.2 column 2.

3.7 Fuel Consumption Measurement

The signals from both P.W.P.F. are the control accelerations and are proportional to the fuel consumption. The fuel consumption measurement (Fig. 3.7.1) includes two absolute value circuits for both channels and an integrator. Six diodes are used to increase the accuracy of the measurement system (see Figure 3.7.2)

3.8 Maximum Range Measurement

The problem of finding the gain setting of the P.W.P.F. control which corresponds to minimum fuel consumption is a state constrained problem. Clearly, if one does not impose any constraints on the range of x and y, the problem is trivial, since by not controlling the plant the fuel consumption is minimized. Therefore, it is necessary to measure the maximum range. The maximum range simulation is shown in Figure 3.8.1. Since most of the amplifiers of both computers were used, it was not possible to construct an absolute value circuit; instead, it was assumed that

$$\begin{aligned} |x_{min}| &= |x_{max}| \\ |y_{min}| &= |y_{max}| \end{aligned} \tag{3.8.1}$$

where

$$\begin{aligned} x_{min} \leq x \leq x_{max} \\ y_{min} \leq y \leq y_{max} \end{aligned} \tag{3.8.2}$$

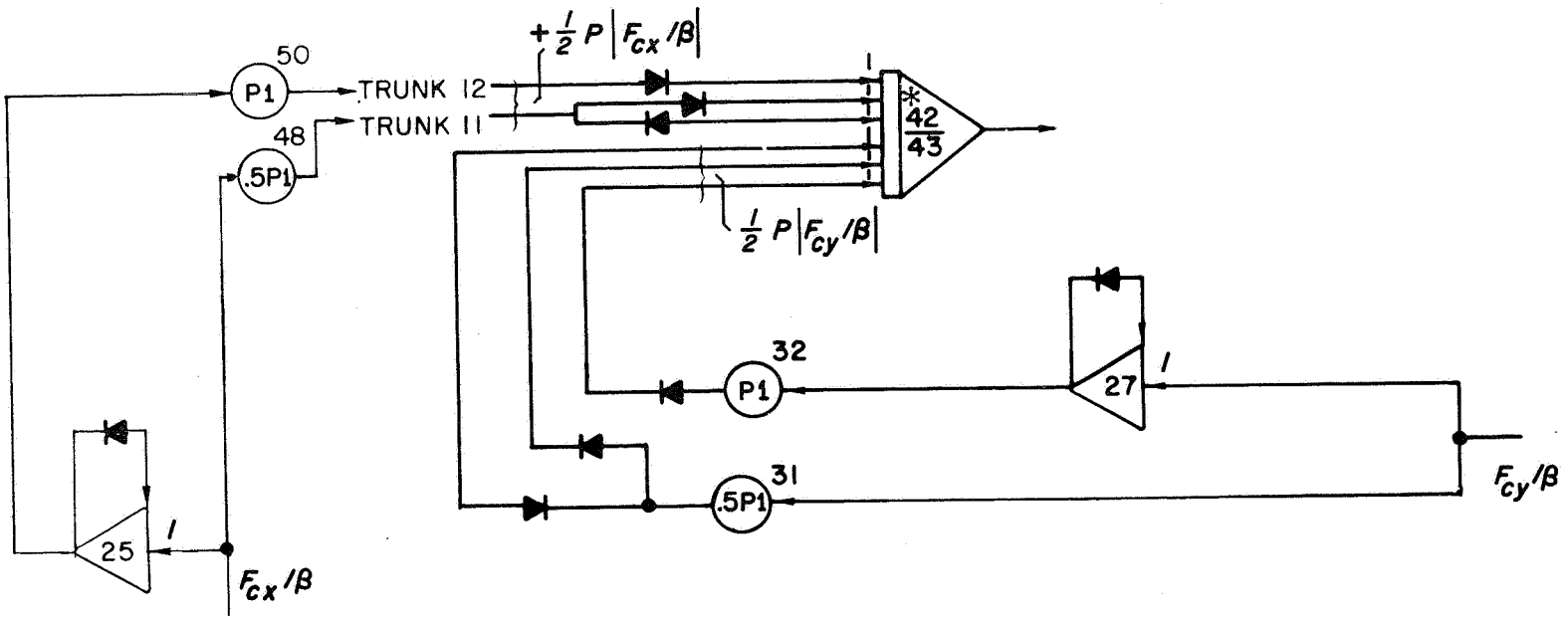

Figure 3 7 1 Fuel consumption measurement.

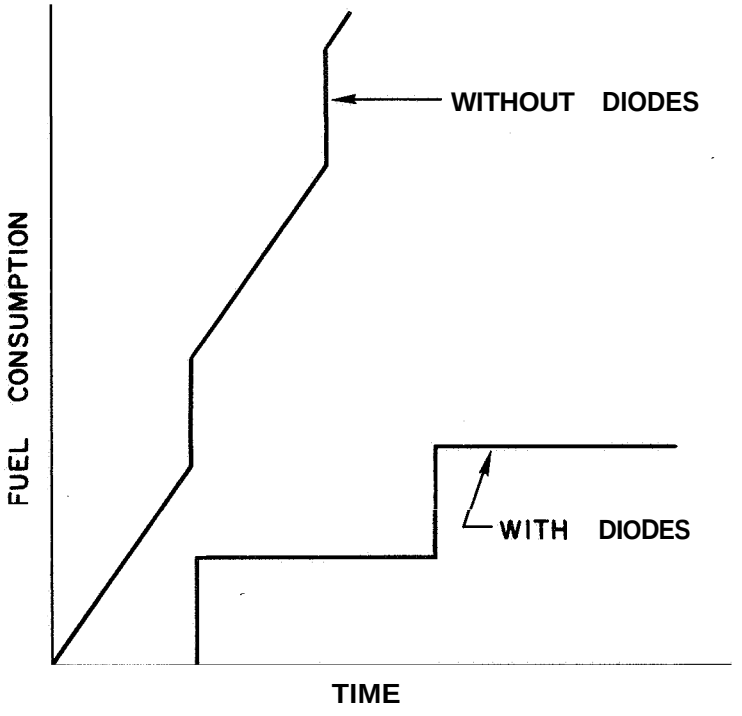

Figure 3.7.2. Effect of a small dead zone generated by two diodes on fuel consumption integration.

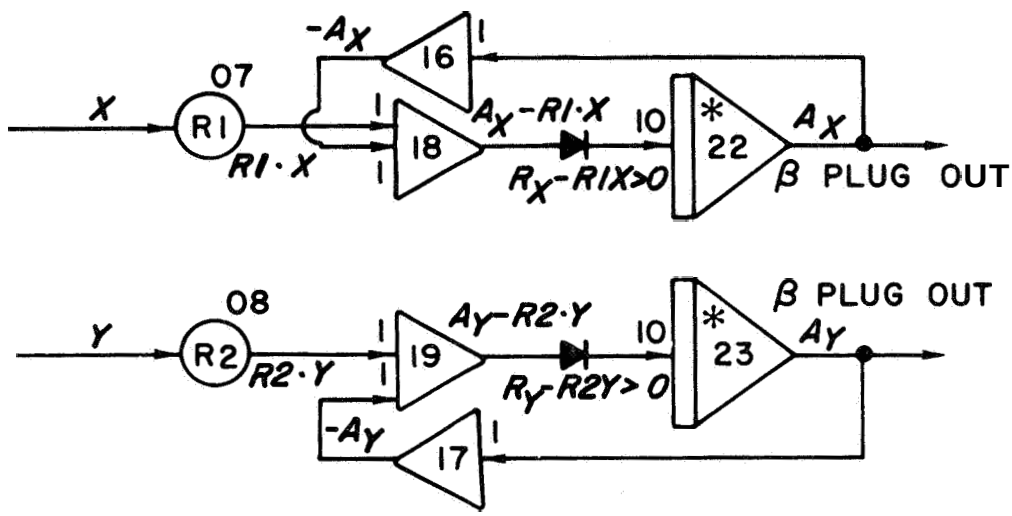

Figure 3.8.1. Maximum range measurement

which is true when the vehicle is rotating. In cases-where the vehicle does not rotate, it is always possible to adjust (Equation 3.2.1) so that

$$x_{max} = \text{Max } |x|$$
$$y_{max} = \text{Max } |y| \qquad (3.8.3)$$

Attenuators 07, 08 were set equal to 1.0.

3.9 Noise Generators and Noise Analyzer

In this simulation two electronic noise generators, E.A.I. Model 201A, were used. The output spectrum is uniform ($\pm$ 0.1 db) from 0 to 35 cps. Output falls off rapidly above 40 cps. The maximum output level is 15 volts rms. More details can be found in PACE Catalog. [Reference 5]. The two noise filters and noise analyzers are identical and are shown in Figure 3.9.1. It includes attenuators 35 and 36 for reducing the noise level and then the noise is passed through a filter

$$G(s) = \frac{1}{(0.01s+1)^4} \qquad (3.9.1)$$

As the order of the filter is increased, the influence of the nonuniform portion of the generator is diminished.

The noise level which passes the fourth order filter is very low, and to increase the accuracy of the analyzer it is passed through amplifiers 40 and 41, then it is fed into an absolute value circuit and integrated. In order to increase the integration time and yet avoid the overload of the analog amplifiers, the integrator initial value is set at -10 volts.

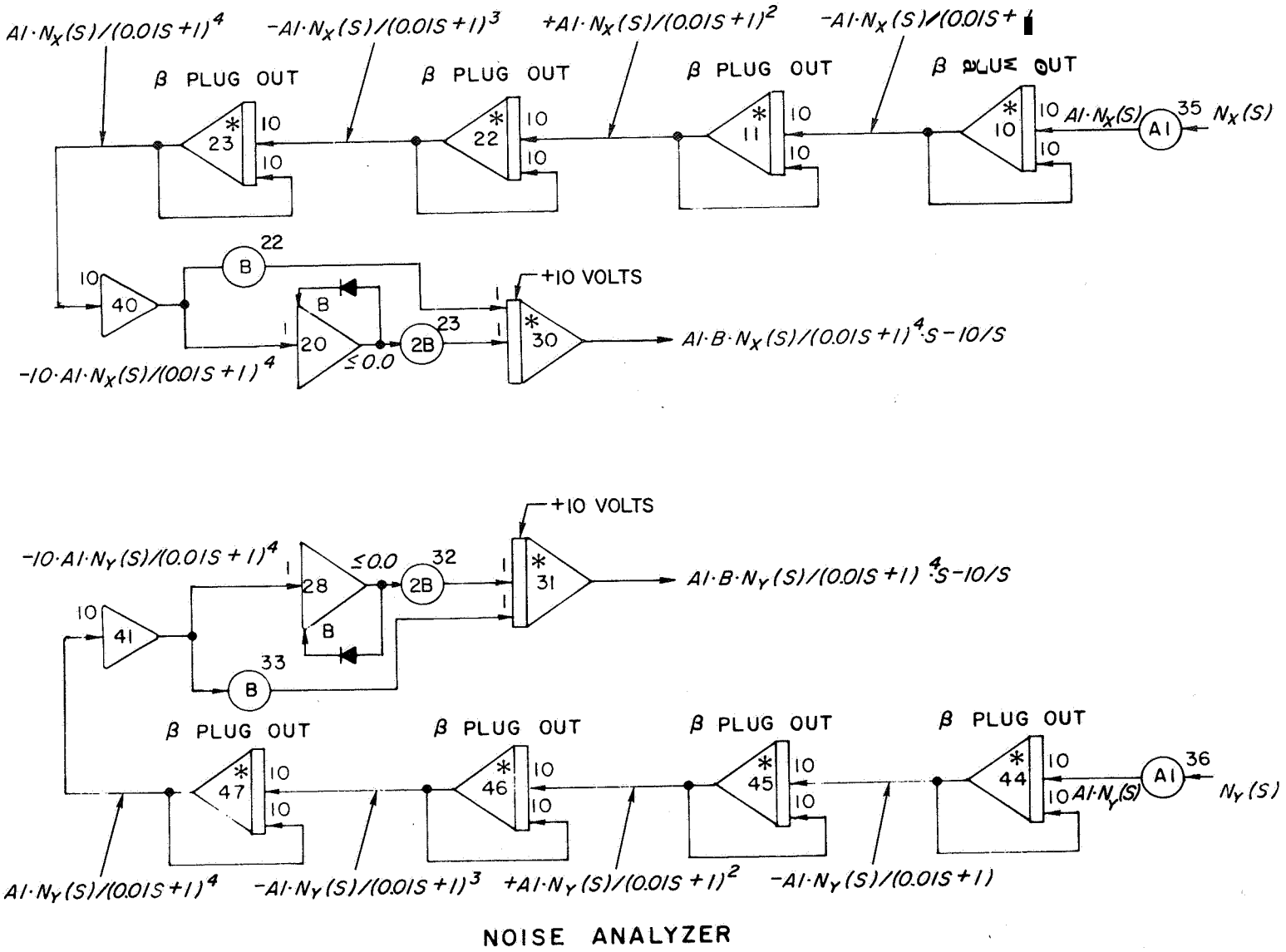

NOISE ANALYZER

Figure 3.9.1. Noise analyzer and filter

The noise spectrum is related to the output of these integrators by

$$N = \left[\frac{8}{500T^2}\left(\int_0^T n(t)dt - 10\right)^2\right] \qquad (3.9.2)$$

3.10 Simulation Results

The complete simulation is shown in Figures 3.10.1 and 3.10.2. In the first figure the equations of motion are given in body-fixed coordinates (Equations 3.2.1) while in Figure 3.10.2 the equations of motion are given in inertial coordinates. Two parameters are still to be identified:

1) The equivalent control jet pressure simulated by attenuators 02 and 17 (TR-48 # 2) for inertial coordinates and attenuators 20 and 21 for the first simulation.

2) The complete correlation between fuel consumption of the simulated vehicle and fuel consumption of the ACV.

These experiments were performed only on the system shown in Figure 3.10.2, therefore all calibration curves are valid for the attenuators setting shown in column 3 of table 3.10.2.

In the first set of experiments the fuel consumption was measured as a function of the control jet pressure (Attenuators 02 and 17) for zero tilt. The results obtained are given in Figure 3.10.3.

The tangent to the fuel consumption curve which passes through the origin is also included. Any tangent to the curve at points greater than 0.145 intersects the negative part of the fuel consumption axis. From the experimental results (Figure 2.8.1, "Table Leveled") it is clear that

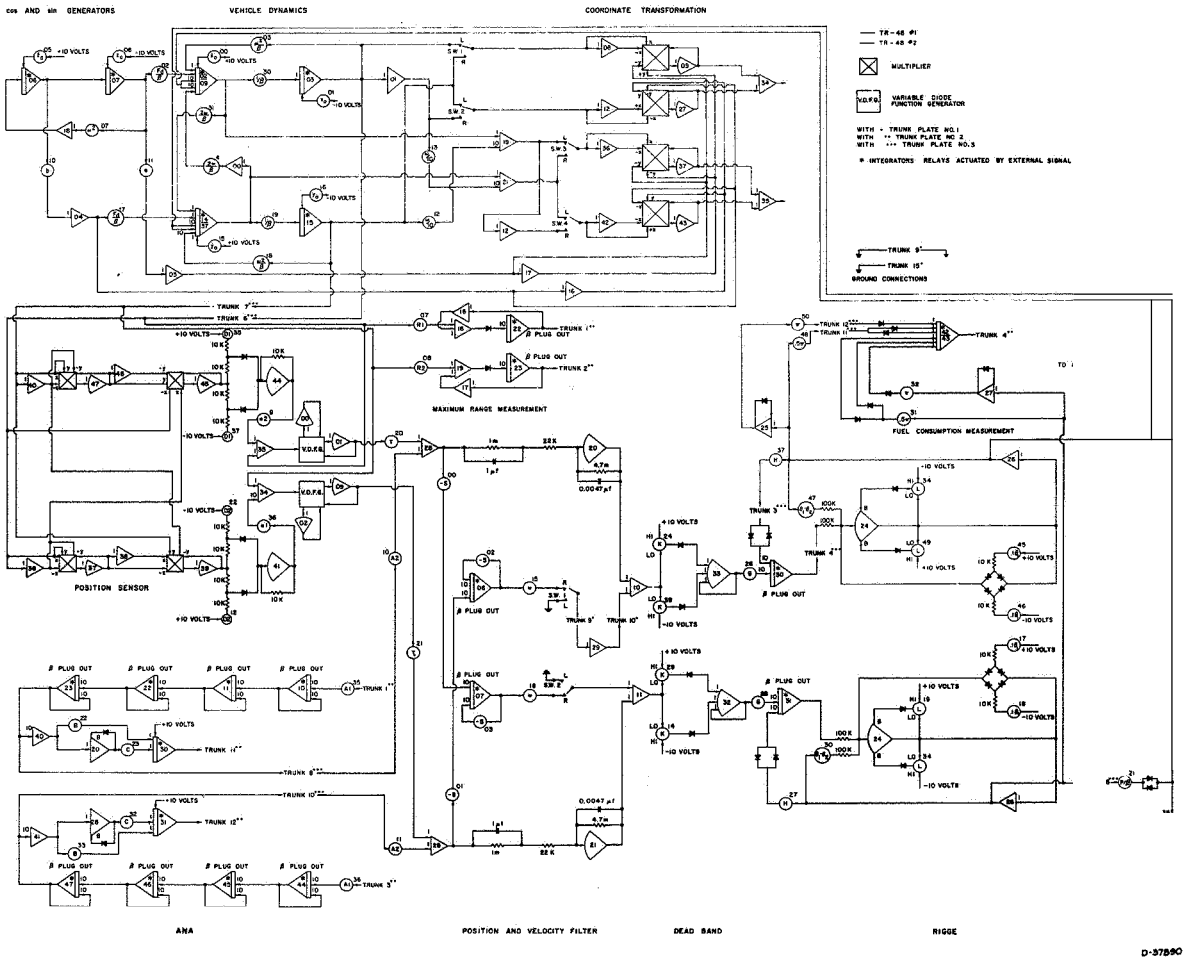

Figure 3.10 1 Complete vehicle simulation. Vehicle dynamics equations in body-fixed coordinates

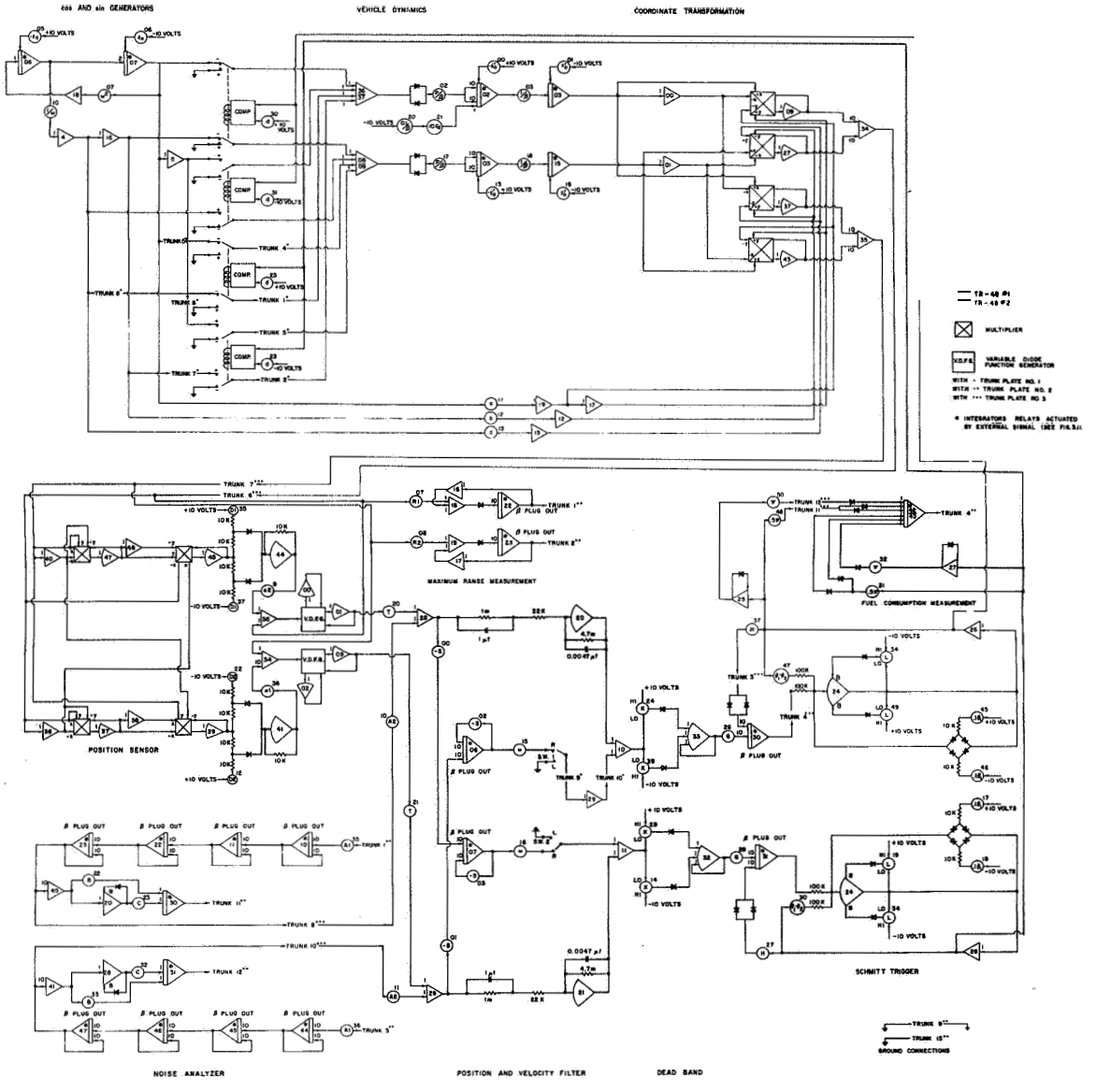

Figure 3.10.2. Complete vehicle simulation. Vehicle dynamics equation in inertial coordinates.

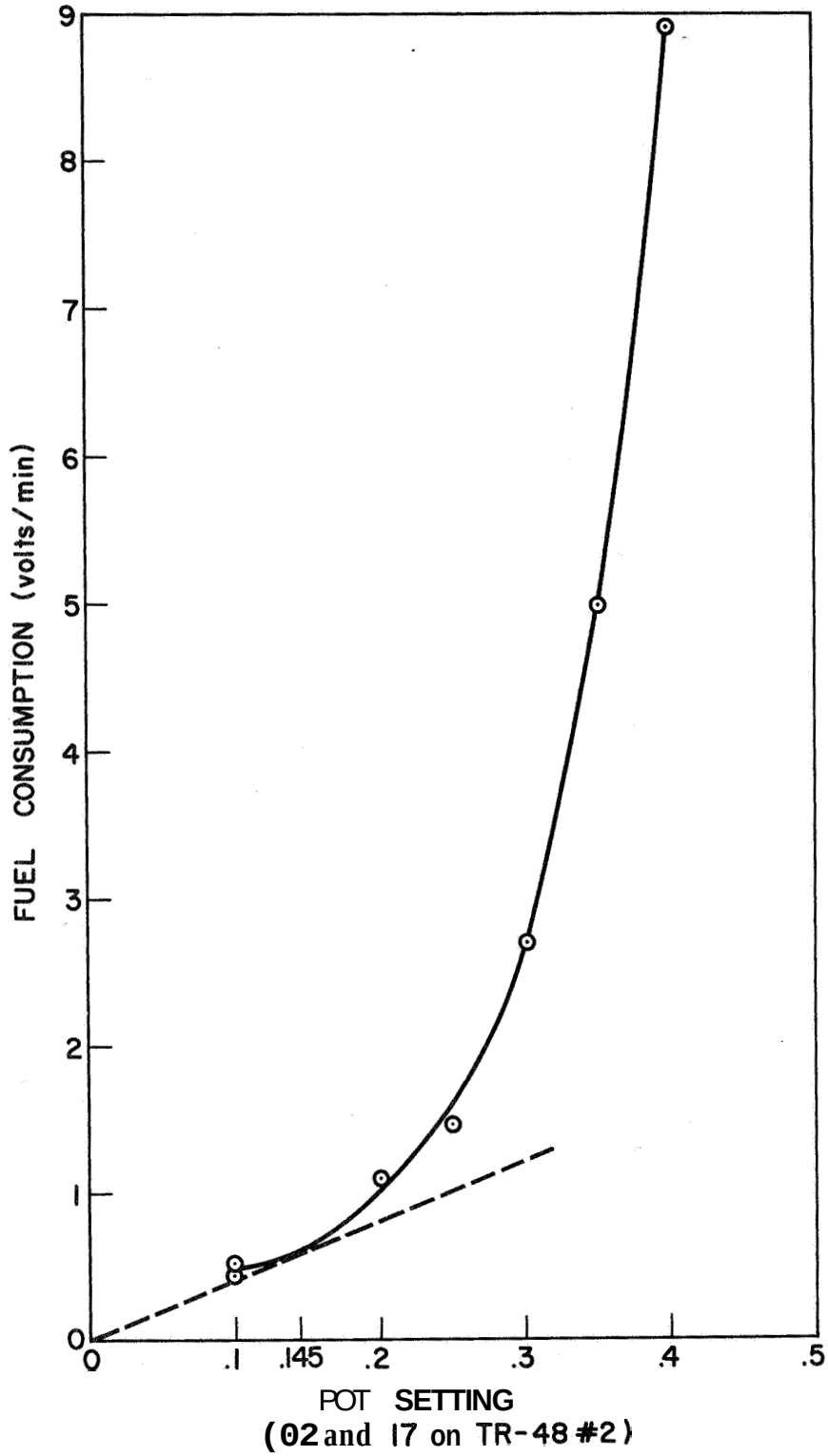

Figure 3.10.3. Gas consumption (volts/min) as a function of simulated control jet pressure. Control jet pressure is simulated by attenuators 02 and 17 for the simulation shown in Figure 3.10.2.

the intersection occurs at positive values of the fuel consumption axis. Therefore the attenuator setting should be less than ~ 0.145.

In order to find the exact attenuator setting the trajectory of the vehicle in the x direction was measured as a function of three different attenuator settings (0.10, 0.15, 0.17) and four different table tilt angles (1", 2", 3", 4").

The trajectory is shown in Figure 3.10.4. The signals shown in this figure are similar to those shown in Figures (2.8.4, 2.8.6), but the amplitude of the signals was amplified 50 times and only one pair of parabolas was included. For each attenuator setting there are four pairs of parabolas. Each corresponds to a different table tilt angle, starting with 4 arcsec. - the lower parabolas. By comparing the shape of the different parabolas obtained in the simulation with that obtained in the experiments it was found that an attenuator setting of 0.1 resulted in the best correspondence between simulator and experiment.

Table Tilt					
Theoretical Values		a Calculated Values (seconds)	Second/ Cycle	Amplitude/50 mv	αt = Const.
Seconds	Equivalent Pot. Setting				
1"	0.0188	0.98	2	92	2
2"	0.0375	1.7	1	40	2
3"	0.0565	2.54	0.4	28	2.1
4"	0.0752	3.4	0.5	20	2.0

Table 3.10.1 Trajectory of simulated vehicle in x direction (Control jet attenuators set at 0.1, Figure 3.10.4 a)

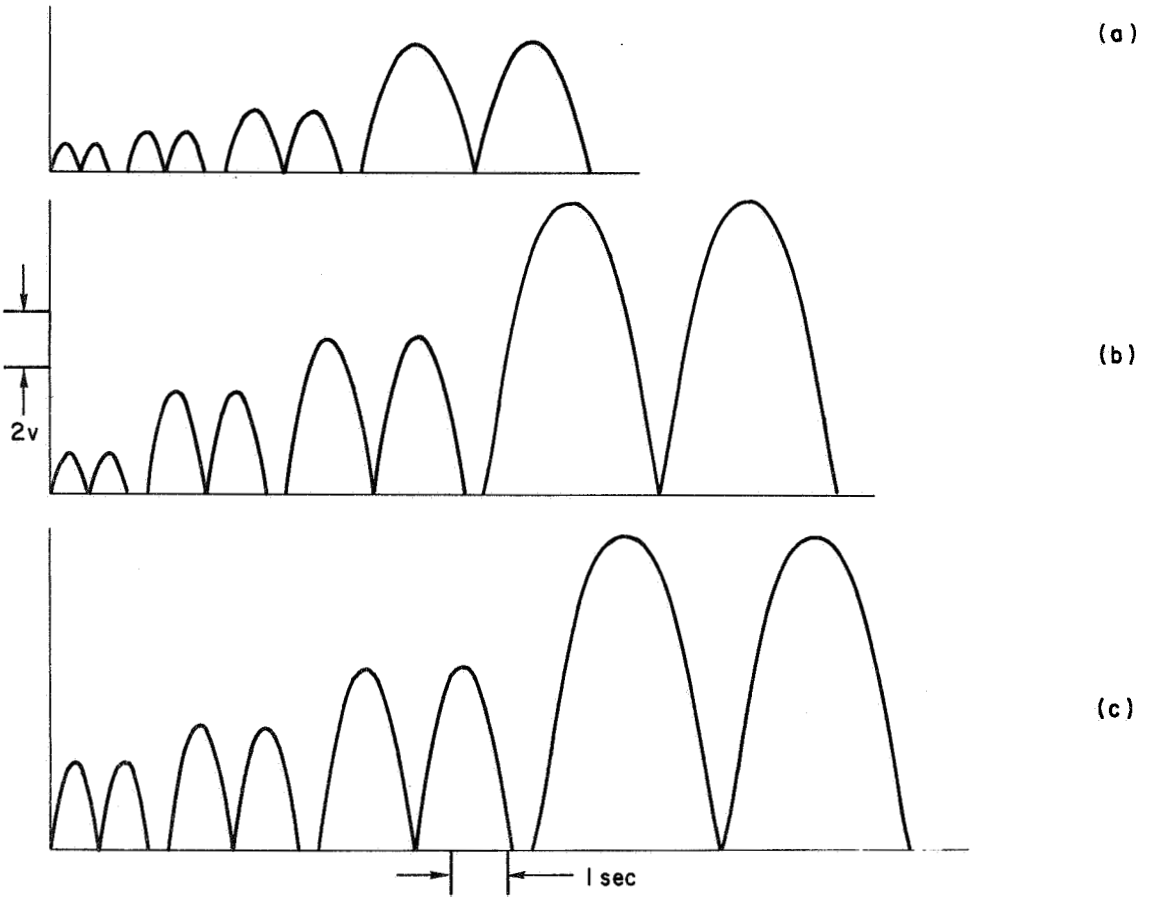

Figure 3.10.4. Vehicle trajectory in x direction. Since the gravitational force coincides only with channel x, the trajectory in y direction is not affected and therefore is not shown.

(a) Attenuators simulating control jet pressure are set at 0.1, and table tilt angle is 1, 2, 3, 4 arc sec.

(b) Attenuators simulating control jet pressure are set at 0.15, and table tilt angle is 1, 2, 3, 4 arc sec.

(c) Attenuators simulating control jet pressure are set at 0.17, and table tilt angle is 1, 2, 3, 4 arc sec.

Signal is shown after amplification of 50 times. Complete program is shown in Fig. 3.10.2.

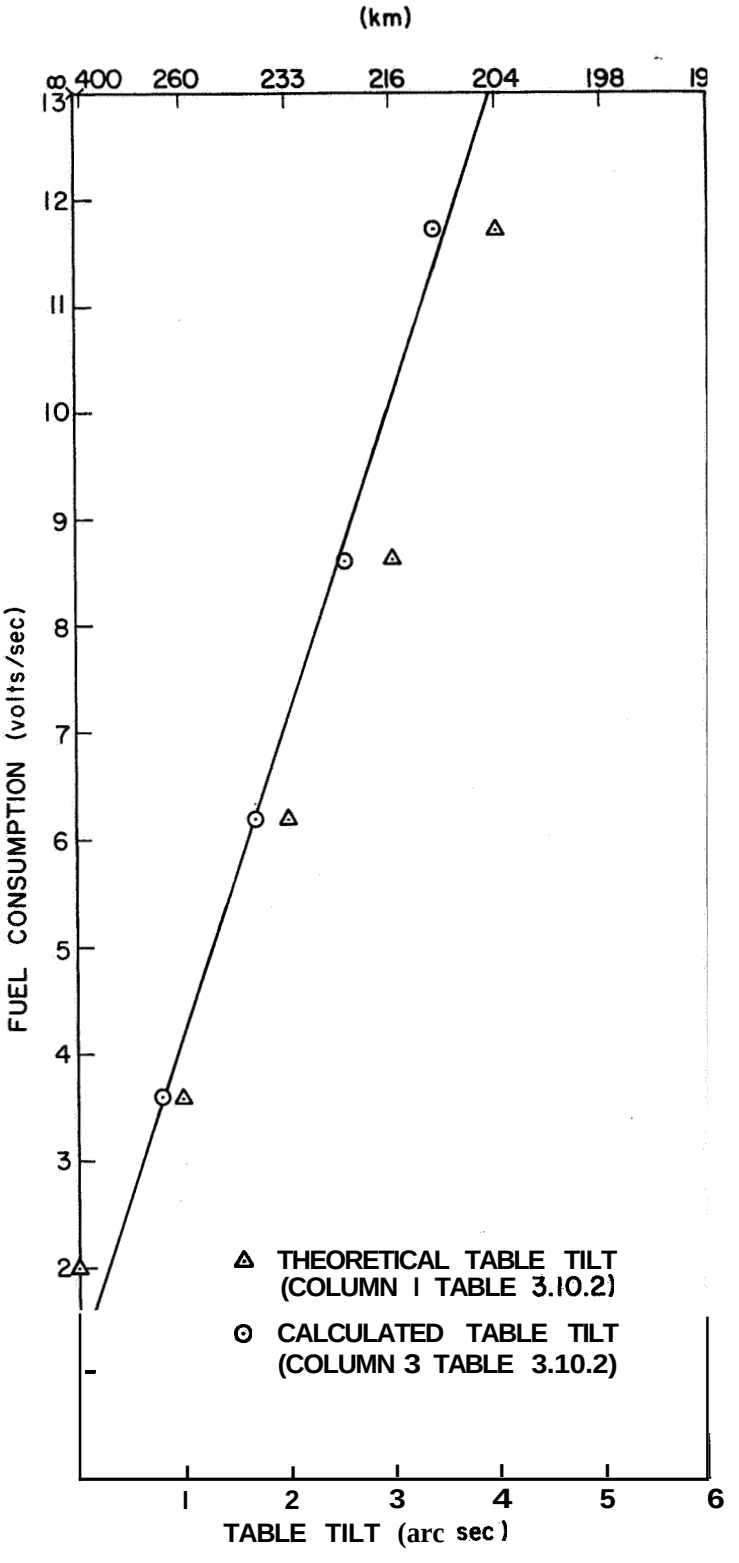

Figure 3.10.5. Fuel consumption as a function of different table tilts. The corresponding attenuator settings are shown in Table 3.10.1, Column 2. (Attenuators 20 and 21, TR-40 #2).

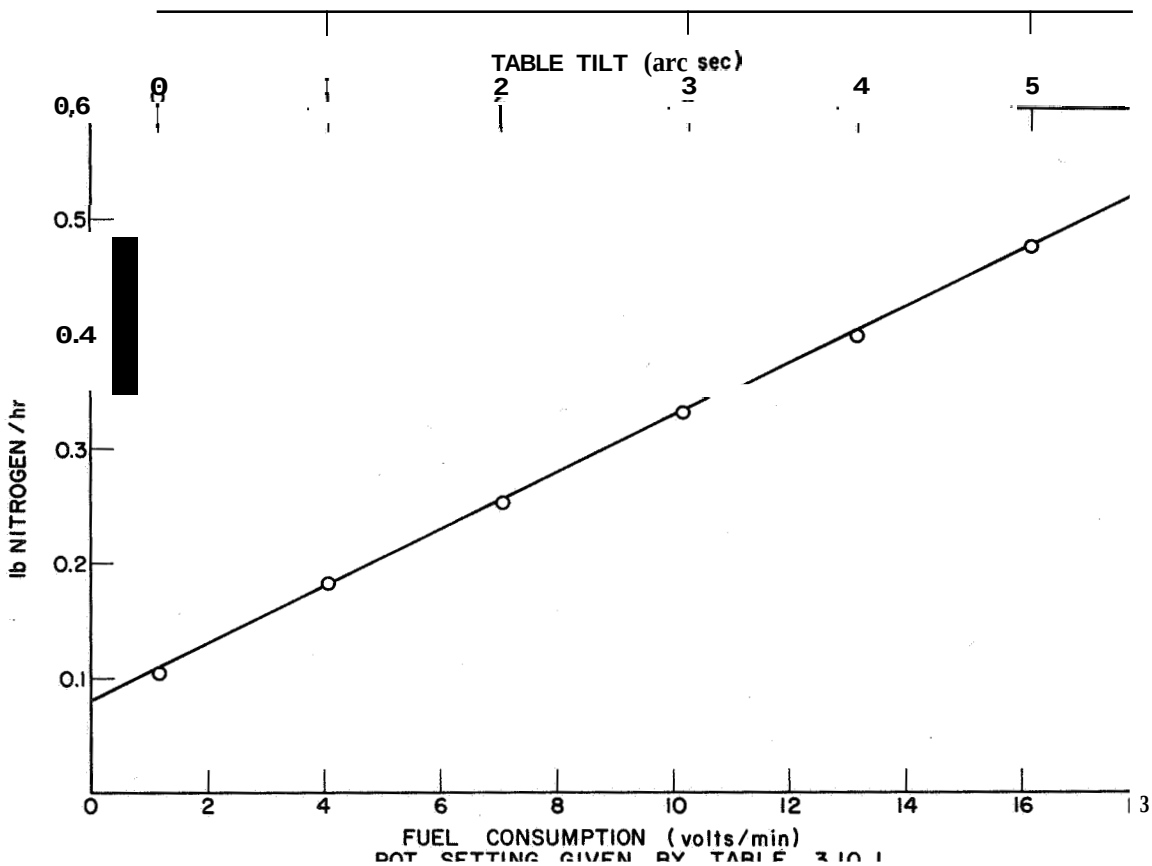

Figure 3.10.6. Correlation curve for fuel consumption. (Valid for the simulation shown in Fig. 3.10.2). ±15%

The attenuator settings given in Column 2 were obtained by

$$[\text{Acceleration due to Table Tilt}] = 0.188 \quad \frac{\text{volts}}{\text{sec}^2 \text{ arc sec}} \qquad (3.10.1)$$

The calculated table tilts, column 3, were obtained from

$$a = \frac{\ell}{(t/2)^2} \qquad (3.10.2)$$

where

a = acceleration

ℓ = distance (column 5 Table 3.10.1)

t = second/cycle. (column 4 Table 3.10.1)

After finding the equivalent attenuator for the control jet simulation, fuel consumption measurement at different table tilts was performed. The results of that experiment are shown in Figure 3.10.5. Again the corresponding attenuator settings were equal to those given in Column 2, Table 3.10.1. The relation between fuel consumption obtained from the simulation experiments and the actual gas consumption of the vehicle is given in Figure 3.10.6. This completes the identification part of the simulation..

In the following table a list of all attenuators used in the simulation is given, together with its functions and its values. Since two different programs were used (Figure 3.10.1 and 3.10.2) and the use of "digital attenuators" (see Section 3.11) is optional, there are three different columns with three different attenuator settings. Program number one will refer always to the simulation given by Figure 3.10.1,

TR-48 Pot.No.		Pot. Settings			Function
		Program No. 1	Digital Connected	Program No. 2	
Sin and Co Generators					
2	05	0.0	⟷	*0.0*	$-\dot{z}_o$ Initial condition of $A\omega \sin(\omega t)$
2	06	0.1	⟷	1.0	z_o Initial condition of $A \cos(\omega t)$ For program 1 A = 1 For program 2 A = F_c = height of the PWPF pulse
2	07	Variable	⟷	Variable	ω^2 Frequency of oscillation
2	10	Variable	⟷	Variable	$b = 1/\omega$
2	11	Variable	⟷	0.1	For program 1, a was used for adjusting the amplitude of cos(ωt) For Program 2 $1/F_c$
2	12	Variable	⟷	0.1	For program 1 ω/10 For program 2 1/F
2	13	Variable	⟷	0.1	For program 1 ω/10 For program 2 $1/F_c$
Vehicle Dy amics					
2	00	0.0	⟷	*0.0*	$-\dot{x}_o$ Initial condition
2	01	0.0	⟷	*0.0*	x_o Initial condition
2	15	0.0	⟷	*0.0*	$-\dot{y}_o$ Initial condition
2	16	0.0	⟷	*0.0*	y_o Initial condition
2	04*	Variable	⟷	Not Used	2ω/β cross coupling
2	31	Variable	⟷	Not Used	2ω/β cross coupling
2	03	Variable	⟷	1.0	For program 1 ω^2/β For program 2 1/β Scaling Factor
2	18	Variable	⟷	1.0	For program 1 ω^2/β For program 2 1/β Scaling Factor
2	19*	1.0	⟷	Not use	1/β Scaling Factor
2	30	1.0	⟷	Not use	1/β Scaling Factor
Gravitational Force					
2	02	Variable	⟷	Not use	F_d/β for x direction
2	17	Variable	⟷	Not use	F_d/β for y direction
2	20	Not used	⟷	0.1	0.1 F_d
2	21	Not used	⟷	Variabl	0.1 F_d
Noise Analyzer					
2	35	Variable	⟷	Variabl	A1 noise level in x channel
2	36	Variable	⟷	Variabl	A1 noise level in y channel
2	22	0.5	⟷	0.5	B for absolute value
2	23	1.0	⟷	1.0	2B unit in x channel
2	32	1.0	⟷	1.0	2B for absolute value
2	33	*0.5*	⟷	0.5	B unit in y channel
Position Sensor					
1	35	0.08	⟷	*0.08*	D1 adjusting the breaking point in x channel
1	37	0.08	⟷	*0.08*	
1	22	0.08	⟷	*0.08*	D2 adjusting the breaking point in y charnel
1	12	0.08	⟷	*0.08*	
1	09*	1.00	⟷	1.00	α2 contour shape x channel
1	36	0.11	⟷	0.11	α1 contour shape y channel

TR-48 Pot No.		Pot. Settings			Function
		Program No. 1	Digital Connected	Program No. 2	
Position and Velocity Filter					
1	20	0.4	⟷	0.4	T amplifier in x direction
1	21	0.4	⟷	0.4	T amplifier in y direction
1	00	0.5	⟷	*0.5*	c pole of the lag filter
1	01	0.5	⟷	0.5	c x channel
1	02	0.5	⟷	0.5	c pole of the lag filter
1	03	0.5	⟷	0.5	c y channel
1	15	Variable	⟷	Variable	Gyro coupling
1	16	Variable	⟷	Variable	Gyro coupling
1	10	0.05	⟷	0.05	A2 Noise level in x channel
1	11	0.05	⟷	0.05	A2 Noise level in y channel
Dead Band and P.W.P.F.					
1	24	0.0366	⟷	0.0366	K determine Dead Band width
1	39	0.0407	⟷	0.0407	K in x channel
1	29	0.03	⟷	0.03	K determine Dead Band width
1	14	0.03	⟷	0.03	K in y channel
1	26	0 525	⟷	0.525	G Determine the input value
1	28	0.412	⟷	0.412	G which causes saturation of the P.W.P.F.
2	37	0.115	⟷	0.115	H Determine the reset signal
1	27	0.115	⟷	0.115	H for the P.W.P.F.
2	47	0.113	1.0	0.113	$\theta_1-\theta_2$ width of hysteresis loop
1	30	0.113	1.0	0.113	$\theta_1-\theta_2$ width of hysteresis loop
2	34	0.472	⟷	0.472	L Pulse height in x
2	49	0.472	⟷	0.472	L channel
1	19	0.472	⟷	0.472	L Pulse height in y
1	34	0.472	⟷	0.472	L channel
2	45	0.10	0.14	0.10	$0.1\theta_1$ Threshold voltage
2	46	0 10	0.14	0.10	$0.1\theta_1$ x channel
1	14	0.10	0.14	0.10	$0.1\theta_1$ Threshold voltage
1	18	0 10	0.14	0.10	$0.1\theta_1$ y channel
Fuel Consumption					
2	20	0 17	⟷	Not use	P/β control jet pressure
2	21	0.17	⟷	Not use	P/β control jet pressure
2	02	Not used	⟷	0.1	P/β control jet pressure
2	17	Not used	⟷	0.1	P/β control jet pressure
2	48	0.5	⟷	*0.5*	0.5π absolute value circuit
2	50	1.0	⟷	1.0	1.0π for x channel
2	32	1.0	⟷	1.0	1.0π absolute value circuit
2	31	0.5	⟷	*0.5*	0.5π for y channel
2	24	Variable	⟷	Not use	CRX cross effect jet
2	25	Variable	⟷	Not use	CRY cross effect jet
Control Relay Circuits					
2	30	Not used	⟷	*0.5*	Transforming the control signal from body-fixed coordinates to inertial coordinates.
2	31	Not used	⟷	*0.5*	
1	33	Not used	⟷	*0.5*	
1	23	Not used	⟷	*0.5*	
Digital Control Relays					
1	13	Not used	0.5	Not use	D1 Relay setting for
1	25	Not used	0.5	Not use	D2 digital signals

1	38**	Not used	−0.2	Not used	T2 determine time needed for all transient to decay
1	06**	Not used	0.06	Not used	T1 rate of time change for operating mode
1	05**	Not used	0.6	Not used	T2 rate of time change for reset mode

*

These attenuators should be grounded.

**

With this setting the operating time is 21 sec, but the fuel consumption is measured only after 8 sec. thus for a period of 13 sec.

Table 3.10.2. Attenuator setting of the simulation

Column 1	Setting for body-fixed coordinates
Column 2	Digital connections
Column 3	Setting for inertial fixed coordinates

For the setting of attenuators 07 and 08 (TR-48#1) see Sec. 3.8.

while program two refers to the simulation given by Figure 3.10.2. The symbol (←→) means that when using the digital the setting can be either that of Program 1 if it is desired to work with body-fixed coordinates, or the setting of Program 2 if it is desired to simulate the vehicle in inertial frame.

When the settings given in columns 1 or 3 are used, the program will simulate the existing vehicle with the existing control parameters. If one uses "digital attenuators'' the control law of the simulation does not simulate the present P.W.P.F. control installed on the A.C.V.

Some attenuator are set at 0.0. These attenuators were used only for static check of the simulation.

3.11 Input-Output Signals

With the present facilities it is possible to convert to digital numbers six different analog outputs. The patching for analog output readings is shown in Figure 3.11.1. The first input is coming from the 1620 control out and is used for checking the multiverter. The signal on this input equals -6.6 volts. If a digital output number 1 of the multiverter is ≥ 7 volts or ≤ 6 volts, the digital computer will discard the present data read from the multiverter.

The analog computer receives two different inputs:

I) Attenuator setting of the simulated vehicle control;

11) Signals for starting, holding, and resetting the analog.

Attenuator setting is done by using the six channels of the D/A Converter. The patching of this part of the program is shown in Figure 3.11.2. The D/A converter can be used in two different ways, as can be seen from the

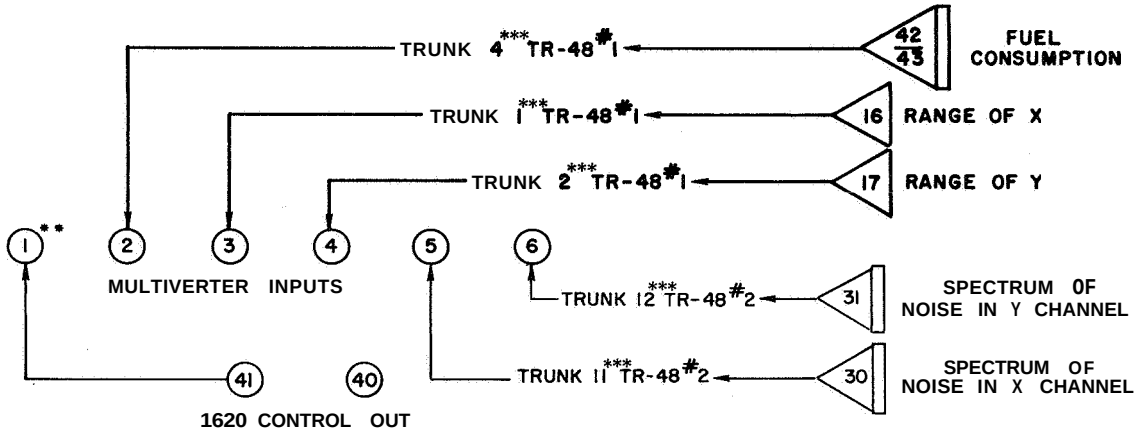

Figure 3.11.1. Digital setting of attenuators. D/A converter patching (subprogram RINO).

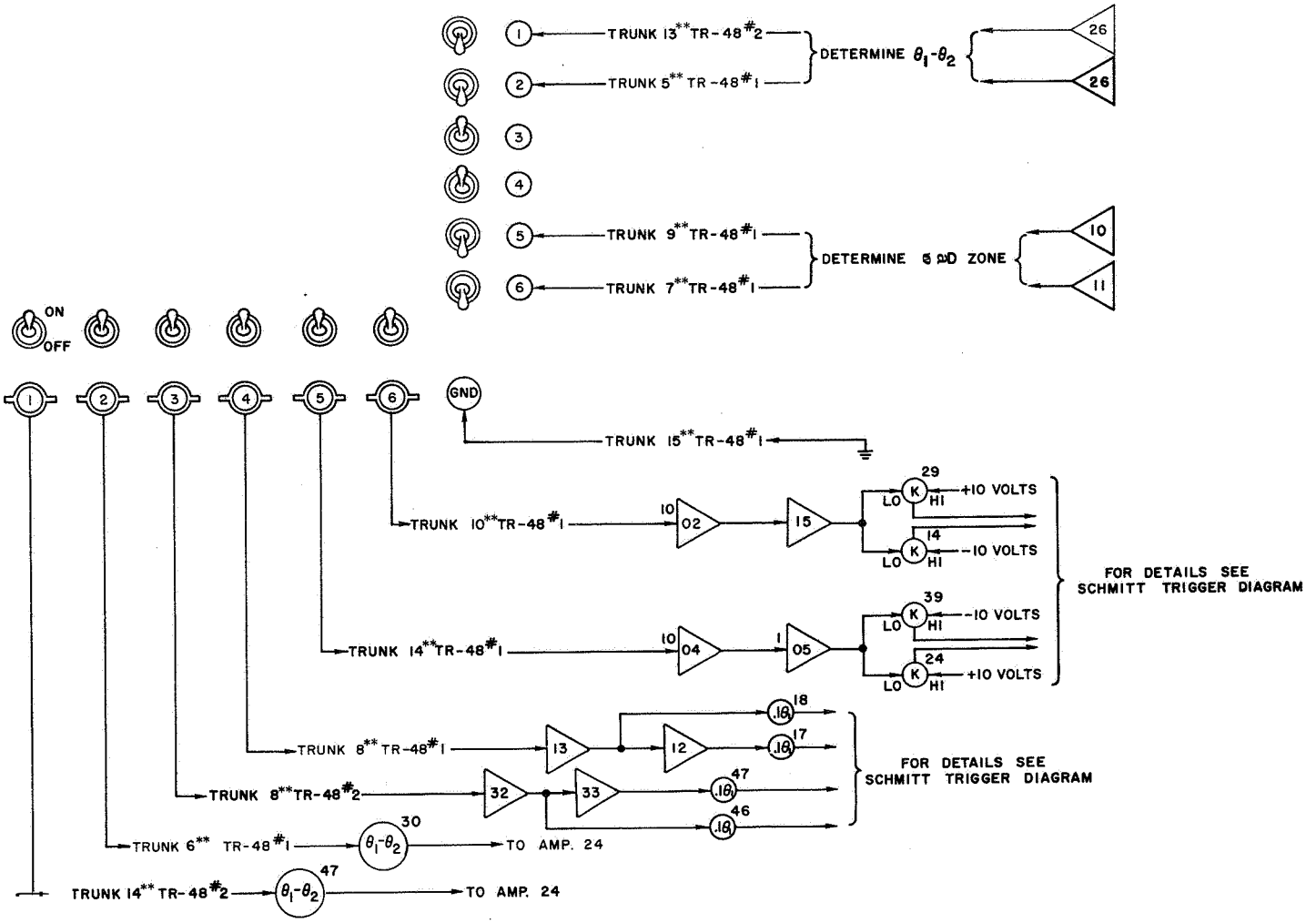

Figure 3.11.2. Digital setting of attenuators D/A converter patching (subprogram WINO).

input switch position. If the switch is raised (as switches 3 and 4), the output signal leaving the unit is generated in the unit. If the switch is lowered, the internal power supply is disconnected from that channel and the channel is used as a regular attenuator for signals coming from the analog (inputs 1, 2, 5, 6). Since the internal signal is ±24.7 volts, while the analog signals are at most ±10 volts, the range of "digital attenuator" settings for analog signals (inputs 1, 2, 5, and 6) is only between 0.0-0.393, while for internal signals (positions 3 and 4) the setting is between 0.0-1.0. (0.393 = 10/24.7)

Since only three parameters of the control law can be adjusted by the digital computers, while the controller has a few more adjustable parameters, it was felt unnecessary to include the "digital attenuators" in the complete simulation description given by Figures 3.10.1 and 3.10.2, however, by using both Figures 3.10.1 or 3.10.2 and Figure 3.11.2 it can be easily transplanted into the general simulation. In Figure 3.10.1 a signal is passed directly from amplifier 26 to attenuator 47 (see Schmitt trigger for x channel, middle right side of Figure 3.10.1). If $(0, -\theta_2)$ is to be adjusted by the digital computer, the signal leaving amplifier 26 is passed first through the "digital attenuator" No. 1 and back to attenuator 47. Similarly, all other signals can be passed through the corresponding "digital attenuators". Thus, with twelve minor changes (six inputs and six outputs) the simulation can be switched from "pure analog" simulation which employs only analog attenuators, to "analog-digital" simulation, in which six analog attenuators were replaced by "digital attenuators".

By transplanting the "digital attenuators" into the simulation, it was possible to adjust automatically three different parameters:

a) θ_1 - the threshold voltage of the Schmitt trigger;

b) θ_1-θ_2 - the width of the Schmitt trigger hysteresis loop;

c) Dead-zone.

Actually, the dead zone was kept constant since the setting of attenuators 24, 39, 16, and 29 was kept constant; but the amplification of the signal entering the dead zone component was adjusted by the "digital attenuators" 5 and 6. Therefore, changing that parameter changed the dead-zone and also, indirectly, the saturation voltage of the P.W.P.F.

Since by using attenuators the signal is attenuated and not amplified, two amplifiers were added (04 and 05 for x channel and 02 and 15 for y channel) to the attenuated signal so the range of amplification/attenuation obtained by this arrangement was 0.0-3.93.

The digital computer controls the mode of analog computer operation through the 1620 control out. With the use of this unit it was possible

Control Unit	10	11	40	41	Analog Computer Mode of Operation
Logical Signal	No	Yes	No	Yes	Hold
	No	Yes	Yes	No	Reset *
	Yes	No	Yes	No	Hold
	Yes	No	No	Yes	Operate *

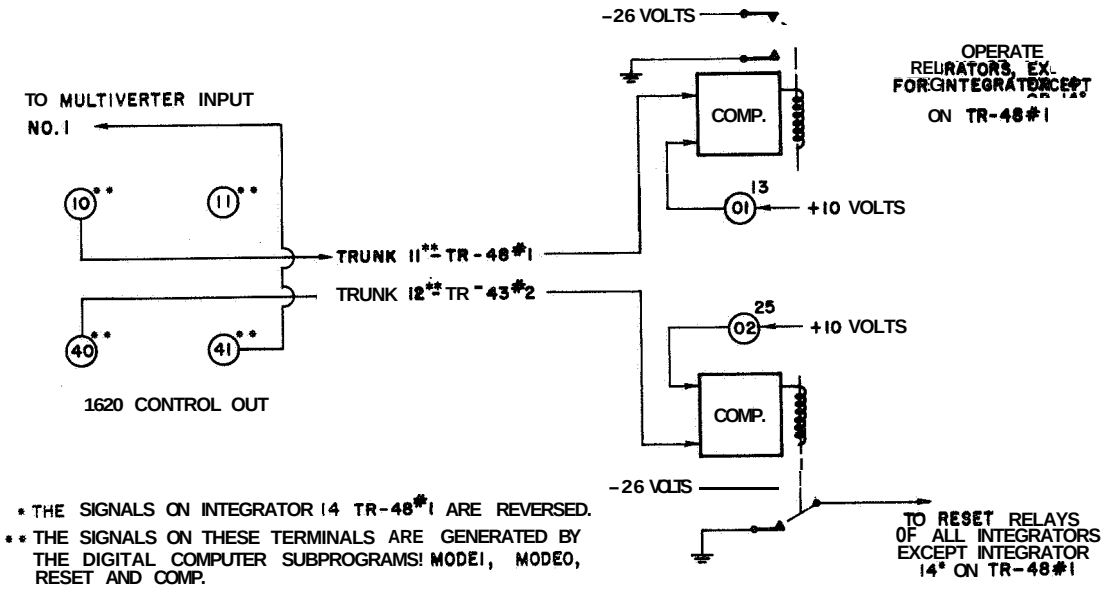

Figure 3.11.3. Use of digital control out logic for operating the analog computer (*see* Table 3.11.1).

The patching of this control unit is, shown in Figure 3.11.3.

Three other control units are shown in Figure 3.11.4. Integrators 03 and 14 are used as clocks. Integrator 03 determines the length of time in which the analog is in operating mode, while integrator 14 determines reset time. Moreover, since the fuel consumption is to be measured only when the vehicle is in its limit-cycle, i.e., all the effects of initial conditions have been decayed, it is necessary to divide the "operating time" into two intervals:

a) time necessary for reaching "equilibrium" trajectory;

b) time necessary for measuring the fuel consumption.

This division was achieved by connecting the output of the fuel consumption integrator (42/43) with its summing junction thus grounding this unit through a relay. The switching point of the relay depends on the setting of attenuator 38.

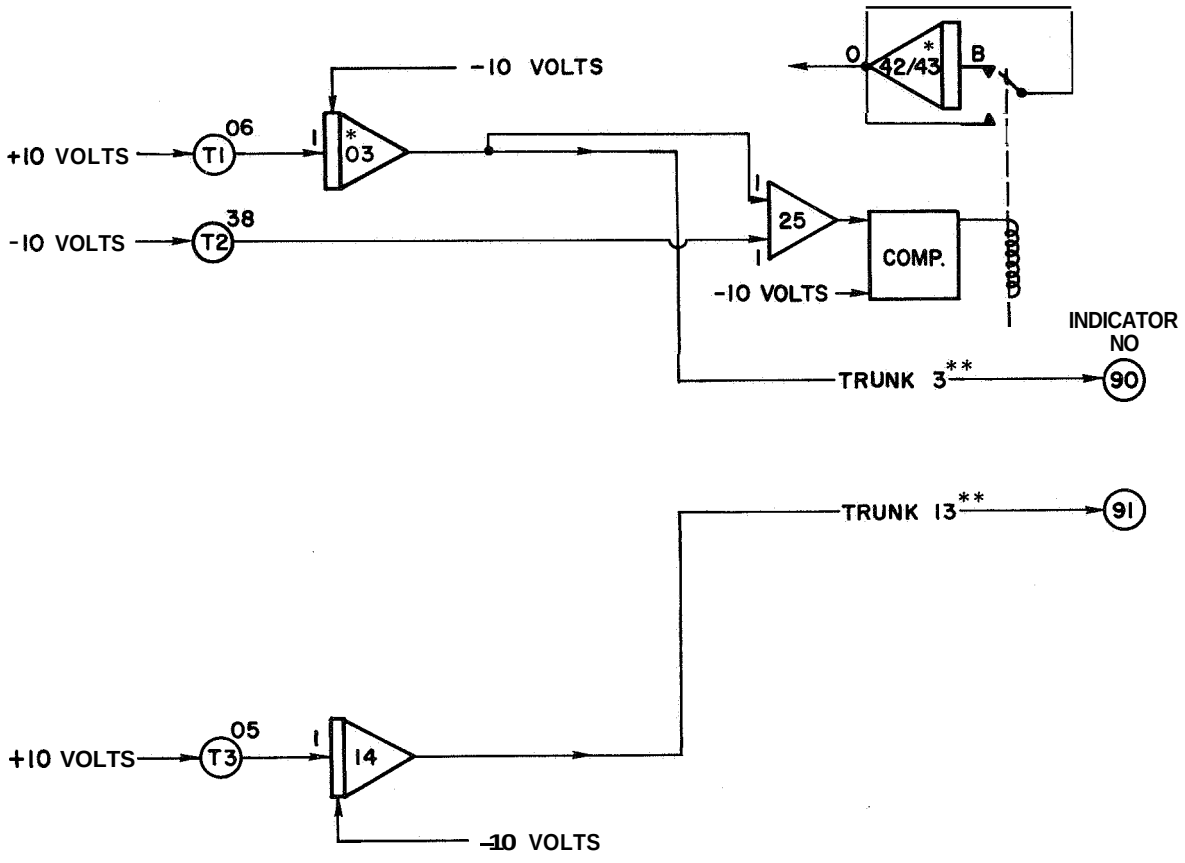

Figure 3.11.4. Analog clocks, determine length of operating mode, reset mode, and time necessary for reaching the limit cycle.

CHAPTER IV

DIGITAL CONTROL AND OPTIMIZATION

4.1 Introduction

The optimization of the plant control parameters was done by slaving the two analogs to a 1620 IBM Digital computer. The digital program consists of four parts:

1) The main program, used mainly for input/output purposes;

2) "DIRECT" - Maximization subprogram;

3) "CHECK" - It checks whether the values of the parameters adjusted by "DIRECT" are within the range of the D/A converter;

4) "EVAL1" - This subprogram controls the analog computer through the subprograms WINO, RINO, MODE1, MODEO, RESET, COMP, WAIT1, WAITO, WSETO, WSET1.

Sometimes it is desired not to minimize the fuel consumption, but rather to find the values of the fuel consumption functional near a given point. For this reason a second subprogram named "DIRECT" was written. If it is desired to perform the above operation, one simply replaces the maximization* subprogram called "DIRECT" with the functional evaluator subprogram called "DIRECT", hopping that confusion can still be avoided and some saving of time can be achieved.

4.2 The Program

The schematics of the main program are shown in Figure 4.2.1. It can be seen that the program is used only for establishing the necessary

* The fuel consumption as measured by the analog is represented by negative -voltage, and in order to minimize the fuel consumption it is necessary to maximize the output of the fuel consumption integrator.

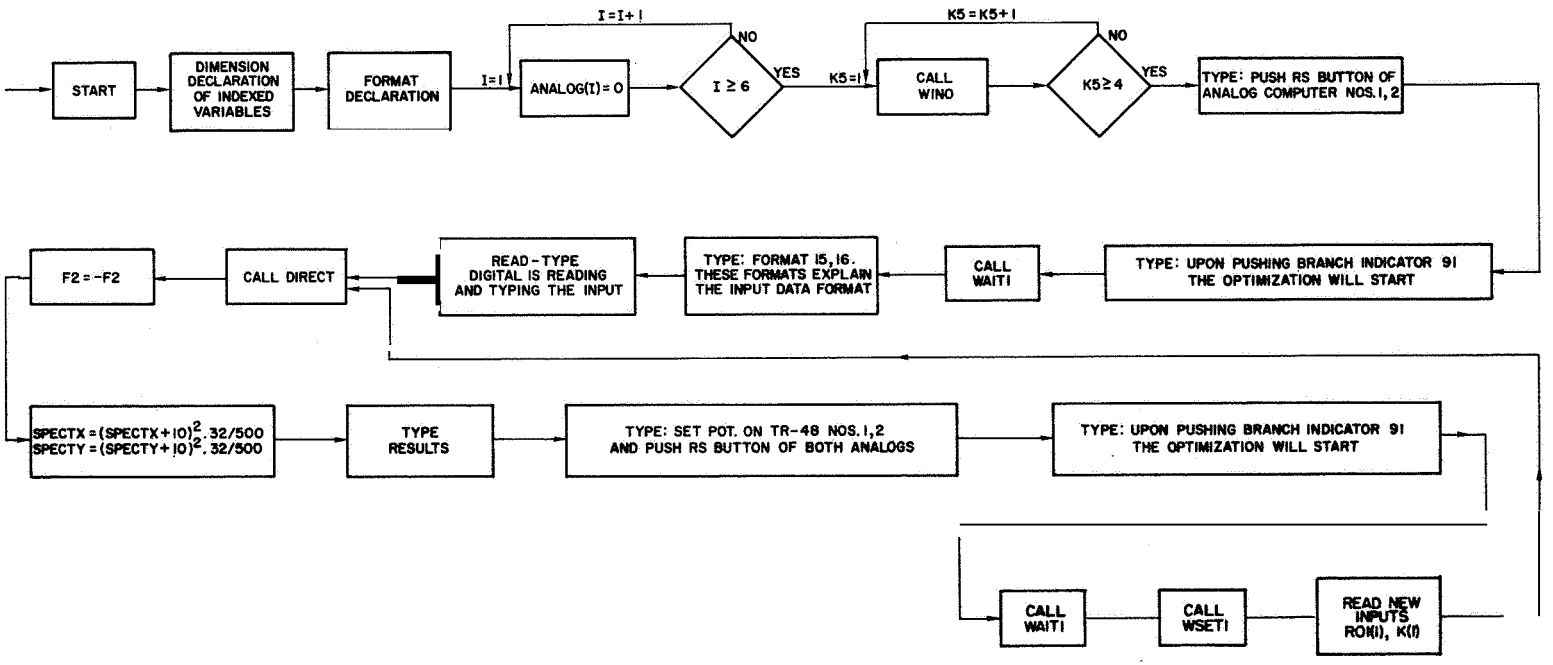

N- NUMBER OF ADJUSTABLE PARAMETERS	I1
EPSI- MINIMUM STEP SIZE	E 9.2
X(1), X(2), X(3)- STARTING POINT OF THE SEARCH	E 9.2
ROI(1), ROI(2), ROI(3)- INITIAL STEP SIZE	E 9.2
RANGX, RANGY- CONSTRAINTS ON STATE VARIABLES	E 9.2
K(I)- STEP SIZE REDUCTION FACTOR (K(I)/K(I)+1)	I1

Figure 4.2.1. Schematics of the main program

output/input relations with the computer. The input data should be given on punched cards following this order:

1)	N - Number of variables	Format I1
2)	EPSI - Smallest step size	Format E9.2
3)	x(1) - First parameter: Determine the width of the Schmitt trigger	Format E9.2
4)	x(2) - Second adjustable parameter: Determine the threshold of the Schmitt trigger	Format E9.2
5)	x(3) - Third parameter: Determine the dead-band width and indirectly the P.W.P.F. saturation voltage	Format E9.2
6,7,8)	ROl(1), ROl(2), ROl(3) - Initial Step Size	Format E9.2
9,10)	RANGX, RANGY - Maximum travelling distance allowed	Format E9.2
11)	K(1) - Step size reduction factor [Step size n+1] = [K(i)/(K(i) + n)]ROl(i)	Format I1

By following the instructions typed by the typewriter, the optimization can be carried without the knowledge of the algorithm.

When the optimum for a given angular velocity, noise level, and table tilt is found, the computer will be at WAITl, waiting for the next optimization which will start after reading the following inputs:

1,2,3)	ROl(1), ROl(2), ROl(3) - Initial step size
4)	K(1) - Step reduction factor

All other parameters remain unchanged, and the adjustable parameters [x(1), x(2), x(3)] have the value of the previous minimum. The listing of the main program is given in Appendix A.

4.3 Direct-Search

Subprogram DIRECT will search for a maximum of the functional defined by the system shown in Figure 3.10.1 or 3.10.2, subject to state constraints (see Section 3.8)

$$\begin{aligned} |X_{max}| &\leq \text{RANGX} \\ |Y_{max}| &\leq \text{RANGY} \end{aligned} \tag{4.3.1}$$

To define the point found by the subprogram Direct it is necessary to introduce the following definitions:

$$f(t_1,\tau,x_1,x_2,x_3) = \int_{t_1}^{t_1+\tau} [\text{Input to fuel consumption integrator}]\, dw \tag{4.3.2}$$

Since there is always unavoidable noise in the measurement of $f(t_1,\tau,\underset{\sim}{x})$ and an additional noise is introduced artificially into the system, it was implicitly assumed that

$$F(\tau,\underset{\sim}{x}) = E\left\{f(t_1,\tau,\underset{\sim}{x})\right\} = \int_{-\infty}^{+\infty} P(f)\, f(t_1,\tau,\underset{\sim}{x})\, df \tag{4.3.3}$$

exists for all feasible $\underset{\sim}{x}$ and all finite τ.

$P(f)$ is the probability density function of the values of $f(t_1,\tau,\underset{\sim}{x})$. It will be assumed that

$$F(\tau,\underset{\sim}{x}) = \lim_{T \to \infty} \frac{1}{2T} \int_{-co}^{+co} f(t_1,\tau,\underset{\sim}{x})\, dt_1 \qquad (4.3.4)$$

Let D be a domain defined by the system equations and the system constraints, so that whenever $(x_1,x_2,x_3) \in D$, the system equations, together with the state constraints, hold.

Let

$$B_i[(x_1^*,x_2^*,x_3^*),\ \delta_i] \quad i = 1,2,3 \quad \delta_i > 0 \qquad (4.3.5)$$

be a closed interval of length δ_i parallel to the x_i axis with (x_1^*,x_2^*,x_3^*) as its midpoint. Let

$$\underset{\sim}{e}_1 = [1,0,0], \quad \underset{\sim}{e}_2 = [0,1,0], \quad \underset{\sim}{e}_3 = [0,0,1] \qquad (4.3.6)$$

be three independent unit vectors.

The subprogram Direct will find a feasible point $(\ddot{x}_1^*,\ddot{x}_2^*,\ddot{x}_3^*)$ i.e., a point which satisfies Equation 4.3.1 such that

$$F(\tau,\underset{\sim}{x}^*) \geq F(\tau,\underset{\sim}{x}^* + \xi_i e_i) \quad \text{for all} \quad i = 1,2,3 \qquad (4.3.7)$$

and for all ξ_1 given by

$$|\xi_i| = \begin{cases} \leq \delta_i \quad \text{if} \quad B_i[(x_1^*,x_2^*,x_3^*),\delta_i] \cap D \neq \{x_1^*,x_2^*,x_3^*\} \\ \quad \text{and is not empty for some} \quad \delta_i > 0 \\ = 0\ . \quad \text{Elsewhere} \end{cases} \qquad (4.3.8)$$

Since the system is noisy, a few modifications had to be done before using the regular Direct search [Reference 6].

1) The step size is not halved after each iteration; instead, the step size reduction factor is given by

$$ROl(I)_n = [K(I)/(K(I) + n)]ROl(I) \qquad (4.3.9)$$

where

$ROl(I)_n$ - Step size in $x(I)$ direction after the n^{th} iteration;

$K(I)$ - Step size reduction factor

$ROl(I)$ - Initial step size.

2) The total number of iterations done by the subprogram Direct depends upon the initial and final step size and on $K(I)$. Each iteration consists of at least twelve fuel consumption measurements. Let $f(\underset{\sim}{x}_{ni})$ be the outcome of the i^{th} fuel consumption measurement done during the n^{th} iteration, and let $\overline{f}_n(\underset{\sim}{y})$ be the reference value stored in the computer when starting the n^{th} iteration. If

$$\overline{f}_n(\underset{\sim}{y}) > f(\underset{\sim}{x}_{ni}) \quad \text{for some } i \qquad (4.3.10)$$

the value of $f(\underset{\sim}{x}_{ni})$ is discarded and $\overline{f}_n(\underset{\sim}{y})$ remains unchanged, but if

$$\overline{f}_n(\underset{\sim}{y}) \leq f(\underset{\sim}{x}_{ni}) \qquad (4.3.11)$$

the computer will evaluate

$$f(\underset{\sim}{x}) = \sum_{i=1}^{3} f(\underset{\sim}{x}_{n,i+1})/3 \qquad \underset{\sim}{x}_{n,i+1} = \underset{\sim}{x}_{n,i+2} = \underset{\sim}{x}_{n,i+3} = \underset{\sim}{x}_{n,i} \qquad (4.3.12)$$

and will set a new reference value

$$\bar{f}_n(\underset{\sim}{x}) = \hat{f}(\underset{\sim}{x}) \qquad (4.3.13)$$

This arrangement is done in order to avoid fuel-consumption reference values $\hat{f}_n(\underset{\sim}{y})$ which, because of its stochastic nature, are far from $F(\underset{\sim}{y})$.

Moreover, if during the n^{th} iteration

$$\bar{f}_n(\underset{\sim}{y}) \geq f(\underset{\sim}{x}_{ni}) \quad \text{for all} \quad i \qquad (4.3.14)$$

the computer will set a new reference value equal to

$$\bar{f}_n(\underset{\sim}{y}) = \sum_{i=1}^{3} f(\underset{\sim}{y}_i)/3 \qquad \underset{\sim}{y}_i = \underset{\sim}{y} \quad \text{for all} \quad i \qquad (4.3.15)$$

Therefore, after each iteration the value of $\bar{f}_n$ is recalculated. These two midifications made possible the use of Direct search for the present program.

A flow diagram which shows the main features of the search is shown in Figure 4.3.1. It should be noted that the first fuel consumption evaluation should be feasible, i.e., satisfies the constraints of Equation 4.3.1. This can be achieved by either setting attenuators 07 and 08 at a proper value, or by making a clever choice of RANGX RANGY, e.g., starting the program once for arbitrary values of RANGX RANGY and finding the values of ALLOWX, ALLOWY which are typed after the first functional evaluation and then setting

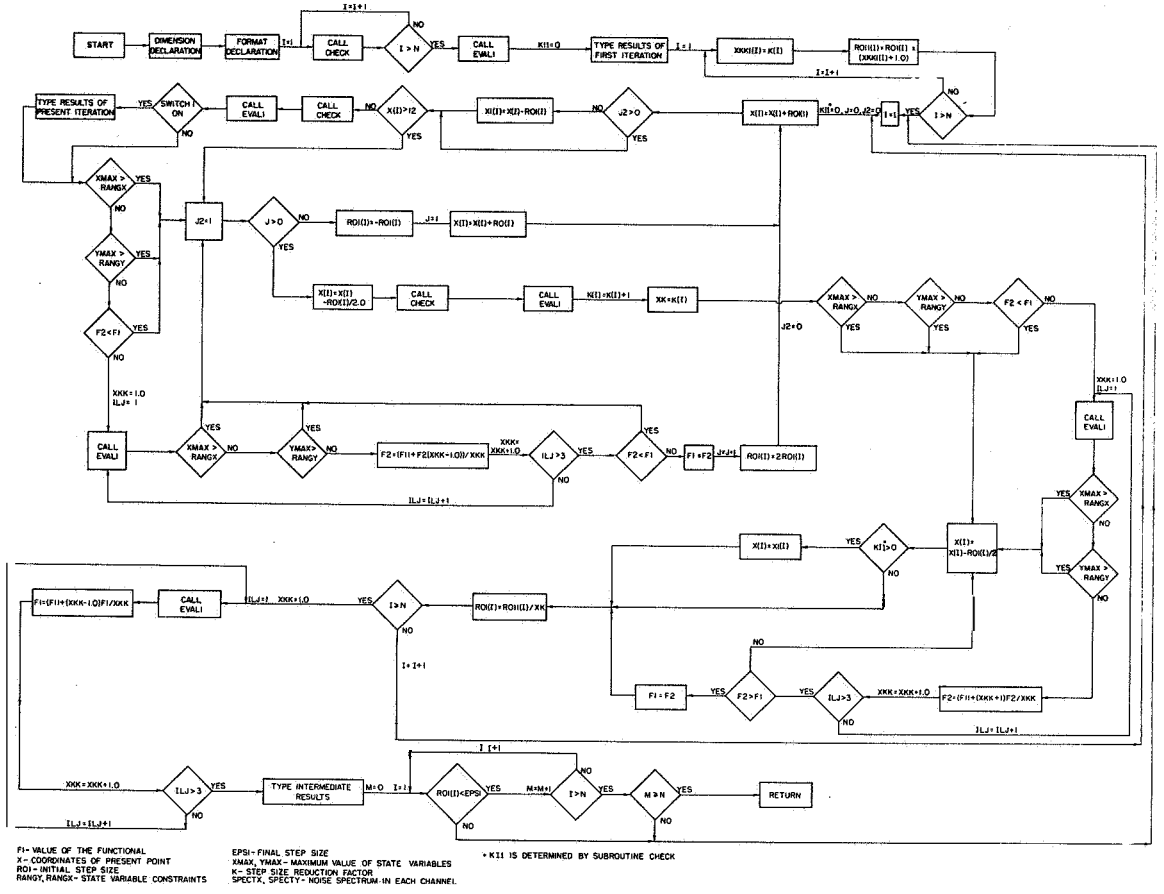

Figure 4.3.1. Schematics of the subprogram DIRECT

$$a \cdot ALLOWX = RANGX$$
$$a \geq 1 \qquad (4.3.16)$$
$$a \cdot ALLOWY = RANGY$$

and starting the program again. Note also that if switch one is on, $f(\underset{\sim}{x}_{ni})$ will be typed after almost each evaluation.

The suggested value of the minimum step size EPSI, is 0.1, which corresponds to attenuator setting difference of (0.1 · 0.393) (see Section 3.11). The maximum step size is 9.99/2 since the maximum input to the D/A converter is 9.99 volts. The complete listing of subprogram DIRECT is given in Appendix A.

In order to use the second "DIRECT" subprogram (see Sec. 4.1) one should replace the maximization subprogram "DIRECT" described above with the functional evaluator subprogram called "DIRECT". One should also delete subprogram "CHECK", since it is not used by the functional evaluator subprogram. The listing ofthissubprogram is given in Appendix A.

4.4 Subprogram CHECK

The range of the D/A converter is -9.99 to +9.99 volts. Whenever the value written on the D/A converter exceeds these values, the D/A output is not correct. Moreover, at the present set-up all adjustable parameters of the P.W.P.F. are positive, thus the range of these parameters is 0.00-9.99. The subprogram CHECK will check the values to be written on the converter and adjust them, according to the following scheme: any value higher than 10 volts will be reduced to 9.99 volts, and any value less than zero will be increased to 0.00.

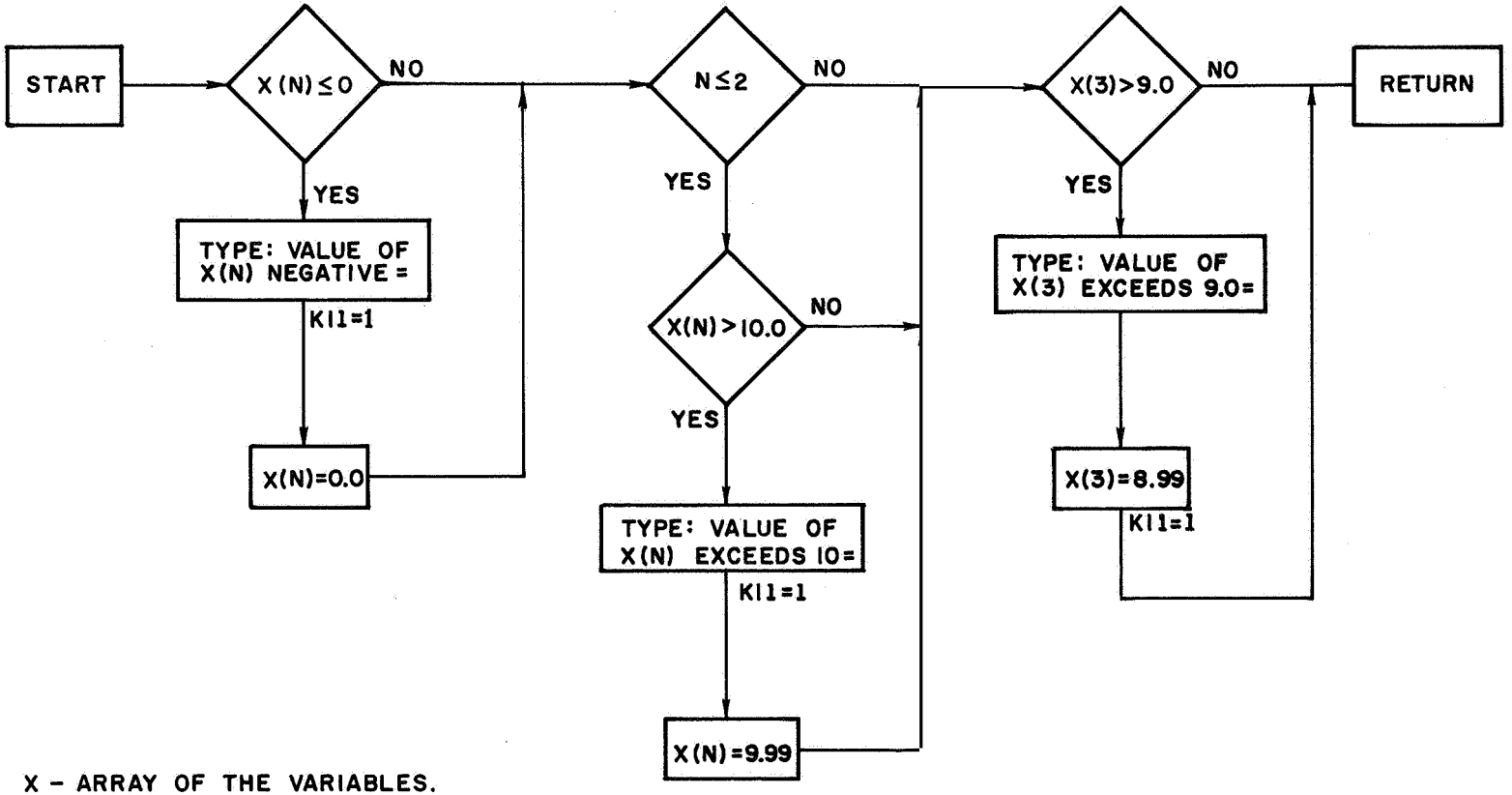

X - ARRAY OF THE VARIABLES.
KI1- INDICATOR IF THE BOUNDARY WAS REACHED.
N- INDEX OF THE VARIABLE.

Figure 4.4.1. Schematics of the subprogram Check

Experimentally, it was found that if x(3) exceeds 9, amplifiers 13, 12, 32, and 33 overload, Figure 3.11.2. Therefore, this parameter is restricted to the range 0.00-8.99.

Whenever a parameter value is adjusted by subprogram check, the typewriter will type the corresponding change. For more details, see the complete listing given in Appendix A.

4.5 Subprogram EVAL1

The main features of this subprogram are shown in Figure 4.5.1. This subprogram controls the analog operation mode through 1620 control out and Indicators 90, 91. This subprogram adjusts the parameters using WINO subprogram and reads the results of the simulation using RINO subprogram. The complete listing of the subprogram is given in Appendix A.

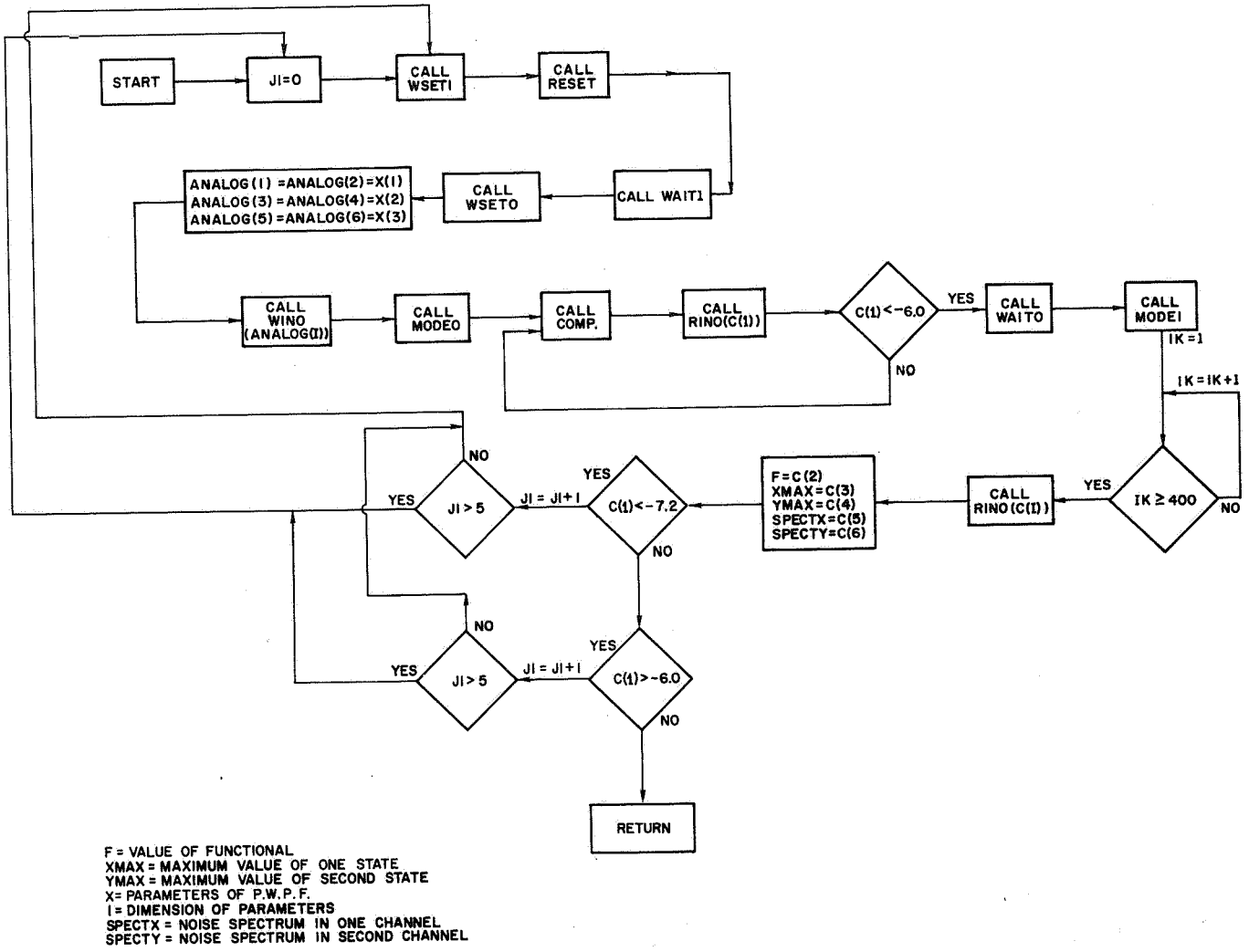

Figure 4.5.1. Schematics of the subprogram EVAL1

CHAPTER V

OPTIMIZATION STUDIES AND RESULTS

5.1 Introduction

The results obtained from the simulation experiments are given in the following sections.

Most of the measurements were performed with a nonrotating vehicle. As was already mentioned, two different simulations exist: a) body-fixed coordinates; b) inertial coordinates. Generally the two programs are almost identical in their behavior, but there is a difference in the fuel consumption measurement; because a) it is very difficult to adjust the control jet pressure, and b) there exist some minor differences between the two programs, as can be seen by comparing Figure 3.2.1 with Figure 3.2.2. However, these differences will not affect the shape of the fuel consumption function (compare Figure 5.2.2 with Figure 5.2.4) and therefore will not affect the optimal value of the control parameters. The results shown in Table 5.2.1 and Figures 5.2.1, 5.2.2, and 5.2.3 were obtained from the simulation shown in Figure 3.10.1 (body-fixed coordinates). While the results shown in Figure 5.2.4 were obtained from the second simulation.

The main underlying idea of the optimization was the studying of the shape of the fuel consumption functional and its dependence on the control parameters for different table tilts, noise levels, and angular velocities.

5.2 Results

The results of the optimization studies for different table tilts and angular velocities are given in Table 5.2.1. The fuel consumption

was measured during equal time intervals. But, the length of the interval was not measured accurately (approximately 18 see). Therefore, fuel consumption measurements given in Table 5.2.1 can be compared with each other but not with a different set of experiments.

To convert the optimal attenuator settings found by the optimization to optimal P.W.P.F. parameters:

1) Width of the Schmitt trigger hysteresis (See Figure 3.6.3)

2) Threshold of Schmitt trigger (see Figure 3.6.4) (5.2.1)

3) [Dead-band width] = $12.5/(x_3/10)$ mils

where 12.5 mils = Dead-band width when $(x_3/10)$ 3.93 = 1.0

3.93 = Dead-band attenuator amplification (see Section 3.11)

Observe that for some experiments the width of the hysteresis loop is bigger than the threshold of the Schmitt trigger.

In all above optimization studies

$$\text{RANGX} = \text{RANGY} = 1.8 \text{ volts} \qquad (5.2.2)$$

From the results obtained (Table 5.2.1) it was not possible to deduce any clear conclusions concerning the dependence of the fuel consumption on the control parameters; therefore, it was felt that the reason for that is due to the fact that near the optimum the functional may be almost constant. In the remaining experiments this hypothesis was checked.

The dependence of the fuel consumption functional on the control parameters is shown in Figure 5.2.1. Table tilt was 1 arc sec and in each set of: experiments only one parameter was changed, while the value of the remaining two parameters was kept constant and equal to the value

Table Tilt (Table 3.10.1 Column 1) arc sec	XMAX Volts	XMAX Volts	Fuel Consumption volts/min	Optimal Setting x_1 ± 0.2	x_2 ± 0.2	x_3 ± 0.2	Optimal Control Parameters $\theta_1-\theta_2$ Volts	θ_1 Volts	Dead Band Mils	ω rad/sec
1	0 97	0.96	3.57	2.96	6.63	2.74	1.80	3.6	11.6	0
2	1 42	1.14	6.40	3.96	4.90	2.15	1.15	1.7	15.1	0
3	1 65	1.25	9.47	2.67	4.40	1.92	1.7	1.0	16.6	0
3	0 73	0.56	9.15	4.4	5.89	4.09	2.3	2.8	7.8	0
4	0 83	0.60	12.4	2.81	6.29	3.70	1.75	3.4	8.6	0
4	0 48	0.45	12.5	1.99	8.20	5.30	1.5	5.6	6.0	0
1	0 26	0.46	7.9	1.54	9.24	7.88	1.3	6.8	4.04	0 3

Table 5 2 1 Optimal control parameters for different table tilts ω angular velocities. (Using body-fixed coordinates) Minimum step size 0.2.

obtained in the corresponding optimization experiment. (Table 5.2.1, first row). Clearly, with this choice of parameters, the fuel consumption functional is almost constant over the investigated range. The same behavior was observed when a somewhat different set of control variables was chosen and the fuel consumption was measured at 1 arcsec. and 3 arc-sec. table tilts (Figure 5.2.2). However, when a set of different parameters was chosen (Figure 5.2.3) the shape was radically changed, which indicates again that only in a narrow range the fuel consumption functional depends strongly on the control parameters while near the optimum it is almost constant.

The results shown in Figure 5.2.1, 5.2.2 and 5.2.3 and Table 5.2.1 were obtained from the system shown in Figure 3.10.1 (body-fixed coordinates), while the results shown in Figure 5.2.4 were obtained from the system shown in Figure 3.10.2. In spite of that, the shape of the graphs shown in Figure 5.2.4 (without noise) is almost identical with the graphs shown in Figure 5.2.2 (table tilt 3 arc sec), and there is only a difference in the fuel consumption ($\sim$ 30%).

The effect of noise on the system is shown in Figure 5.2.4. The table tilt for these experiments was 3 arcsec. The different signal to noise value can be deduced from the shape of the trajectories shown in the right corner of Figure 5.2.4.

5.3 Conclusions

It was found that the fuel consumption is almost constant over a wide range. It seems that any choice of control parameters within this range will be adequate, depending, of course, on the a priori constraints

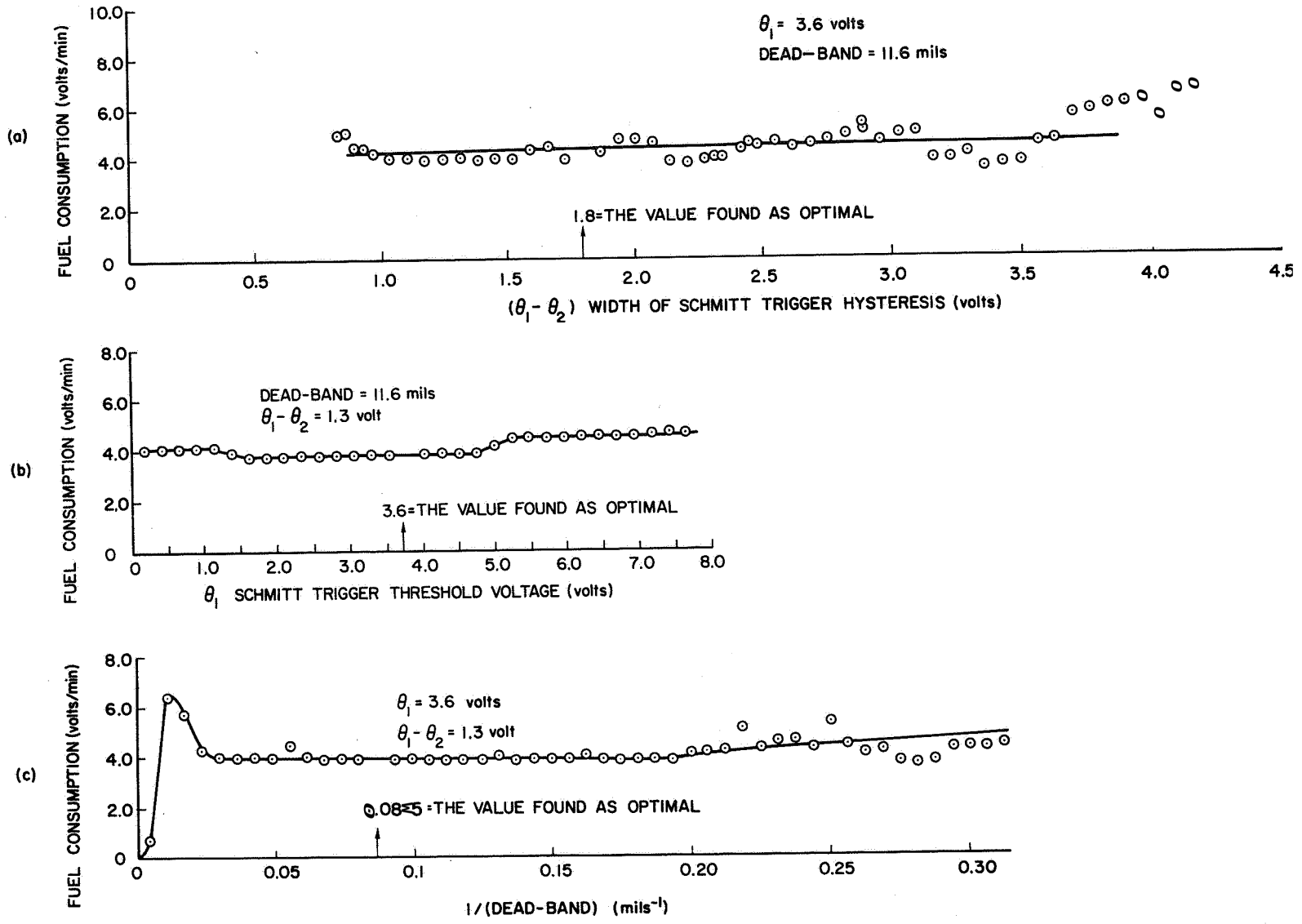

Figure 5.2.1. Fuel consumption vs. different control parameters
(a) Changing only the width of Schmitt trigger hysteresis
(b) Changing only the Schmitt-trigger threshold voltage
(c) Changing only the Dead Band width

Table tilt is 1 arc sec. The value of the optimal parameters are indicated on the graph, (Experiments performed on the system shown by Figure 3.10.1).

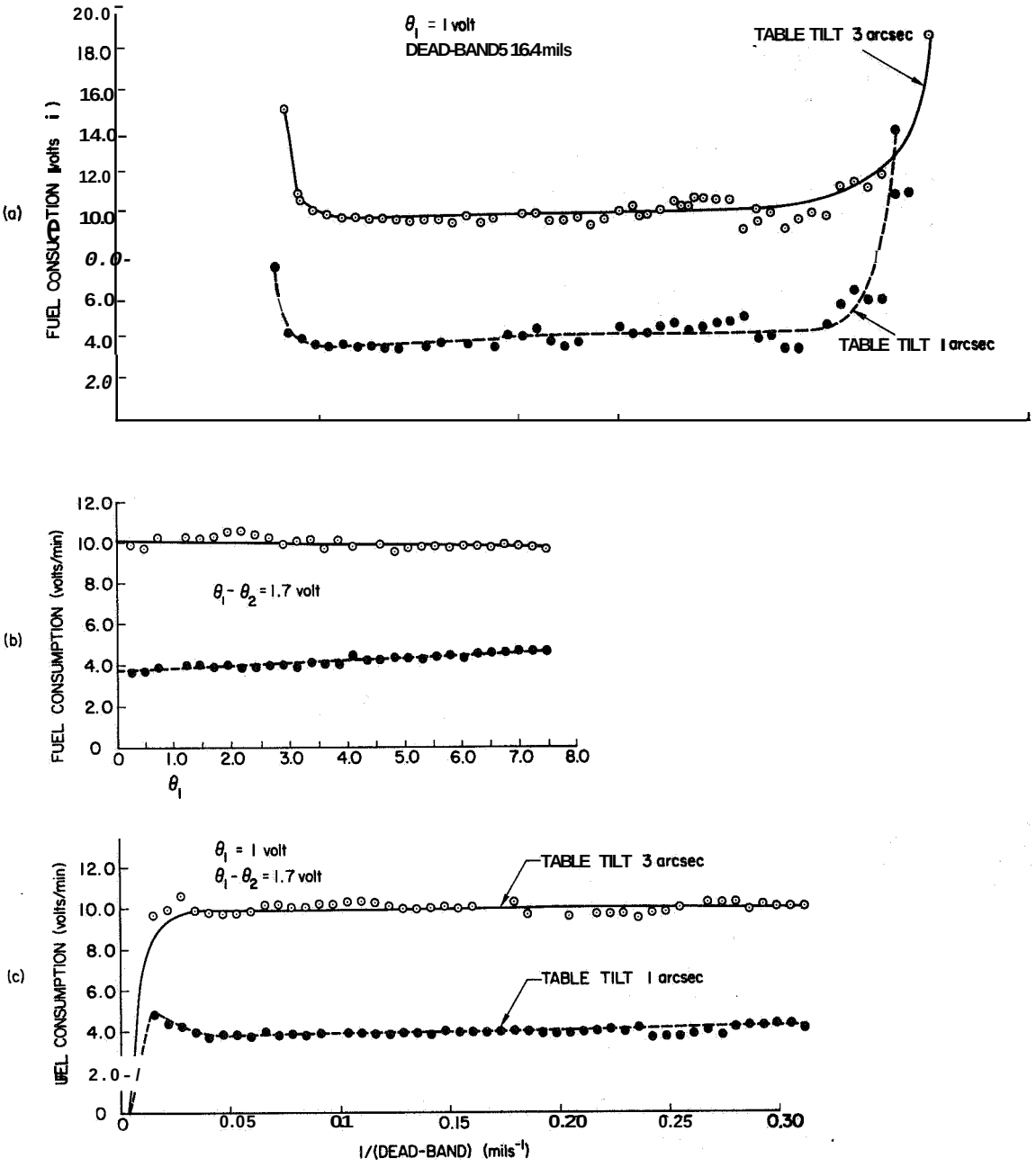

Figure 5.2.2. Fuel consumption vs. different control parameters and two different table tilts.

(a) Changing only the width of Schmitt trigger hysteresis

(b) Changing only the Schmitt-trigger threshold voltage

(c) Changing only the Dead Band width

(Experiments performed on the system shown by Figure 3.10.1)

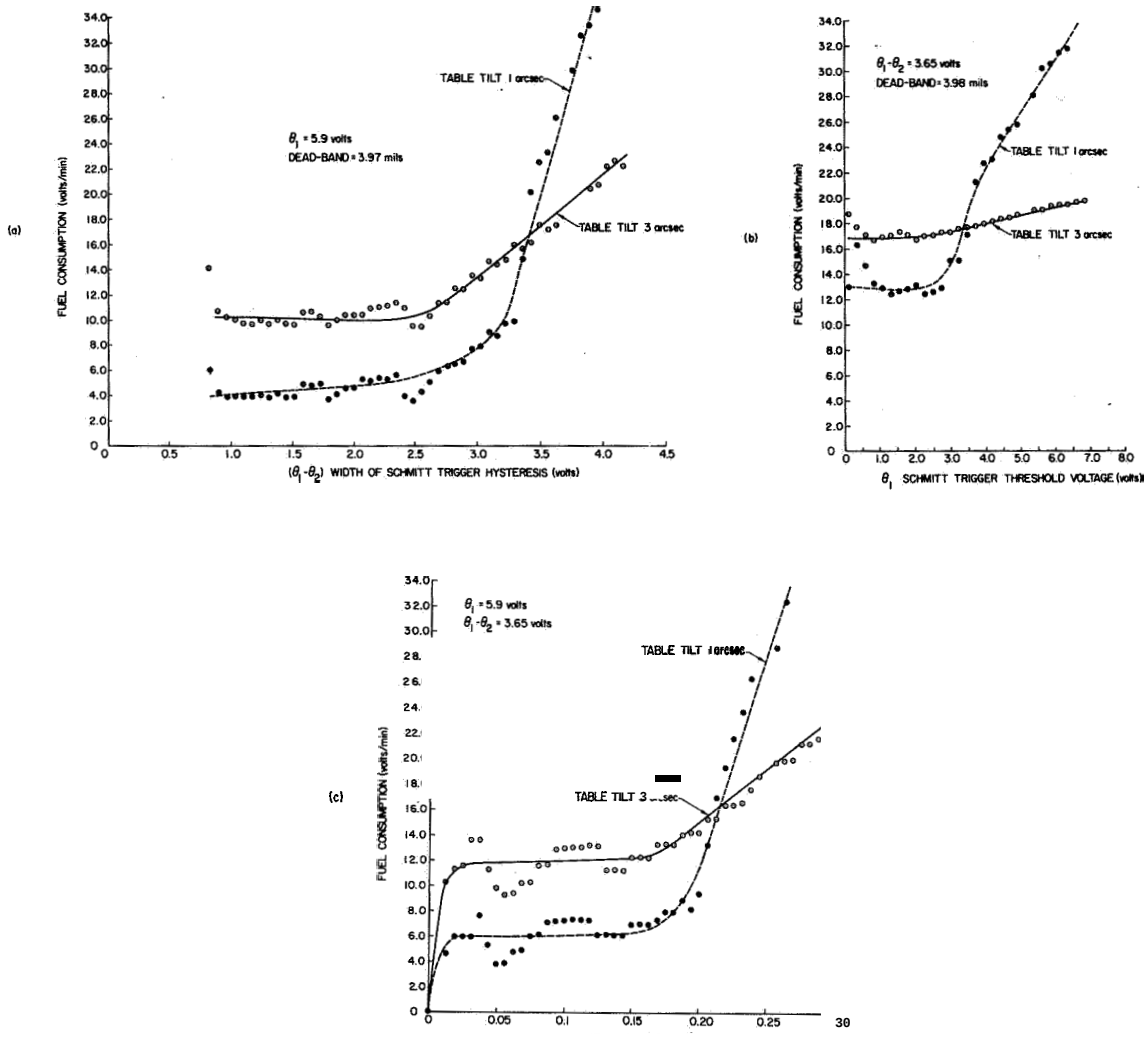

Figure 5.2.3. Fuel consumption vs. different control parameters and two different table tilts

(a) Changing only the width of Schmitt trigger hysteresis

(b) Changing only the Schmitt-trigger threshold voltage

(c) Changing only the Dead Band width

(Experiments performed on the system shown by Figure 3.10.1)

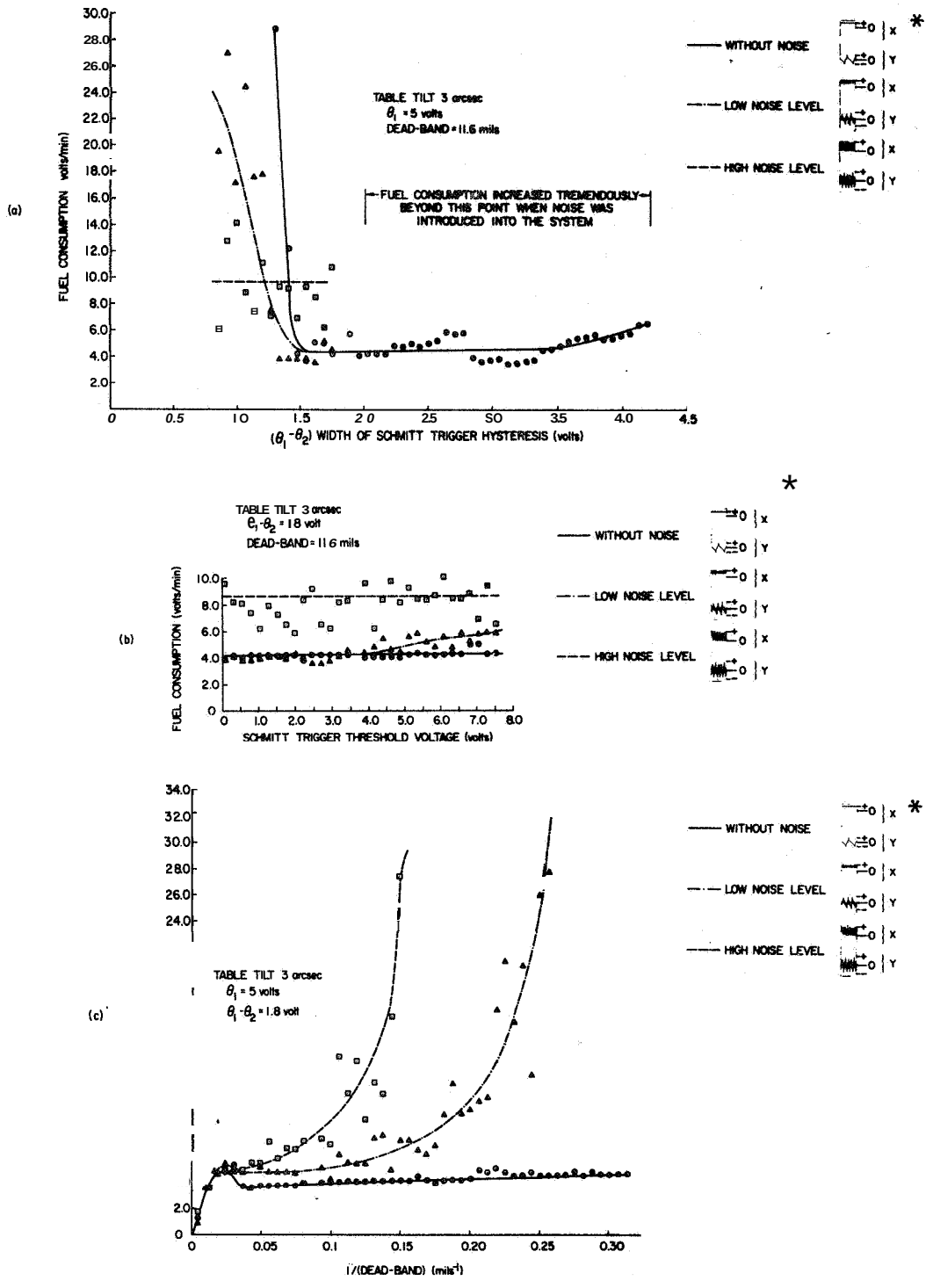

Figure 5.2.4. Effect of noise on the fule consumption

(a) Changing only the width of Schmitt trigger hysteresis
(b) Changing only the Schmitt-trigger threshold voltage
(c) Changing only the Dead Band width
* Pictorial representation of the noise influence on the vehicle trajectory.

on the state variables x and y. However, it was felt that the information collected is not enough. It is necessary to check the behavior of the vehicle for higher angular velocities and different signal-noise ratios. And last but, not least to take longer measurements of fuel consumption during the optimization.

APPENDIX A

MAIN PROGRAM

```
      DIMENSION X(5),RO1(5) ,K(3)
    4 FORMAT (~9.2)
    5 FORMAT (38HPUSH RS BUTTON OF ANALOG TR-48 NOS.1,2)
    6 FORMAT (60HUPON PUSHING BRANCH INDICATOR 91 THE OPTIMIZATION WILL
   1START)
    7 FORMAT (80HFUEL CONSUMPTION    RANGEX    RANGEY    TETA1    TETA1-
   1TETA2    SPECTX    SPECTY)
   12 FORMAT (80H1
   1          NOISE LEVEL    )
    8 FORMAT(4H    ,F8.3,6H       ,F8.3,2H  ,F8.3,1H  F8.3,3H    ,F8.3,
   16H      ,F8.3,2H  ,F8.3)
    9 FORMAT (11)
   11 FORMAT (61HSET POT. ON TR-48 NOS. 1,2 AND PUSH RS BUTTON OF BOTH A
   1NALOGS)
   13 FORMAT(1H1/48H                                          DEAD ZONE)
   14 FORMAT(39H                                          F8.3)
   15 FORMAT(50HREAD THROUGH CARD READER THE FOLLOWING PARAMETERS )
   16 FORMAT( 66H1)N=NUMBER OF ADJUSTABLE PARAMETERS 2) EPSI=THE SMALLES
   1T STEP SIZE)
   17 FORMAT(32H3) X(1),X(2),X(3)=STARTING POINT)
   18 FORMAT(40H4)RO1(1),RO1(2),RO1(3)=INITIAL STEP SIZE)
   19 FORMAT(44H5)RANGX,RANGY=CONSTRAINTS ON STATE VARIABLES)
   20 FORMAT(38H6)K(1),K(2),K(3)=STEP REDUCTION FACTOR)
   21 FORMAT(55HTHE STEP SIZE IS REDUCED BY K(1)/(K(I)+(ITERATION NO. )))
   22 FORMAT(53HFORMAT OF ALL INTEGERS IS I1 AND OF ALL REALS IS E9.2)
      M=6
      DIMENSION ANALOG(6)
      DO 221 1=1,6
  221 ANALOG(I)=0.0
      DO 222 K5=1,4
      CALL WINO(ANALOG(1))
  222 CONTINUE
      CALL COMP
      CALL MODE1
      TYPE 5
      TYPE 6
      CALL WAIT1
      TYPE 15
      TYPE 16
      TYPE 17
      TYPE 18
      TYPE 19
      TYPE 20
      TYPE 21
      TYPE 22
      READ 9,N
      TYPE 9,N
      READ 4,EPSI
      TYPE 4,EPSI
      READ 4,X(1)
```

```
      TYPE 4,X(1)
      READ 4,X(2)
      TYPE 4,X(2)
      READ 4,X(3)
      TYPE 4,X(3)
      READ 4,RO1(1)
      TYPE 4,RO1(1)
      READ 4,RO1(2)
      TYPE 4,RO1(2)
      READ 4,RO1(3)
      TYPE 4,RO1(3)
      READ 4,RANGX
      TYPE 4,RANGX
      READ 4,RANGY
      TYPE 4,RANGY
      READ 9,K(1)
      K(2)=K(1)
      K(3)=K(1)
      TYPE 9,K(1)
    1 CALL DIRECT (F2,X,N,RO1,RANGX,RANGY,EPSI,XMAX,YMAX,K   ,SPECTX,SPEC
     1TY)
      F2=-F2
      SPECTX=(SPECTX+10.0)**2*32.0/5.0/100.0
      SPECTY=(SPECTY+10.0)**2*32.0/5.0/100.0
      TYPE 12
      TYPE 7
      TYPE 8,F2,XMAX,YMAX,X(1),X(2),SPECTX,SPECTY
      TYPE 13
      TYPE 14,X(3)
      TYPE 11
      TYPE 5
      CALL WAIT1
      CALL WSET1
      READ 4,RO1(1)
      TYPE 4,RO1(1)
      READ 4,RO1(2)
      TYPE 4,RO1(2)
      READ 4,RO1(3)
      TYPE 4,RO1(3)
      READ 9,K(1)
      K(2)=K(1)
      K(3)=K(1)
      TYPE 9,K(1)
      GO TO  1
      END
```

```
1         SUBROUTINE DIRECT( F1,X,N,RO1,RANGX,RANGY,EPSI, XMAX,YMAX,K   ,SPECT
         1X, SPECTY)
2         DIMENSION RO11(5)
3         DIMENSION X(5),RO1(5),K(5)
4         DIMENSION XKK1(3)
5    98   FORMAT (11F7.3)
6         DIMENSION X1(5)
7         DO 97 1=1,N
8    97   CALL CHECK(X  ,KI1,I)
9         CALL EVAL1(F1,ALLOWX,ALLOWY,X,N, SPECTX,SPECTY)
10        K I1=0
11        TYPE 98,F1,ALLOWX,ALLOWY, SPECTX, SPECTY, (X(K2),RO1(K2),K2=1,N)
12        DO 99 I=1,N
13        XKK1(I)=K(I)
14        RO11(I)=RO1(I)*( XKK1(I)+1.0)
15   99   CONTINUE
16   100  DO 200 I=1,N
17        J2=0
18        J=0
19        KI1=0
20   101  X(I)=X(I)+RO1(I)
21        IF (J2)107,107,108
22   107  X1(I)=X(I)-RO1(I)
23        KI1=0
24   108  CONTINUE
25        IF (X(1)-12.0) 102,102,150
26   102  CALL CHECK (X  ,KI1,I)
27        CALL EVAL1 (F2,XMAX,YMAX,X,N,SPECTX, SPECTY)
28   105  IF (SENSE SWITCH 1) 104,103
29   104  TYPE 98,F2,XMAX,YMAX, SPECTX, SPECTY, (X(K2),RO1(K2),K2=1,N)
30   103  CONTINUE
31        IF (XMAX-RANGX) 120,120,150
32   120  IF (YMAX-RANGY) 130,130,150
33   130  IF (F2-F1) 150,140,140
34   140  XKK=1.0
35        DO 142 ILJ=1,3
36        CALL EVAL1 (F11,XMAX,YMAX,X, N,SPECTX, SPECTY)
37        IF (XMAX-RANGX) 141,141,150
38   141  IF (YMAX-RANGY) 1422,1422,150
39   1422 F2=(F11+F2*(XKK-1.0))/XKK
40   142  XKK=XKK+1.0
41        IF (F2-F1) 150,143,143
42   143  F1=F2
43        J=J+1
44        RO1(1)=2.0*RO1(I)
45        J2=0
46        GO TO 101
47   150  J2=1
48        IF (J  ) 160,160,170
49   160  RO1(I)=-RO1(I)
50        J=1
51        X(I)=X(I)+RO1(I)
52        GO TO 101.
```

```
170   X(I)=X(I)-RO1(I)/2.0
      CALL CHECK (X ,KI1,I)
      CALL EVAL1 (F2,XMAX,YMAX,X,N,SPECTX,SPECTY)
      K(I)=K(I)+1
      XK=K(I)
      IF (XMAX-RANGX) 180,180,195
180   IF (YMAX-RANGY) 190,190,195
190   IF (F2-F1) 195,191,191
191   XKK=1.0
DO    DO 1913 ILJ=1,3
      CALL EVAL1(F11,XMAX,YMAX,X,N,SPECTX,SPECTY)
      IF (XMAX-RANGX)1911,1911,195
1911  IF (YMAX-RANGY) 1912,1912,195
1912  F2=(F11+(XKK-1.0)*F2)/XKK
1913  XKK=XKK+1.0
      IF (F2-F1)195,1914,1914
1914  F1=F2
      GO TO 200
195   X(1)=X(I)-RO1(1)/2.0
      IF (KI1) 200,200,196
196   X(1)=X1(I)
200   RO1(I)=RO11(I)/XK
      XKK=1.0
      DO 1915 ILJ=1,3
      CALL EVAL1(F11,XAMX,YMAX,X,N,SPECTX,SPECTY)
      F1=(F11+(XKK-1.0)*F1)/XKK
1915  XKK=XKK+1.0
      TYPE 98,F1,XAMX,YMAX,SPECTX,SPECTY,(X(K2),RO1(K2=1,N)
      M=0
      DO 203 I=1,N
      IF (RO1(I)-EPSI) 203,203,100
203   M=M+1
      IF (M-N) 100,220,220
220   CONTINUE
      RETURN
      END
```

SUBROUTINE CHECK

```
1         SUBROUTINE CHECK(X,KI1,N)
2    400  FORMATION(12H VALUE OF X(,I1,13H) NEGATIVE =,F8.3)
3         DIMENSION X(5)
4    401  FORMAT (12H VALUE OF X(,I1,15H) EXCEEDS 10 = ,F8.3)
5    402  FORMAT (25HVALUE OF X(3) EXCEEDS 9 =,F8.3            )
6    300  IF (X( N)) 301, 302, 302
7    301  TYPE 400,N,X(N)
8         KI1=1
9         X(N)=0 .0
10   302  IF (N-2)304,304,306
11   304  IF (X(N)-10 .0) 306,306,303
12   303  TYPE 401,N,X(N)
13        KI1=1
14        X(N)=9.99
15   306  IF (X( 3)-9.0)310,311,311
16   311  X(3)=8.99
17        TYPE 402     ,X(3)
18        KI1=1
19   310   CONTINUE
20        RETURN
21        END
```

```
1         SUBROUTINE EVAL1 (F,XMAX,YMAX,X,I,SPECTX,SPECTY)
2    7401 FORMAT ( 36HMULTIVERTOR DOES NOT CONVERT CORRECT)
3    7499 J1=0
4    7501 CALL WSET1
5         CALL RESET
6    701  CALL WAIT1
7         CALL WSET0
8         DIMENSION X(5)
9         M=6
10        DIMENSION ANALOG(6)
11        ANALOG(1)=X(1)
12        ANALOG(2)=X(1)
13        ANALOG(3)=X(2)
14        ANALOG(4)=X(2)
15        ANALOG(5)=X(3)
16        ANALOG(6)=X(3)
17        CALL WIND(ANALOG(1))
18   709  CALL MODE0
19   710  CALL COMP
20        M2=1
21        DIMENSION C(6)
22   708  CALL RIN0(C(1))
23        IF (C(1)+6.0) 711,710,710
24   711  CALL WAIT0
25        CALL MODE1
26   IK=1 IK=1
27     1  IF (IK- 400)2,3,3
28     2  IK=IK+1
29        GO TO 1
30     3  CONTINUE
31        M2=6
32   748  CALL RIN0(C(1))
33   749  F=C(2)
34        XMAX=C(3)
35        YMAX=C(4)
36        SPECTX=C(5)
37        SPECTY=C(6)
38        IF (C(1)+7.2)7511,7512,7512
39   7511 J1=J1+1
40        IF (J1-5)7501,7501,7500
41   7512 IF (C(1)+6.0) 750,750,7513
42   7513 J1=J1+1
43        IF (J1-5)7501,7501,7500
44   7500 TYPE       7401
45        GO TO 7499
46   750  RETURN
47        END
```

REFERENCES

[1] Lange, B., "The Control and Use of Drag-Free Satellite", SUDAER No. 194, June 1966.

[2] Sherwood, R. B. and Wu, S. H., "Analysis of a Pulse Width-Pulse Frequency Modulator", TRW Space Technology Lab., 65.93521-12, April 1965.

[3] DeBra, B. D. and Mathieson, J. C., "A Precision, Active, Table Leveling System", 1966 AIAA Guidance and Control Specialist Conference, Seattle, Washington, August 1966.

[4] TR-48 Computer Operators Manual, E. A. I., Long Branch, New Jersey.

[5] Electronic Noise Generator Model 201D, E. A. I., Long Branch, New Jersey.

[6] Wilde, D. J., "Optimium Seeking Methods", Prentice-Hall, Inc., Englewood Cliffs, New Jersey.

ERRATA SHEET

SIMULATION AND OPTIMIZATION STUDIES OF DRAG FREE SATELLITE

Ury Passy

Sudaar No. 295
November 1966

Page 47 Under 3.4 heading, third line, Figure 2.4.5 should read "Figure 2.4.4".

Page 50 Middle of the page, Table 3.4.1, were obtained . . . ., should read "Table 3.4.2, were obtained . . . .".

Page 51 Caption at bottom of the page, Table 3.5.3, should read "Table 3.4.4".

Page 52 Caption for first table, Table 3.6.4, should read "Table 3.4.5".

Page 52 Caption for second table, Table 3.7.5, should read "Table 3.4.6.

Page 73 Lettering inside of the figure, (COLUMN 1 TABLE 3.10.2) should read "(COLUMN 1 TABLE 3.10.1)".

Page 73 Lettering inside of figure, (COLUMN 3 TABLE 3.10.2) should read "(COLUMN 3 TABLE 3.10.1)".

Page 52 First line after second table, (Table 3.4.5) should read "(Table 3.4.6)".